UCLouvain

AGRO LOUVAIN

Faculté des bioingénieurs

A coupled 3D hydrodynamic and ecosystemic model of Lake Titicaca.

How to grasp the complexity of Lake Titicaca in an easy to use model that enables water quality analyses and facilitates informed decision making?

Auteur :	François Duquesne
Promoteurs :	Emmanuel Hanert
	Eric Deleersnijder
Lecteurs :	Charles Bielders
	Prem Jai Vidaurre
Année Académique :	2018 - 2019
Bioingénieur :	Sciences et technologies de l'environnement

Abstract

Mathematical models are essential in the quest to better understand the human impact on the world's ecosystems.

In this thesis, we have provided a new tool that can be used to study Lake Titicaca's hydrodynamics and water quality. This was achieved by coupling NPZD (for Nitrogen-based nutrients, Phytoplankton, Zooplankton and Detritus) ecosystem-type model to an underlying three dimensional hydrodynamic model: the 3D version of the Second-generation Louvain-la-Neuve Ice-Ocean Model. SLIM3D leverages the finite elements method to solve the three-dimensional hydrodynamic equations on each element of an unstructured 3D mesh.

Our study focused on the entire Lake Titicaca, and we developed a case study on the smaller section of this lake: Lago Menor. Indeed, in the Cohana bay, eastern part of Lago Menor, a significant nitrogen discharge is caused by anthropogenic activities of the upstream Katari watershed. This discharge is most likely responsible for the algal bloom event occurred in March-April 2015. We thus applied a nitrogen forcing to our NPZD ecosystem-type model in order to replicate the proliferation of phytoplankton.

Our model covered the period of January 2014 to May 2015 and required the following inputs: the bathymetry, surface temperatures, and the horizontal wind speeds. Winds and surface temperatures are the major forcings that affect the hydrodynamics of the lake.

The results generated by the coupled SLIM3D-NPZD model we chose to exploit were: lake temperatures, the u and v components of water velocity, and the NPZD components.

Overall, the validation of our coupled SLIM3D-NPZD model suggests that the task of simulating Lake Titicaca's hydrodynamics was achieved but that our model lacks a more site-specific calibration in order to correctly simulate water quality. We managed to simulate the bloom of 2015 but observed some erroneous simulations in other parts of the lake. Nevertheless, we were able to foresee a few promising applications for this coupled model. These range from the use of the model for research purposes to the forecasting and analysis of different contamination scenarios.

We have thus manged to implement a fairly simple ecosystemic model that could be used as a predictive tool in the planification for the environmental protection of Lake Titicaca. Offering new opportunities for research and expanding the potential uses of the SLIM hydrodynamic model.

Acknowledgements

This Master's Thesis represents an important milestone in my life and its completion wouldn't have been possible without the support of many people whose names may not all be mentioned hereunder.

First and foremost I would like to thank professor Emmanuel Hanert, who has proven to be an exceptional thesis supervisor. Always supportive and open to new ideas, he has been a key element that helped to make this thesis such a pleasant experience.

I would also like to thank my co-supervisor, professor Eric Deleersnijder, whose work with SLIM has inspired me in numerous ways to complete this Master's thesis.

I owe my gratitude to Valentin Valerys for all his work regarding the implementation of the NPZD model as well as for all the time he spent helping and guiding me.

A very special gratitude goes out to the SLIM team and the PhD. students that where always happy to answer my numerous questions.

I would also like to acknowledge my readers: Prem Jai Vidaurre and professor Charles Bielders of the Earth and Life Institute at UCLouvain, and I am gratefully indebted to them for their valuable comments on this thesis. With a special mention to Prem for his crucial help gathering data in La Paz.

Finally, I must express my very profound gratitude to my family and to my girlfriend for providing me with unfailing support and continuous encouragement throughout my years of study and through the process of researching and writing this thesis. This accomplishment would not have been possible without them. Thank you.

Glossary

ALT: Binational Autonomous Authority of Lake Titicaca.

CFS: Climate Forecast System.

C3S: Copernicus Climate Change Service.

ECMWF: European Centre for Medium-Range Weather Forecasts.

ERA5: ERA refers to "ECMWF ReAnalysis", with ERA5 being the fifth major global reanalysis produced by ECMWF.

IRD: The french Research Institute for Development.

MMAyA: Bolivian Ministry of the Environment and Water (Ministerio del Medio Ambiente y Agua).

NOAA: National Oceanic and Atmospheric Administration.

NPZD: Nitrogen based nutriments, Phytoplankton, Zooplankton, Detritus.

SLIM: Second-generation Louvain-la-Neuve Ice-Ocean Model.

Key words

Lake Titicaca • hydrodynamic model • SLIM • ecosystemic model • NPZD • algal bloom • water quality

Contents

1 Introduction **1**

2 Context **5**
2.1 Lake Titicaca . . . 5
2.1.1 Main physical characteristics . . . 6
2.1.2 Climate variability . . . 8
2.2 Anthropogenic impact on the Lake . . . 9
2.2.1 Algal bloom event of March - April 2015 . . . 9
2.2.2 The Katari watershed . . . 11
2.2.3 Contaminant sources . . . 12

3 Methods **13**
3.1 The hydrodynamic model . . . 13
3.1.1 The domain . . . 14
3.1.2 Hydrostatic pressure and Boussinesq approximation . . . 14
3.1.3 The three-dimensional hydrodynamic equations . . . 15
3.1.4 Boundary conditions . . . 16
3.1.5 Unstructured mesh . . . 17
3.1.6 Model Forcings . . . 20
3.1.7 Limitations concerning the hydrodynamic model . . . 22
3.2 The NPZD model . . . 24
3.2.1 Governing equations . . . 25
3.2.2 Initial conditions . . . 28
3.2.3 Model forcings . . . 29
3.2.4 Limitations concerning the NPZD model . . . 31

4 Results **33**
4.1 Water velocity . . . 33
4.2 Water temperatures . . . 35
4.3 Tracer . . . 38
4.4 NPZD components . . . 39
4.4.1 Nitrogen . . . 39
4.4.2 Phytoplankton . . . 40
4.4.3 Zooplankton . . . 42
4.4.4 Detritus . . . 43

5 Discussion **45**
5.1 The Physical model validation . . . 45
5.2 The NPZD model validation . . . 50
5.2.1 Vertical distribution of P in Lago Mayor . . . 50
5.2.2 Comparison with Landsat 8 image . . . 51
5.3 Limitations of our model . . . 54
5.4 Potential applications . . . 56

6 Conclusion **57**
6.1 Summary . . . 57
6.2 Elements of response to our main scientific question . . . 58
6.3 Future research suggestions . . . 59

Appendices **65**

A Land use (2010) **66**

B Horizontal water velocity (February 2014) **67**

C Monomictic property of the lake **68**

D Phytoplankton on the 15^{th} of August **69**

E Flood prone areas **70**

F Chlorophyll a (August 2011) **71**

List of Figures

2.1 Lake Titicaca and the neighboring cities. 5
2.2 Map of the TDPS system 7
2.3 Average climate variables for the year of 2018 8
2.4 Representation of the eutrophication process. Source: Scannone (2016) . . 9
2.5 A dead Telmatobius culeus is found on the lake bottom. 10
2.6 The Katari watershed and Lago Menor. 11

3.1 Three-dimentional domain for SLIM3D equations 14
3.2 Bathymetry construction procedure 18
3.3 3D mesh generated by SLIM. 19
3.4 Windrose for Lake Titicaca region. 20
3.5 Wind speeds for the Lake Titicaca region. 20
3.6 Mean surface temperatures on Lake Titicaca. 21
3.7 Typical evolution of temperatures over the lake following the diurnal cycle 21
3.8 Comparison between an adapted σ-level mesh and an adapted z-level mesh 23
3.9 Schematic NPZD model. 25
3.10 Nitrite and nitrate concentrations in Lake Titicaca 28
3.11 History of outflow of the Katari watershed. 30
3.12 Discharge and estimated nitrite input from the Katari river 31

4.1 Water horizontal velocity (m/s) for the 15^{th} of March 2015 34
4.2 Water horizontal velocity (m/s) in Lago Menor for the 15^{th} of March 2015 34
4.3 Annual evolution of the temperature profile. 35
4.4 Water temperatures for mid February 36
4.5 Water temperatures for mid August 37
4.6 Tracer dispersion during the year 2014. 38
4.7 Nitrogen based nutrients concentrations in Lake Titicaca 40
4.8 Phytoplankton concentrations in Lake Titicaca 41
4.9 Zooplankton concentrations in Lake Titicaca 42
4.10 Detritus concentrations in Lake Titicaca 43

5.1 Sampling stations of the CR.1407 cruise. 46
5.2 Temperature profiles over the 27 sampling points. 47
5.3 Annual evolution of the temperature profile in Lake Titicaca 48
5.4 Phytoplankton and zooplankton during vertical mixing. 49
5.5 Vertical algal biomass distribution 50
5.6 Vertical phytoplankton distribution between Isla del sol and Isla de la Luna. 51
5.7 Comparison between simulated phytoplankton and Landsat 8 image. . . . 52
5.8 NDVI and the Tenjo et al. (2014) chlorophyll a index in Lago Menor. . . . 54

A.1 Land use (2010) 66

B.1 Water horizontal velocity for the 15^{th} of February 2014. 67

C.1 Isotherms versus depth and time. 68
C.2 Dissolved oxygen concentrations at three depths in Lago Mayor 68

D.1 Phytoplankton on the 15^{th} of August 69

E.1 Flood prone areas. 70

F.1 Chlorophyll a (August 2011) 71

1 | Introduction

Nowadays, it is widely known that human activities can have considerable impact on the environment (IPCC, 2014). However, it is not always easy to quantify the impact of such activities, and it is even harder to consider all systemic variables that contribute to a given impact.

A good example of human impact on the environment can be seen in Lake Titicaca, the largest fresh water lake in South America, which is currently suffering from major degradation caused by anthropogenic activities. The algal bloom of 2015 serves as an example of the impact of such activities on the lake (Achá et al., 2018; Ap et al., 2017). This bloom, located in the south-eastern part of the lake (Lago Menor) was caused by eutrophic water conditions and resulted in high aquatic mortality. Not only the environmental impact is high but its social and economic consequences are even more important. It is clear that there is a lot at stake. Lake Titicaca and its interactions with its surroundings being a complex system, it is hard to understand the intrinsic forces that are at play. During and after the bloom, several questions arose: What is the extent of the the affected areas? What could have been done to prevent it? How to tackle the problem?

The use of models can help us answer these questions, by providing supportive information to decision makers. Indeed, by internalizing the complexity of the system, they can allow us to replicate real life behaviors. Not only can we do a retrospective analysis but we can also project ourselves in the future by performing predictive analytics. However, in the quest of hyperrealism, models can reach a high level of complexity, thus requiring tedious calibration of many parameters (for which in-situ data can be scarce). This makes their usage less accessible. Yet, for the models to have tangible impact, their usability needs to meet the expectations of the people who use them. Simpler models on the other hand, do not always cover all the complexity of the system but are easier to use and more accessible. The effect of the complexity of marine ecosystemic models on their effectiveness has been studied by Fulton et al. (2003). As the author well said: "Too much complexity leads to too much uncertainty and problems with interpretation of the model's dynamics and predictions, while too little detail results in models that cannot produce realistic behaviours". This highlights the importance and the need for simple models that can simulate as best as possible the environment that one chooses to study.

Our motivations for this thesis are of two types. Firstly, the environmental aspect regarding Lake Titicaca is a major concern. Indeed, the contamination of the lake is not limited to Lago Menor. Other shallow areas in the lake are subject to eutrophization. The Puno bay for instance, on the Peruvian side, is particularly affected (Lazzaro et al., 2016). The multiple cities surrounding the lake also take part in the overall water quality degradation due to uncontrolled waste water discharges. Furthermore, the contaminants are not always of the same nature, other types of contaminants can be found in the lake. Mercury pollution, for instance, linked to illegal mining activities in the mountains north of the lake, is affecting the fish and therefore the humans who feed on them (Gammons et al., 2006). On a larger scale, it is the whole lake that is suffering from different types of pollution originating in different parts of the lake. The multiple sources of contamination of Lake Titicaca show the vulnerability of the ecosystem. Consequently, it seems that prevention and on-going water quality management are of the utmost importance. People involved in the environmental management of the lake can benefit from tools as model to take informed decisions for the conservation of the lake.

Our second motivation is the research gap that we have identified. In fact, there are two main research gaps that we aim at filling with this thesis. First of all, we want to enlarge the scope of applications of the SLIM3D model. Even though there are several models that simulate lake hydrodynamics, in this thesis we will be using SLIM3D which is the 3D version of the Second-generation Louvain-la-Neuve Ice-Ocean Model (SLIM, https://www.slim-ocean.be/). What is interesting is that this model has not often been used for water quality analyses. Secondly, few hydrological models of Lake Titicaca have been made. One example is the mathematical model developed by Aguirre Céspedes (2009). For this study, the author used the Estuary and Lake Computer Model (ELCOM) of the University of Western Australia. Additionnaly, in spite of the availability of research regarding Lake Titicaca's ecosystem, hydrological models incorporating a ecosystemic component seem to be nonexistent for the lake. This represents a promising avenue for research, considering that there are multiple sources of data: independent studies on the one hand, and state research on the other. Indeed, in the efforts of safeguarding the lake and the people who depend on it, many independent studies have been made to asses the water quality in different parts of the lake. Moreover, research projects have been conducted as part of joint efforts combining Peruvian and Bolivian forces such as the scientific cruises gathering limnological and fishery resources data providing a larger coverage of the lake (Cruz et al. (2013);Cruz et al. (2014)). The research made in this area has provided sustainable knowledge concerning the quality of the marine habitat and the species that live in it.

Hydrological models can be very useful since they can simulate and predict the evolution of multiple parameters such as water temperatures, surface elevation and, current directions and intensities in a given water body. But in order to study water quality the best tool would be one that can combine the predictive power of a hydrological model with the complexity of marine ecosystems. Such a tool could enable us to analyze and forecast

the evolution of basic marine populations such as phytoplankton and zooplankton. This tool would also allow us to to simulate and predict the levels, distributions, and risks of chemical pollutants.

With this background in mind, we wanted to build a model that could help in the efforts of conserving the water quality and therefore the biodiversity of Lake Titicaca. Which leads us to our main question:

How to grasp the complexity of Lake Titicaca in a easy to use model that enables water quality analyses and facilitates informed decision making?

We chose to focus on the entire **Lake Titicaca** since our aim is to provide a tool that could be used both in the study of the lake as a whole and for particular applications in any part of it. What we consider a **easy to use model** is one that can be easily understood by any competent user, providing transparency on its internal workings (white box) and that does not require fastidious calibration or numerous inputs. **Water quality** in this thesis will be limited to the nitrogen based nutrients, phytoplankton, zooplankton and detritus concentrations in the lake. **Decision making** concerns mainly political decisions such as environmental policies, as well as other types of regulations regarding waste water discharges, chemical and biological pollution limitations or waste management. These regulations could have a positive impact for the conservation of the lake.

In order to answer our main question, we will present a new tool that can be used to study the water quality and that can help in the efforts of mitigating the impact of human activities on the environment. We will implement a coupled hydrodynamic and ecosystemic model of Lake Titicaca. The hydrodynamic component will be covered by SLIM3D. As for the ecosystemic component, it will be managed by coupling a NPZD (for Nitrogen-based nutrients, Phytoplankton, Zooplankton, and Detritus) ecosystem model to SLIM3D. Such a model enables the exploration of other relevant environmental questions such as the impact of climate change, or of environmental, agricultural or urban policies on the ecosystem.

To achieve this we will proceed as follows:

- Firstly, apply SLIM3D to the lake to simulate its three dimensional hydrodynamics over time and validate it with regards to in-situ observations.

- Secondly, develop, parametrize and validate a NPZD ecosystem-type model that will be coupled to SLIM3D in order to simulate the contamination in Lago Menor.

- Thirdly, use the coupled model to reproduce the algal bloom event of 2015 taking into account the input of nutrients in the the Cohana bay provided by the Katari river.

This combined hydrological-ecosystemic model could be used to study water quality in the efforts of safeguarding the lake and its ecosystem. Apart from providing a better understanding of the lake hydrodynamics, this model could serve in the environmental impact assessment and could support environmental management agencies to take the right decisions. With this new predictive tool we would be able to perform a series simulations showing water pollution under different pollution scenarios. Therefore this tool could be used in the decision making process regarding water treatment in the upstream watersheds.

This thesis will be structured as follows. We will start by giving the general context of the lake and presenting the 2015 algal bloom event that will serve as our case study in Chapter 2. We will then move on to the Chapter 3 in which we will describe the governing equations behind both the hydrodynamic and the ecosystemic models. We will follow by presenting and analyzing our results in Chapter 4. The validation for both models will then be developed in Chapter 5. Finally, we will conclude by answering our research question and by mentioning some possible applications of the model as well as our recommendations for future research in Chapter 6.

2 | Context

2.1 Lake Titicaca

Lake Titicaca is the largest freshwater lake in South America and the highest of the world's large lakes. It is believed that the name Titicaca derived from the Aymara language titi: wild cat and karka: rock. The legend tells that the Titis, that used to live on the rocky islands of the lake, used to swim from the islands to the mainland in search of food. Nowadays the titi cat or the Andean cat is the most endangered cat species in the Americas.

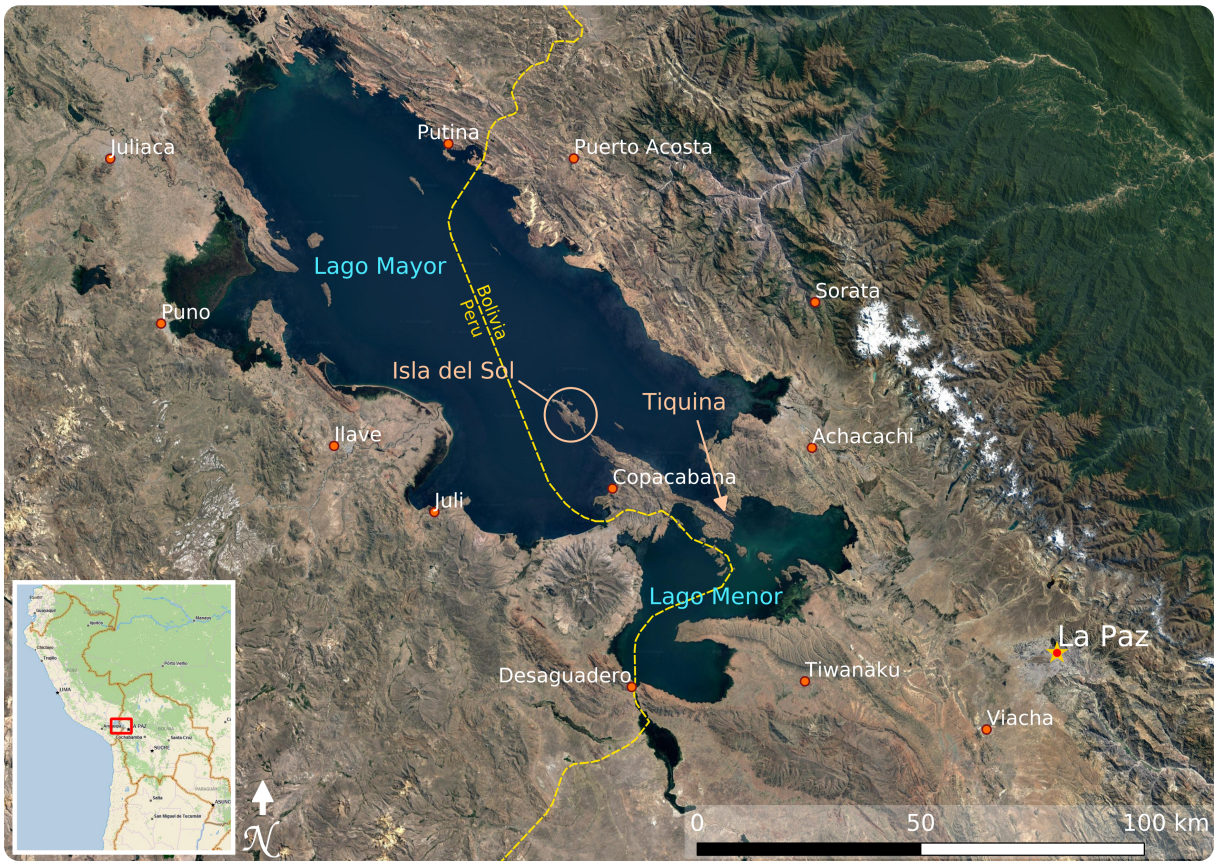

Figure 2.1: Lake Titicaca and the neighboring cities. The yellow border separates Peru on the left of Bolivia on the right. The city of La Paz is visible on the right side.

The lake is nested within the Altiplano, a high plateau region shared by Peru and Bolivia between the eastern and western Andes mountain range. Its formation dates back

approximately 1.8 million years to the Pleistocene - Pliocene transition. Since that time, a series of lakes of different sizes and shapes have succeeded one another following the glacier and inter-glacier periods to give us the lake we know today (Lavenu, 1991).

It is surrounded by multiple cities, which populations are mentioned in Table 2.1, that contribute to the degradation of the lakes water quality.

Country	City	Population
Peru	Juliaca	276,110 (2017)
	Puno	128,637 (2017)
	Ilave	30,000 (2017)
	Juli	21,462 (2014)
	Desaguadero	20,009 (2007)
Bolivia	El Alto	922,598 (2017)
	Viacha	38,457 (2012)
	Tiwanaku	11,309 (2001)
	Achacachi	9,575 (2018)
	Copacabana	3,000 (2010)

Table 2.1: Main cities surounding Lake Titicaca and their populations.

Throughout the years, this land has witnessed the passing of many ancient civilizations. After the Aymaras, the Collas and the Incas, today one can find direct descendants of the Aymaras, the Quechuas, the Urus and other ethnicities.

The high plateau is one of the poorest regions in both Peru and Bolivia. The lake is an important asset for many communities in both countries. Being a natural wonder, it stimulates tourism and sustains economical stability. This intimate link between the lake and the people living around it has been present since the first populations settled in the area. With this in mind, one can understand how crucial the well-being of the lake is for the population to thrive. Yet, paradoxically, today the main cause behind the ecological crisis seems to be human activity.

2.1.1 Main physical characteristics

Lake Titicaca spans on a surface area of 8,372 km^2 and is situated at 3,812 m above sea level. It's geographic extent is between latitudes -16.65 to -15.20 and longitudes -70.10 to -68.50. The southern lake basin, known as Lago Menor or Lago Huinaymarca, is connected to the larger basin, known as the Lago Mayor or Lago Chucuito, by a 800 m wide waterway near the village of Tiquina. Lago Mayor represents 83.4% of the total surface with an average depth of 107m and a maximum depth of 281m, wheras Lago Menor represents 16.6% of the surface averaging a depth of 9m and a max depth of 42m (Dejoux et al., 2013). The main inputs of water to the lake are: rainwater (55%), inflow by rivers (44%) and groundwater inflows (1%). The main outputs are evaporation (95%), output through the desaguadero river (5%) and drainage, other losses are negligible (Martinez Gonzales et al., 2007). Lake Titicaca is part of a larger watershed system: the TDPS system, short for Titicaca-Desaguadero-Poopó-Salar de Coipasa (see Fig. 2.2). This watershed is an endorheic system which means that there is no water output towards the sea. It sustains a global southward water flow from Lake Titicaca

towards Lake Poopó and the Coipasa salar. Lake Titicaca is a monomictic lake meaning that the mixing of the waters between the top and bottom of the lake only occurs during one seasonal period. During the rest of the year, thermal stratification of the water layers is present. This restricts the vertical movement of surface waters towards the depth or deep waters towards the top. Water temperatures usually vary between 14 and 10 degrees Celsius with a thermocline at about 40m depth. This thermocline is the limit where an abrupt change in temperature occurs between hotter waters on top and cooler waters bellow. The thermocline disappears during the dry season, when atmospheric temperatures are cooler, thus, allowing vertical mixing to occur throughout the water column.

Figure 2.2: Map of the TDPS system. Source: *The United Nations World Water Development Report* (WWDR, 2003)

Having such specific physical and morphological characteristics, Lake Titicaca is home to more than 530 aquatic species of which at least 64 are considered endemic (Kroll et al., 2012). The lake was designated as a Ramsar Site on August 26, 1998 –Ramsar being an intergovernmental environmental treaty established in 1971 by UNESCO– for the aquatic diversity that it houses. Indeed, as an example, the majority of the 45 recognized species of this Orestias are found in Lake Titicaca and 23 of these species are endemic. This genus is composed of fish that are restricted to freshwater habitats in the Andes at an altitude of 2,800m to 4,600m. However, some new species have been introduced to Lake Titicaca in order to develop commercial fishery. In 1939, several trout species were introduced. Pejerrey (*Odontesthes bonariensis*) was introduced in Lake Poopoo in 1946 and made its way to Lake Titicaca by 1955-56. These new species have threatened the local fauna and have been responsible for the loss of two Orestias species: *O. cuvieri* and *O. pentlandii* (Ibáñez Luna et al., 2014). It goes without saying that Lake Titicaca, due to its specificity is home to an important variety of fauna and flora. Some species can be found nowhere else on earth. Therefore, it is crucial to protect this rich yet fragile biodiversity.

2.1.2 Climate variability

The Lake's climatology is regulated by three main factors: the geographic and astronomic position, the relief and the atmospheric circulation (Martinez Gonzales et al., 2007). Firstly, the lake being between -15.2 and -16.6 degree's latitude, it is subject to fairly perpendicular solar rays during the entire year. Therefore only two seasons govern in this region: the dry and the rainy season, the latter extending from late September to May. Secondly, being on a high plateau nested within the Andes mountain range, the region is prone to a cold climate. Furthermore, due to the low air density in altitude, solar radiations are stronger on the surface leading to an average horizontal irradiation values of 2563 kWh/m^2. Lastly, the known atmospheric circulation on a global and local scale impacts the seasonal changes in air temperatures, wind speeds and direction and precipitations. The El Niño and La Niña phenomenons can also affect the climate in this region. Average climate data for the year of 2018 are shown in Fig. 2.3. This figure show the annual evolution of temperatures, relative humidity, cloud cover, precipitations, wind speeds and directions. The data was measured on the "Isla del Sol" island near the center of the lake (see Fig. 2.1) during the year 2018.

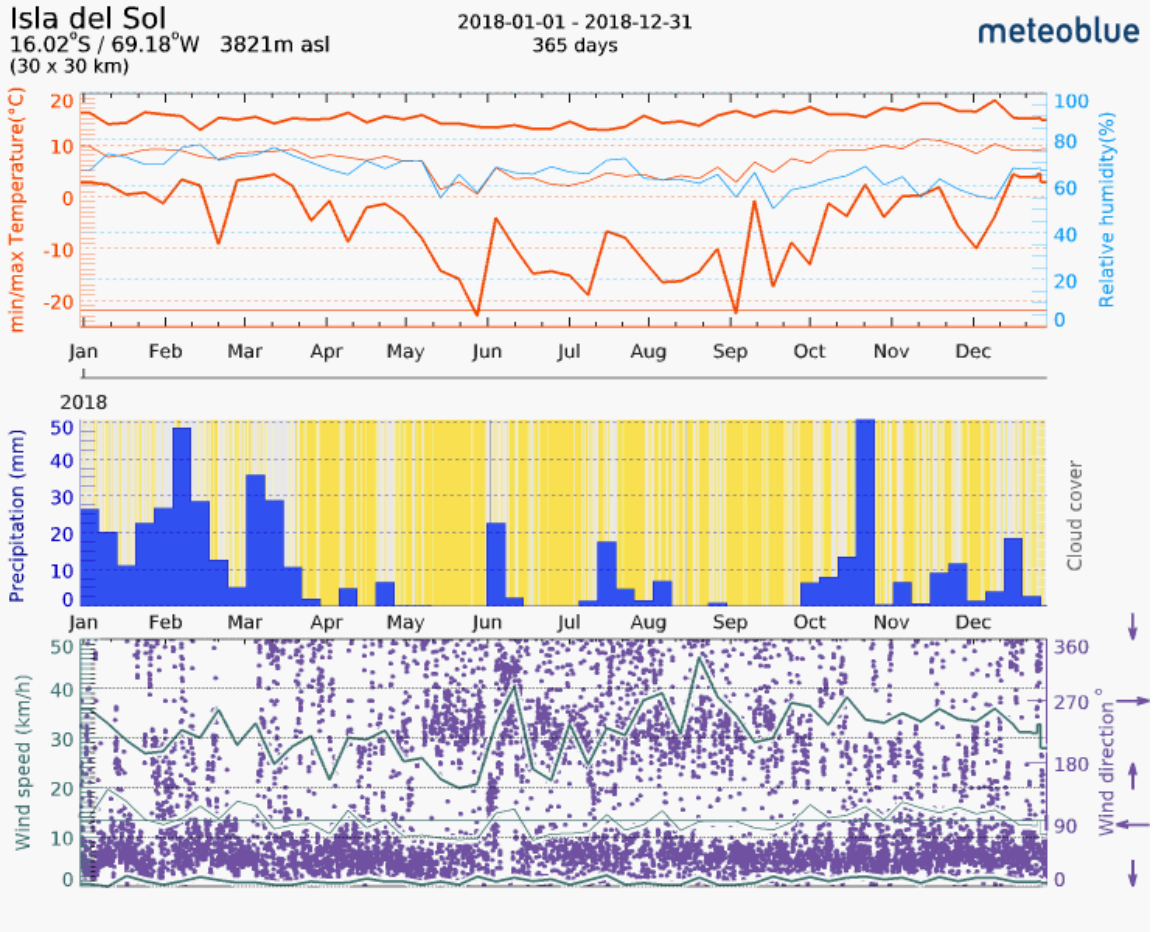

Figure 2.3: Average climate variables for the year of 2018. We can see that the dry season spreads from May to october. Source: meteoblue (2019)

At first glance we can see that the temperature evolution as well as the precipitations show a distinct pattern during the dry season (spanning from May to October) and the rainy season. We can also see that the wind blows predominantly towards the South-West but also towards the North-East during the dry season. As we will see further on, the climate has multiple effects on the lake, it is responsible for introducing a seasonality in the water temperatures and has a significant impact on the water currents.

2.2 Anthropogenic impact on the Lake

With the goal of providing an example of the potential uses of our coupled SLIM3D-NPZD model for lake environments, we worked on a case study in which we study the impact of anthropogenic contamination on the lake. This study mainly focuses on the Cohana bay in Lago Menor and the upstream Katari watershed. Even though this portion of the lake has been subject to algal bloom events in the past years, we will focus on the algal bloom of April-March 2015.

2.2.1 Algal bloom event of March - April 2015

Algal bloom events are known to occur in many lakes across the globe. They are usually due to increased nitrogen and phosphate availability. Both are the result of anthropic activities such as intensive agriculture and waste water discharge. This input of nutrients into the lake can lead to eutrophic conditions in which the proliferation of algae can be observed. Fig. 2.4 shows a schematic representation of this eutrophication process.

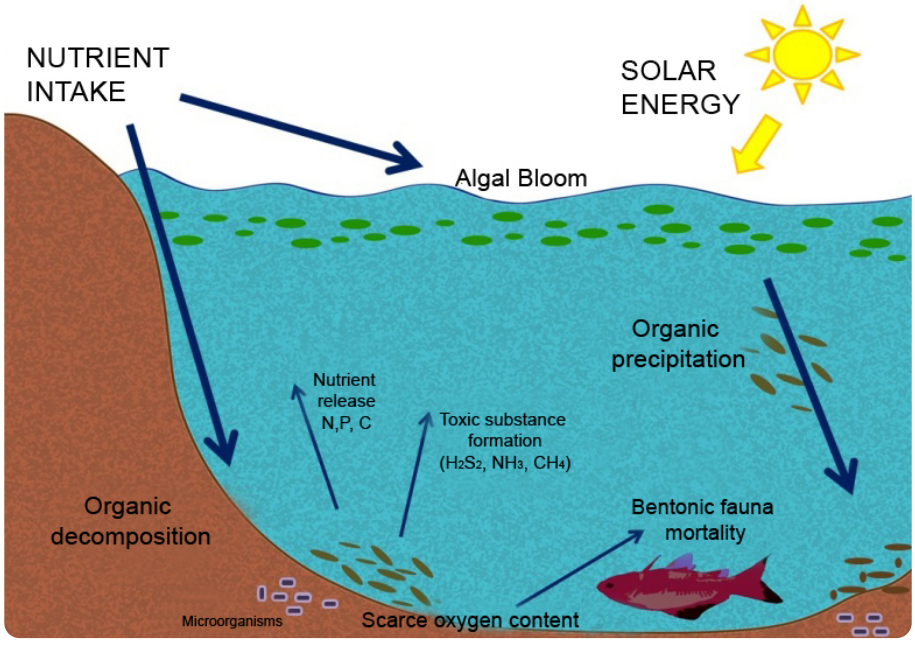

Figure 2.4: Representation of the eutrophication process. Source: Scannone (2016)

The additional nutrients provided to an aquatic environment benefits the phytoplankton population which increases in number. The multiplication of such algae near the water surface creates an opaque layer that limits light penetration through water. The zooplankton that feeds on phytoplankton are able to thrive. However, the lack of sunlight leads to the death of plants living on the bottom of the lake. The microbial decomposition of these plants, and eventually of the dead algae that precipitates, severely depletes the dissolved oxygen present in these waters. This process leads to hypoxic or anoxic dead zones in which marine life is unable to survive.

In March-April 2015, at the end of the rainy season, Lake Titicaca was subject to its first documented massive algal bloom in Lago Menor. The main algae involved was *Carteria sp.*, representing nearly 100% of the algae in the top 10 cm of the water surface (Achá et al., 2018). More than 50% of the lake surface was affected, resulting in more than two tons of aquatic biota death (Pérez, 2015) and, thus, affecting the ecosystem as a whole.

Figure 2.5: A dead Telmatobius culeus is found on the lake bottom.

Among the victims, the already critically endangered and iconic *Telmatobius culeus*, commonly known as the Titicaca water frog was particularly affected. This frog is one of the lake's most important predators. It lives in oxygen-rich waters on the lake's bottom and breaths through its skin. In April 2015 thousands of frogs were found dead on the Bolivian shores. The algal bloom induced a drop in oxygen levels due to algal uptake this in turn led to the death of animals of different species. Since then, conservation efforts have been made. An example is the Bolivian Amphibian Initiative, led by Arturo Muñoz, that launched an emergency project, which included both in situ and ex situ conservation measures. The algal bloom and the ecological collapse related to it raised consciousness among the local population and made it to worldwide news titles. The bloom was likely caused by significant nutrient input from the Katari river which can be explained by upstream anthropogenic activities in the Katari watershed (Achá et al., 2018; Ap et al., 2017).

2.2.2 The Katari watershed

To have a better understanding of the scope of the problem addressed in this thesis, we will focus on the Katari watershed and its components (see Fig. 2.6). The total area of this subcatchment is of about 2022 km^2. It encompasses the city of El Alto (9.22×10^5 inhabitants in 2018 according to the Bolivian national institute of statistics: INE) which borders La Paz. The watershed contains four major rivers of interest: the Katari, Seco, Seke and Pallina rivers. Water flows from its source up in the Cordillera Real and flows towards Lake Miluni north of El Alto. Then, two branches are formed: the Seke and Seco rivers that flow through El Alto. These two then join to the Paillina river, which, has its source further south-east of the catchment and passes through the city of Viacha (8.81×10^4 habitants). The Pallina river continues its flow north-west and joins the Katari river which passes through agricultural (17.88 km^2) and breeding areas (410.72 km^2). The river finally discharges into Lago Menor through the Cohana Bay (Ap et al., 2017). The junction between the Katari river and the Cohana bay is a flood prone area (see Appendix E), which forms a delta with a shape that evolves in time.

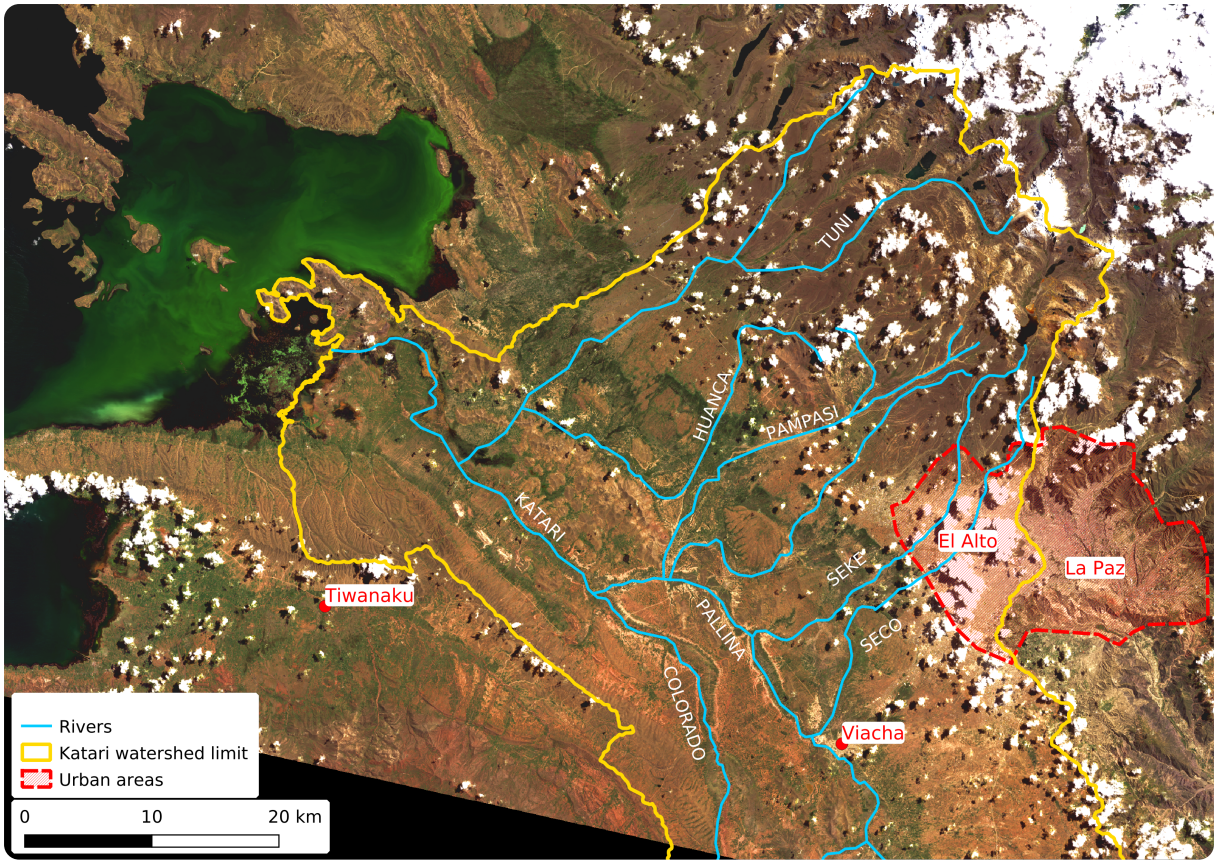

Figure 2.6: The Katari watershed and Lago Menor. The background image is a Landsat 8 image taken on the 24^{th} of March 2014 in which we can appreciate the extent of the algal bloom located in Lago Menor (left side of the image). On the right side, we can see the twin cities of La Paz and El Alto separated by the watershed limit (in yellow). The seco and Seke river pass through El Alto and follow their path towards the Katari river which leads to Lago Menor. The Andes mountain range appears in the upper right corner drawing the watershed limit.

2.2.3 Contaminant sources

The water and soil contamination of the Katari watershed is due to three major sources: the mining activities upstream in the mountains north of the city of El Alto, the urban discharges of El Alto and, the impact of agriculture on the lands downstream.

Starting from the slopes of the snow-capped mountain Huayna Potosí, where the Seco and Seke rivers begin, contamination is present. Indeed, the presence of heavy metals show the impact of past and present mining activities (Ap et al., 2017). This has considerable effect on the water quality as mining residues cause acidification of the water therefore favoring the enrichment in harmful elements such as Cd, Zn, As, Cu,Ni,Pb and Sn (Salvarredy-Aranguren et al., 2008).

Both Seco and Seke rivers make their way through rapidly expanding urban areas of the city of El Alto. Here, they suffer from waste water discharges, and uncontrolled domestic and industrial discharges (Ap et al., 2017; Chudnoff, 2009). Contaminants make their way to the Pallina river and then to the Katari river, where soils and vegetation are affected. The waste water treatment plant of Puchucollo located south-west of the city started its activities in 2010 and was said to manage the removal of 80% of pollutants (in 2016), although it was designed back in 1989 for a capacity of 4.0×10^5 habitants (Molina et al., 2017). Yet, as of 2019, the population of El Alto has an estimated population of 9.3×10^5 habitants (INE: bolivian national institute of statistics). This increase in population brings an increase in water contamination since no major progress has been made regarding waste management. Downstream, abnormal concentations of As, NO_3, Cl^- and SO_4^{2-} were found in village wells close to the Katari river (Lima et al., 2019). Additionally, it has been found that the Katari basin is widely contaminated with antibiotics such as sulfamethoxazole as well as the most common human sulfamethoxazole transformation products (Duwig et al., 2014).

The third source of contamination is agriculture, specifically within the last section of the Katari river, starting from the intersection between the Colorado and the Pallina rivers. This area is predominantly pasture-land, the cattle that feeds on these lands contributes to the increase of total nitrogen in the river and therefore in the Cohana bay. The spread of agricultural surface back in 2010 is shown in the land use map provided in Appendix A for the Titicaca subcatchment.

These contaminated waters are harmful for both the fauna and flora of the Katari watershed and Lago Menor. Since the local populations use this water for drinking and cooking, they are highly exposed to diseases linked to poor water quality (Ap et al., 2017). The consumption of contaminated fish, for instance due to mercury intake, might induce public health problems (Gammons et al., 2006; Guedron et al., 2017; Monroy et al., 2014).

3 | Methods

In this section we will describe both the SLIM3D and the NPZD type models. For both models we will describe the main governing equations as well as their inputs data and the pre-processing manipulations.

3.1 The hydrodynamic model

The physical variables and their respective symbols used for the hydrodynamic model are presented in Table 3.1.

Symbol	Definition	Unit
u	Horizontal velocity vector	m s^{-1}
w	Vertical velocity	m s^{-1}
η	Free surface elevation	m
T	Temperature	°C
p	Hydrostatic pressure	N m^{-2}
ρ	Water density	kg m^{-3}
ρ_0	Reference water density	kg m^{-3}
ρ'	Water density deviation	kg m^{-3}
f	Coriolis parameter	s^{-1}
g	Gravitational acceleration	ms^{-2}
ν	Vertical viscosity	m^2s^{-1}
ν_h	Horizontal viscosity	m^2s^{-1}
κ	Vertical diffusivity	m^2s^{-1}
κ_h	Horizontal diffusivity	m^2s^{-1}
x, y	Horizontal Eulerian coordinates	
z	Vertical Eulerian coordinate	
e_z	Vertical unit vector (pointing upward)	
∇_h	Horizontal derivative operator	
$\wedge$	Vector product	

Table 3.1: Symbols and physical variables for Hydrodynamic model

The Second-generation Louvain-la-Neuve Ice-Ocean Model (SLIM, https://www.slim-ocean.be/) is a hydrodynamic model that uses the finite element method and unstructured meshes to simulate flows as well as dynamics of various tracers such as temperature, salinity, density or any chemical or biological compound. For the task at hand, the 3D version of the model (SLIM3D) was applied to Lake Titicaca lake which allowed us to take into account the vertical dimension of flow. SLIM3D solves the three-dimensional hydrostatic

equations under the Boussinesq approximation on each element of a tri-dimensional mesh made of tetrahedra.

SLIM and its different variants have been used in numerous hydrological studies,teh most relevant works oncerning our study are that of Delandmeter et al. (2018) which used SLIM3D on lake Tanganyka and Naithani et al. (2007) who studied nutrients and plankton dynamics for the same lake.

We will start this section with an overview of the governing equations of this model, for this purpouse, we relied on Vallaeys et al. (2018). For a detailed explanation concerning these equations, numerous papers exist and are available on the slim website. The procedure to generate unstructured meshes will be presented in section 3.1.5.

3.1.1 The domain

SLIM3D solves the hydrodynamic Boussinesq equations on a three-dimentional domain Ω delimited by its fixed lateral Γ_l and bottom Γ_b boundaries and by its moving top surface Γ_s boundary. Vertical coordinates can thus vary between the free surface elevation $z = \eta$, which changes in time, and the bottom boundary $z = -h$, which is defined by the bathymetry.

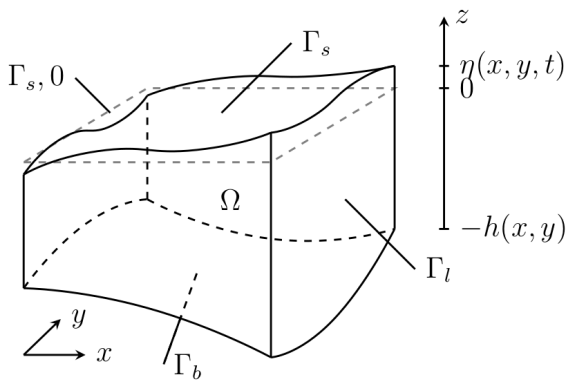

Figure 3.1: Three-dimentional domain for SLIM3D equations

The 3D domain Ω defined by the fixed lateral Γ_l, bottom Γ_b and the free surface Γ_s boundaries. The reference surface boundary $\Gamma_{s,0}$ is located at $\eta = 0$. Credits: P. Delandmeter

3.1.2 Hydrostatic pressure and Boussinesq approximation

For a hydrostatic equilibrium, the Navier-Stokes vertical momentum equation reduces to:

$$\frac{\partial p}{\partial z} = -\rho g \tag{3.1}$$

With $p(t, x, y, z)$ the pressure, g the gravitational acceleration, and $\rho(t, x, y, z)$ the density. This means that the pressure vertical gradient is equal to the weight of the water mass lying above. Integrating from z to η, yields:

$$\begin{aligned} p &= p_a + \int_z^\eta \rho g dz \\ &= p_a + g\rho_0(\eta - z) + g\int_z^\eta (\rho - \rho_0)\, dz \end{aligned} \tag{3.2}$$

In our model, water is assumed to be incompressible. Following the Boussinesq approximation, we assume that the variations of density are small enough to be neglected in the flow field. However, we will take density into consideration in the buoyancy forces found in Eq. (3.4)

3.1.3 The three-dimensional hydrodynamic equations

In the following three-dimensional equations the main unknowns are the horizontal velocity vector $\boldsymbol{u}(t,x,y,z)$, the vertical velocity $w(t,x,y,z)$, the free surface elevation $\eta(t,x,y)$ and the temperature $T(t,x,y,z)$. The density is computed by means of the state equation $\rho = \hat{\rho}(T)$ of Jackett et al. (2006) depending on the temperature.

Pressure:

$$\frac{1}{\rho_0}\nabla_h p = \frac{1}{\rho_0}\nabla_h p_a + g\nabla_h \eta + \frac{g}{\rho_0}\nabla_h \int_z^\eta (\rho - \rho_0)\, dz \tag{3.3}$$

Resulting from the hydrostatic hypothesis. With ∇_h the horizontal gradient operator, $p(t,x,y,z)$ the pressure and $\rho(t,x,y,z)$ the density.

Momentum:

$$\begin{aligned} \frac{\partial u}{\partial t} + \nabla_h \cdot (uu) + \frac{\partial (wu)}{\partial z} &= \nabla_h \cdot (\nu_h \nabla_h u) + \frac{\partial}{\partial z}\left(\nu \frac{\partial u}{\partial z}\right) \\ &\quad - f\boldsymbol{e}_z \wedge u - g\nabla_h \eta \\ &\quad - \frac{g}{\rho_0}\nabla_h \int_z^\eta \rho' dz - \frac{1}{\rho_0}\nabla_h p_a \end{aligned} \tag{3.4}$$

With f the Coriolis factor, $\boldsymbol{e}_z$ is vertical unit vector, $\nu_h(t,x,y,z)$ and $\nu(t,x,y,z)$ the horizontal and vertical viscosities. The symmetric part of the viscosity operator $\left(\nu_h \nabla_h u^T\right)$ is not taken into account in SLIM for the sake of simplicity.

Continuity:

$$\nabla_\mathrm{h} \cdot \boldsymbol{u} + \frac{\partial w}{\partial z} = 0 \tag{3.5}$$

Representing the conservation of mass under the incompressibility assumption.

Temperature:

$$\frac{\partial T}{\partial t} + \nabla_\mathrm{h} \cdot (\boldsymbol{u}T) + \frac{\partial (wT)}{\partial z} = \nabla_\mathrm{h} \cdot (\kappa_\mathrm{h} \nabla_\mathrm{h} T) + \frac{\partial}{\partial z}\left(\kappa \frac{\partial T}{\partial z}\right) + f_\mathrm{relax} \tag{3.6}$$

The temperature T evolution depends on the gain and loss of temperatures due to exchanges both horizontally and vertically with neighboring elements it is computed as an advection-diffusion equation with $\kappa_h(t, x, y, z)$ and $\kappa(t, x, y, z)$ the horizontal and vertical diffusivity, respectively. A temperature relaxation term f_{relax} is added to this equation in order to parameterize the surface heat flux due to the surface temperature forcing on the top layers of the lake:

$$f_{\text{relax}} = \frac{\max(z_{\text{r}} + z, 0)}{z_{\text{r}}\tau_{\text{r}}} (T_{\text{surface}} - T) \tag{3.7}$$

With $z_{\text{r}} = 12$ m the depth of the relaxation zone (affected surface layers) and $\tau_{\text{r}} = 5$ days the relaxation time. We can see that the closer the waters are to the surface, the more they are subject to the temperature forcing. The intensity of the forcing is diminished with depth in a linear manner, until the maximum depth of the relaxation zone z_{r}. Underneath this depth, the forcing is not directly applied.

3.1.4 Boundary conditions

In our model, the lateral boundaries are closed and thus impermeable as a consequence, the normal flow velocity vanishes on the boundary:

$$\boldsymbol{u} \cdot \boldsymbol{n}_h = 0 \tag{3.8}$$

With n_h the horizontal vector normal to the lateral boundary Γ_l, horizontal velocities heading outside of the domain are thus forbidden. Regarding the top and bottom surfaces, the impermeability conditions are computed as follows:

$$w - \frac{\partial \eta}{\partial t} - \boldsymbol{u} \cdot \nabla_h \eta = 0 \quad \mathbf{x} \in \Gamma_s \tag{3.9}$$

$$w + \boldsymbol{u} \cdot \nabla_h h = 0 \quad \mathbf{x} \in \Gamma_b \tag{3.10}$$

Similarly to the lateral boundary, these conditions restrict the water flow within the defined vertical borders. Lastly the wind stress and bottom friction imply additional boundary conditions:

$$\nu \frac{\partial \boldsymbol{u}}{\partial z} = \frac{\boldsymbol{\tau_s}}{\rho_0}, \quad x \in \Gamma_s \tag{3.11}$$

$$\nu \frac{\partial \boldsymbol{u}}{\partial z} = \frac{\boldsymbol{\tau_b}}{\rho_0}, \quad x \in \Gamma_b \tag{3.12}$$

Where $\boldsymbol{\tau_s}(t, x, y)$ is the wind stress and $\boldsymbol{\tau_b}(t, x, y)$ the bottom friction.

3.1.5 Unstructured mesh

Following the finite elements method, the objective of the meshing phase is to build a 3D mesh that divides the domain into multiple elements of smaller sizes. Our hydrological model solves the above-mentioned governing equations for every element of the system, so the more elements, the greater the resolution. If the domain is too large, or the spatial resolution too great, the computational workload can be constraining. For most application there is no need for a finely resolved mesh on the entire domain, we usually focus on local phenomena. This is precisely why we chose to work with a non-uniform mesh resolution. This way, we can chose to refine our mesh for the area of interest: Lago Menor, allocating resources where they matter.

The first step in building an unstructured mesh is to determine the system boundaries. Our three-dimensional mesh is defined horizontally by the perimeter of the lake and vertically by its bathymetry. The lake perimeter varies from one year to another given that some parts of the lake are relatively shallow and are affected by inter-annual surface elevation variations (Ronchail et al., 2014). To implement this boundary, a shape-file of the 2013 lake perimeter, elaborated by the french Research Institute for Development (IRD) in Bolivia was used. In the vertical direction, a simple tiff file of the bathymetry can be fed to SLIM3D to fix the bottom limit of the domain. In practice, we had to face the difficulties of obtaining such a file. Somme punctual bathymetry measures gathered during the Cruz et al. (2014) cruise (see Fig. 3.2a) where found on the geoportal of the Autonomous Binational Authority of Lake Titicaca (ALT) website (*http://geotiticaca.org/web/*). After adding some points with values of zero on the contour of the lake we where able to build a realistic bathymetry by performing a inverse distance squared weighting interpolation (see Fig. 3.2b). For homogenization purposes, SLIM uses a smoothed bathymetry based on the provided bathymetry file (see Fig. 3.2c).

Once the boundaries where clearly defined, we started by generating a 2D mesh. This process is achieved by introducing a set of rules that dictate where the resolution of the mesh should be greater. Through this process, we decided to create a mesh that provides high resolution for regions of smaller depth and/or close to the coastline where currents tend to be most important. Additionally, a greater resolution was allocated for Lago Menor for our case study.

The 3D mesh was then established by extruding the preliminary 2D mesh towards the depth (see Figs. 3.3b and 3.3c). For this purpose we used the z-level method, which consists in creating horizontal levels at given depths. Higher resolution was allocated closer to the top of the lake in order to better capture the surface dynamics. Additionally, since the Cohana bay is relatively shallow, the top 5m were further refined by establishing a 1m-resolution layer. The final Model used a mesh composed of 28,017 triangles extruded over 15 layers which generated a total of approximately 209,680 tetrahedral elements. The horizontal layers correspond to the following depth in meters 0,1,2,3,4,5,10,15,25,35,50,80,110,140,200 and 240.

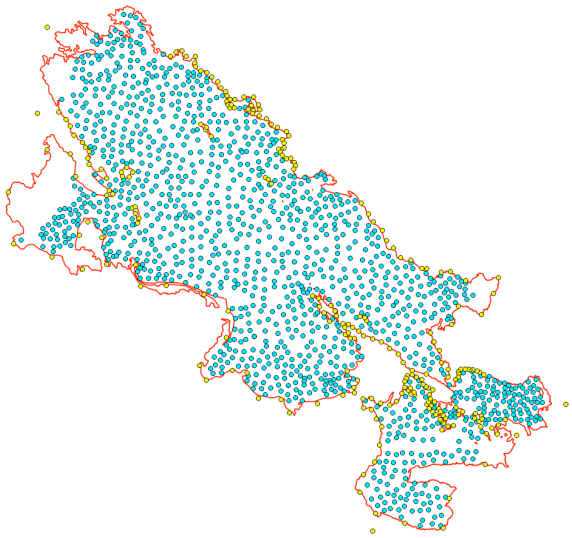

(a) Original data points are in cyan, added points in yellow.

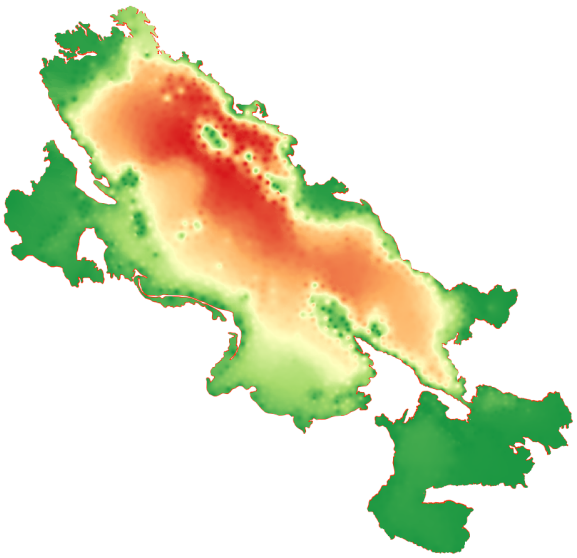

(b) Raw interpolation

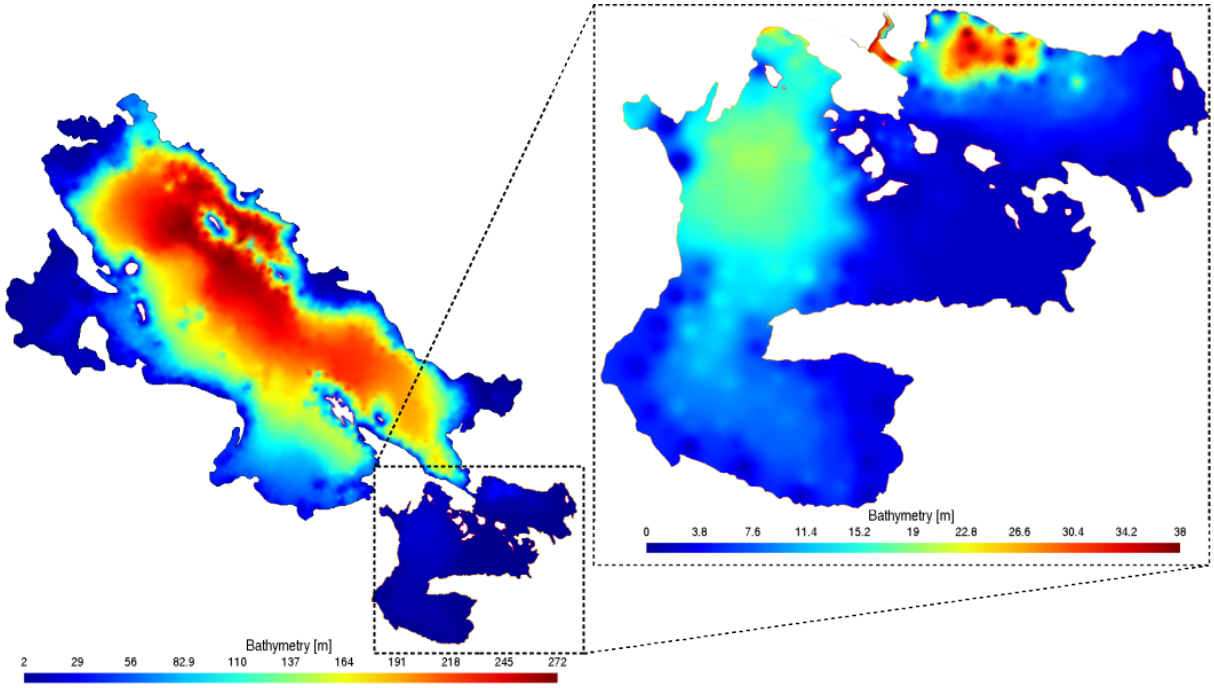

(c) Bathymetry generated by the model.

Figure 3.2: Bathymetry construction procedure from the field measurements (a), their interpolation to the entire lake (b) and the final bathymetry computed on the model mesh (c).

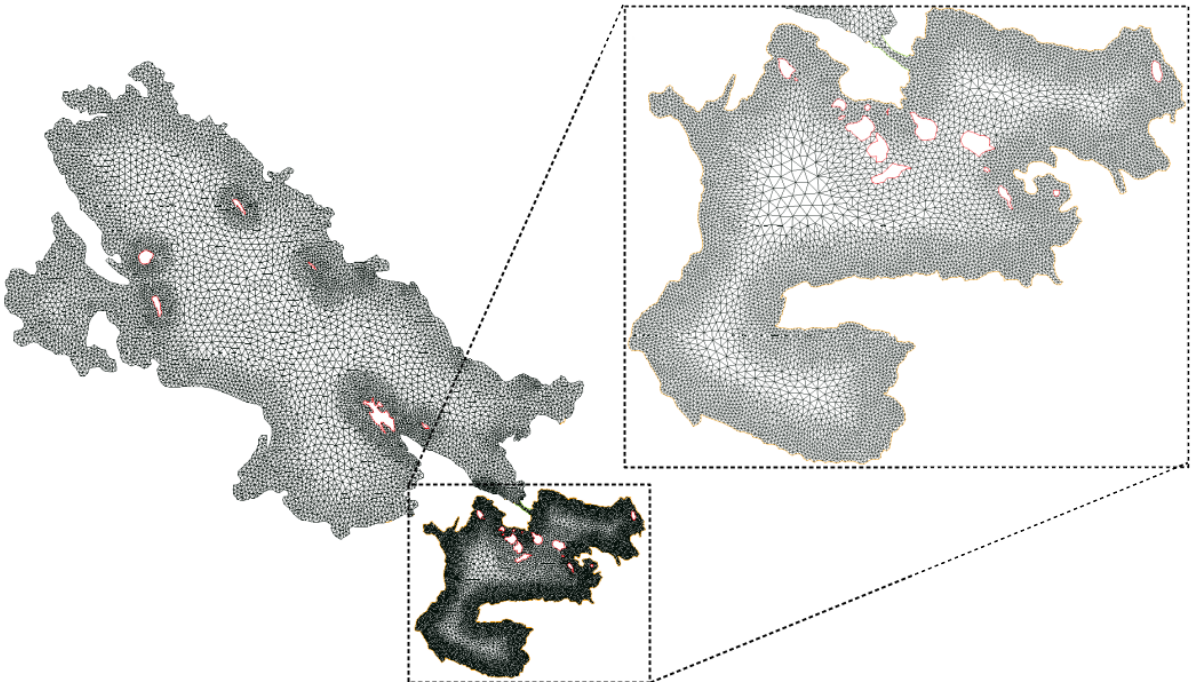

(a) The horizontal mesh is composed of 28,017 triangular elements.

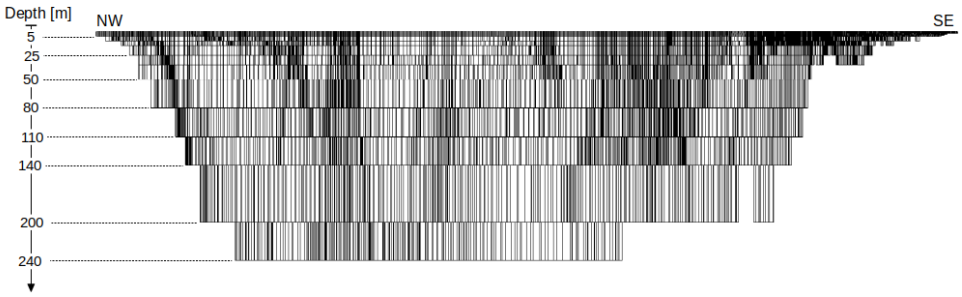

(b) Over the vertical, the horizontal mesh is extruded into up to 15 layers.

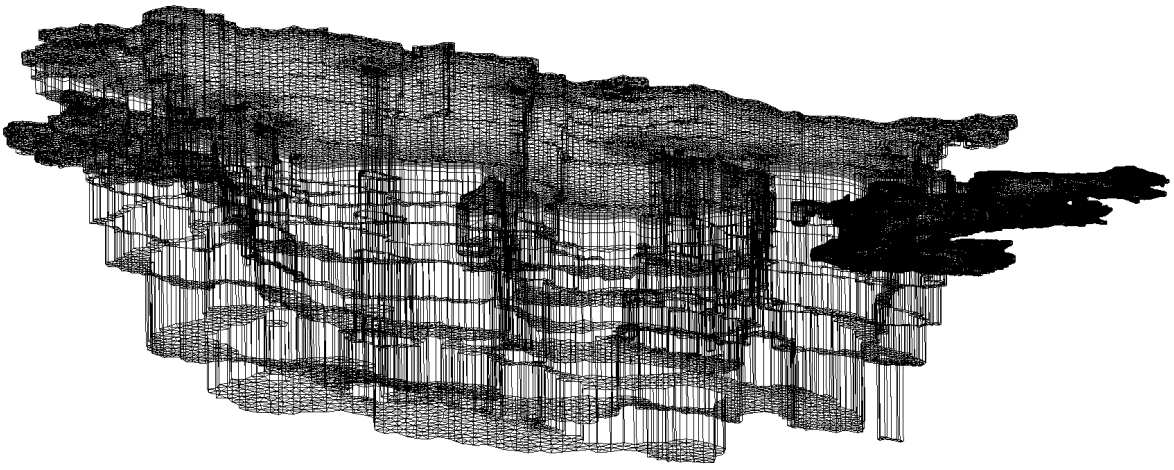

(c) The 3D mesh is finally composed of approximately 209,680 tetrahedral elements.

Figure 3.3: 3D mesh generated by SLIM.

3.1.6 Model Forcings

These forcing are external forces that are applied to the system and that drive the water movements. Surface currents are generated largely by wind but other factors contribute such as the Coriolis forces due to Earth's rotation or the density differences in water masses caused by temperature and salinity variations. Lake Titicaca being a fresh water lake (salinity in general less than 1 g/l (Martinez Gonzales et al., 2007)), the haline effect on circulation has a low impact therefore we chose to neglect it for our study. The major forcings we took into account were: wind and surface temperatures.

Wind forcing

Wind affects the system by introducing surface shear stress, a horizontal force on the water surface which triggers movement. Due to the viscosity, the underlying water layers are affected as well. The intensity and irregularity of wind generates turbulence within the surface layers which tends to create vertical eddies that lead to water mixing. On a larger scale surface waters are dragged by winds, this creates circulation within the lake.

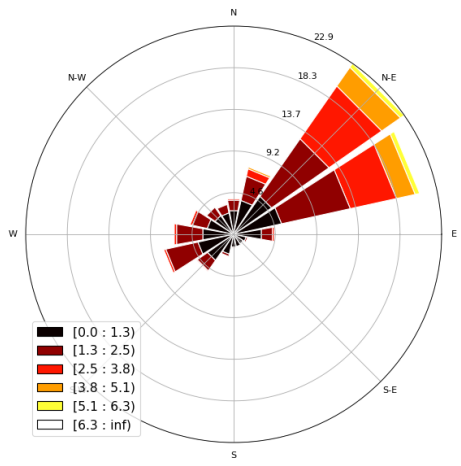

Figure 3.4: Windrose for Lake Titicaca region.

The wind data used for this purpose was that of the Climate Forecast System (CFS) provided by the National Oceanic and Atmospheric Administration (NOAA). This is a modeled hourly time series of the u and v components of wind (in m/s) at 10m over land with a horizontal resolution down to one-half of a degree (approximately 56 km). This data was interpolated in order to create a better spatial resolution for the model. For the area of interest, the wind mainly blows down from the Andes mountains in the north-east towards the south-west (Fig. 3.4). Wind speeds vary diurnally between 0 and 4 m/s with an estimated annual mean of 1.5 m/s (Fig. 3.5). We can appreciate an increase in the maximum wind intensities during the rainy season.

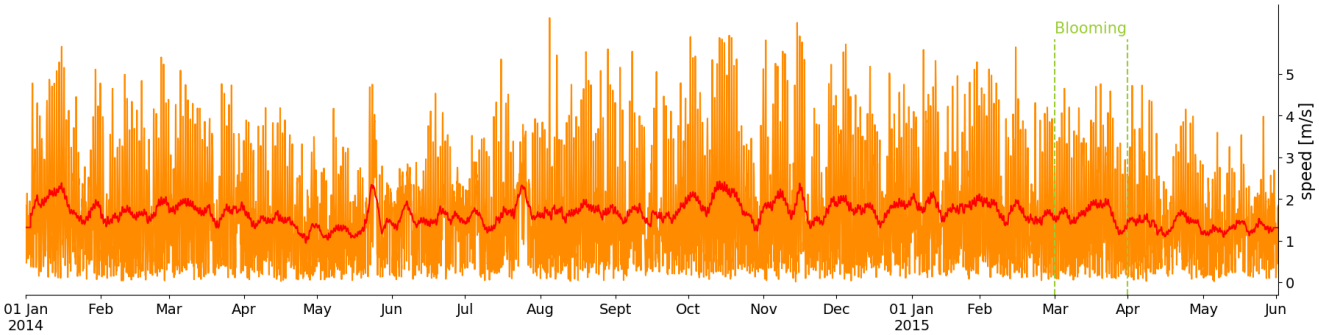

Figure 3.5: Wind speeds (m/s) for the Lake Titicaca region.

Surface temperatures forcing

This second forcing acts on a minor scale compared to wind stress. The impact of surface temperatures on the water flow is explained by the variations induced on the water density. As the sun radiates on the surface of the lake, the latter tends to warm and thus to induce warming of the deeper water layers through vertical mixing. In comparison to the wind effect of creating mixing of the vertical layers, the heating of the surface waters tends to strengthen the stability of the epilimnion due to density differences and thus increasing stratification. Fig. 3.6 shows the annual cycle of the mean skin temperatures - defined as the temperature of the surface at radiative equilibrium - over the lake, we can see that for the year 2014 a minima is reached during the dry season and higher values are present during the rainy season.

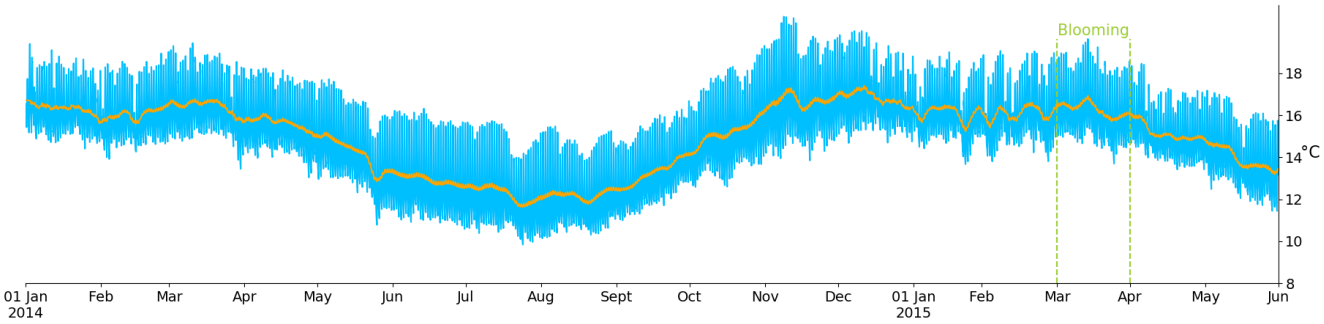

Figure 3.6: Mean surface temperatures (°C) on Lake Titicaca.

The data used for the temperature forcing term was extracted from the ERA5 climate reanalysis dataset provided by the Copernicus Climate Change Service (C3S). This dataset consists of hourly skin temperature with a spatial resolution is of 0.25 degrees (approximately 27 km). ERA5 provided the necessary data for our region of interest with a dozen data points over the lake. Moreover, ERA5 provided water surface temperatures in addition to land surface, taking into account water bodies when computing global skin temperatures.

Surface temperatures evolve following the diurnal and the annual cycle, in Fig. 3.7 we can appreciate a typical diurnal evolution of surface temperatures as well as the thermal inertia of the lake. First of, we can see that the water temperatures are slightly different than the land temperatures. During the night atmospheric temperatures tend to fall bellow the 10°C line, in response

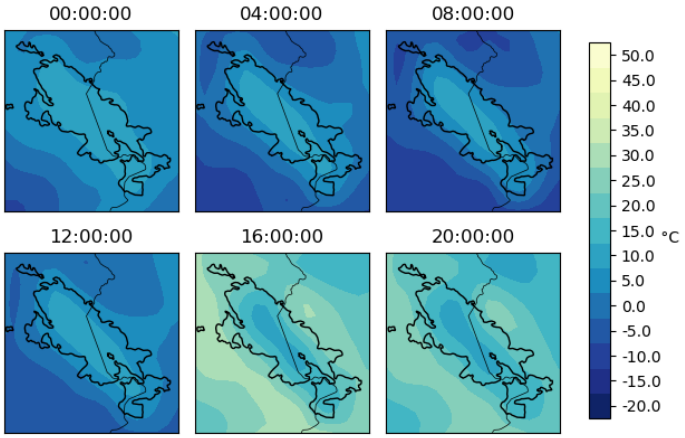

Figure 3.7: Typical evolution of temperatures over the lake following the diurnal cycle on June 30, 2014.

to this, land surface temperatures decrease rapidly. The lake surface however remains at around 15°C and becomes hotter than the surrounding land surface. As the day approaches, solar radiation warms the land to values higher than the water surface. The fact that water takes more time to reach equilibrium in heat transfers is known as the thermal inertia of the lake. The diurnal cycle of the lake surface temperatures is therefore less intense than that of land surface and its amplitude is of about 4°C.

To implement this forcing to our model, a series of manipulations where needed. Similarly as for the wind forcing, a spacial interpolation was realized on each time step in order to homogenize the data. Additionnaly since we are interested in the water surface temperatures, we chose to use only the central points in the center of the lake therefore rejecting the outermost data points that are influenced by the land temperatures. Finally these central points where averaged and this single value was used as the surface temperature for the entire lake.

3.1.7 Limitations concerning the hydrodynamic model

It is known that a model is only as good as the data that is fed into it. In our case, the quality of the model outputs is entirely dependent of that of our two major forcing data.

Poor spatial resolution

For surface temperature forcing, since we chose to homogenize the surface temperature on the entire lake we lost significant information concerning the variation of this forcing in space. Some regions such as the lake borders were consequently badly represented, especially considering that the waters in this region are shallow and thus more subject to thermal relaxation. The use of this homogeneous surface temperature forcing was the result of much time and effort allocated to address the issue. Indeed many alternatives were tested to implement a surface temperature that looked as realistic as possible but, given the poor spatial resolution of the climate model for this region (a dozen points on the lake), none were conclusive. To add precision to the model, more work should be done on this aspect, but given the limited resource at hand we decided to leave it as is.

No external flows considered

For our model, we considered an entirely closed system regarding mass balance, we chose to assume equilibrium between inputs and outputs of water that might affect the system since they where considered relatively small. This allowed us to simplify the model but it also added some errors, for instance, the currents at the Tiquina passage are believed to be under evaluated by the model. Indeed, given that most river inputs are located in the Lago Mayor and that the main output is in Lago Menor (Desaguadero river) this should generate a net southward flow through the Tiquina bottleneck. This net flow is not generated in our model. These water flows may have a more significant and local effect on the hydrodynamics than expected. For instance, regions near river inputs may

contribute to changes in temperature, density or current velocities. This could lead to simulations that misrepresent the reality. Furthermore, other external flows deserve to be taken into account: pluviometry and evaporation could be interesting for our model since they contribute to the water balance, the latter in a significant way (95% of the lake water loss). The validity of this approximation needs to be confirmed.

Errors due to discrete horizontal layers of the mesh bathymetry

We chose to extrude the 2D mesh into 15 layers thus creating artifitial horizontal steps on the borders of the lake. This was found to have some repercussions on the NPZD model as we will see in Chapter 4. Another issue regarding the uppermost layers of this mesh is the misrepresentation of the wetlands surrounding the lake. Some regions around Lake Titicaca are in fact swamps prone to flooding (see Appendix E), the perimeter of the lake in these areas is thus difficult to determine. This applies to the Cohana bay, where our model establishes a depth of 1m to 2m when in reality the bay is shallower. We will also see that this has an impact on our NPZD results.

This artificial lake border effect can always be corrected by providing more resolution to the top layers or by extruding the 2D mesh on a greater number of horizontal layers, though this might result in additional computational resources.

Another way to bypass this unwanted effect, is to extrude the 2D mesh following the addapted σ-level method which provides a continuous bathymetry thus avoiding the horizontal steps (see Fig. 3.8). A combination of σ-level mesh on the Lago Mayor and z-level mesh on Lago Menor could be considered, this would provide greater resolution for the Cohana bay while limiting the computation needs for the larger part of the lake.

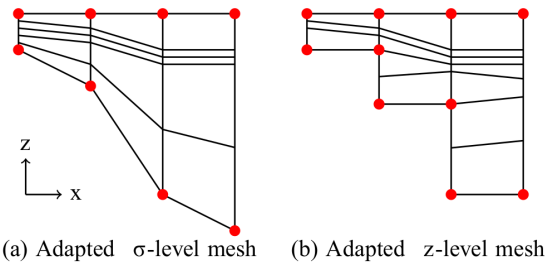

Figure 3.8: Comparison between an adapted σ-level mesh (a) and an adapted z-level mesh (b). The nodes marked with a red dot are fixed during the mesh vertical diffusion process. Source:(Delandmeter et al., 2018)

Insufficient calibration.

The difficulties encountered while searching for qualitative data have forced us to use parameter values that are not specific to the lake. For this thesis, we made the conscious decision to make these approximations regarding the model calibration. However, for further applications of our model, a more rigorous calibration should be done in order to achieve more realistic results.

3.2 The NPZD model

The physical variables and their respective symbols used for the NPZD ecosystem-type model are presented in Table 3.2.

Symbol	Definition	Value	Unit
N	Nitrogen	Variable	mmol N m^{-3}
P	Phytoplankton	Variable	mmol N m^{-3}
Z	Zooplankton	Variable	mmol N m^{-3}
D	Detritus	Variable	mmol N m^{-3}
a	Temperature coefficient	0.07	$°C^{-1}$
g_{max}	Maximum grazing	$0.81e^{-5}$	s^{-1}
I_0	PAR at the surface	275	Wm^2
k_C	Light attenuation by phytoplankton	0.06	$m^2(mmol\ N)^{-1}$
k_D	Light attenuation by detritus	0.01	$m^2(mmol\ N)^{-1}$
k_W	Light attenuation by pure water	0.08	m^{-1}
k_N	Half-saturation constant for nitrogen uptake	0.5	mmol N m^{-3}
k_P	Half-saturation constant for grazing	0.25	mmol N m^{-3}
m_p	Phytoplankton mortality	$9.26e^{-7}$	$s^{-1}(mmol\ N\ m^{-3})^{-1}$
m_z	Zooplankton mortality	$6.94e^{-7}$	$s^{-1}(mmol\ N\ m^{-3})^{-1}$
s_p	Phytoplankton sinking speed	$1.157e^{-5}$	m s^{-1}
s_D	Detritus sinking speed	$1.157e^{-4}$	m s^{-1}
T_{opt}	Optimal temperature	20	°C
$\mu_{\max}$	Phytoplankton maximum growth rate	$3.25e^{-5}$	s^{-1}
α	Light-photosynthesis slope	$1.62e^{-6}$	$m^2s^{-1}w^{-1}$
β	Light inhibition coefficient	$3.24e^{-8}$	$m^2s^{-1}w^{-1}$
ε	Remineralization rate at $0°C$	$1.73e^{-7}$	s^{-1}
λ	Active respiration	0.3	Dimensionless
γ	Zooplankton growth efficiency	0.4	Dimensionless
u	Horizontal velocity vector		m s^{-1}
w	Vertical velocity		m s^{-1}
κ	Vertical diffusivity		m^2s^{-1}
κ_{h}	Horizontal diffusivity		m^2s^{-1}
z	Vertical Eulerian coordinate		
∇_{h}	Horizontal derivative operator		

Table 3.2: Symbols and physical variables for the NPZD model

The second major goal of this thesis was to develop a simple ecological model coupled to the main physical model that would help us study the contamination in the lower part of the Titicaca lake: Lago Menor. With this model, we should be able to replicate the algal bloom event caused by Carteria sp. in the Cohana bay during autumn 2015. For this purpose, a marine ecosystem model of type NPZD was chosen.

These type of models are widely used in marine ecology studies (see for instance Friedrichs and E. Hofmann, 2001; Kawamiya et al., 2000; Olascoaga et al., 2005; R. Hood et al., 2003), and have been subject of research (Anderson, 2005; Heinle and Slawig, 2013). They are simple (as compared to more complex models that often have dozens of equations), tractable (easy to understand the processes at play) and scalable (one can adapt the complexity according to his needs).

In our case, we chose to develop our model following the Tian et al. (2015) formulation, thus we kept most of the parameters suggested by the paper. The model consists of four state variables: Nitrogen N (dissolved inorganic nitrogen: NO_2, NO_3 and NH_4), phytoplankton P, zooplankton Z and detritus D, and six processes governing the evolution of these reservoirs (see Fig. 3.9). These four major components are closely related to one another. In a steady environment, they tend towards an equilibrium state.

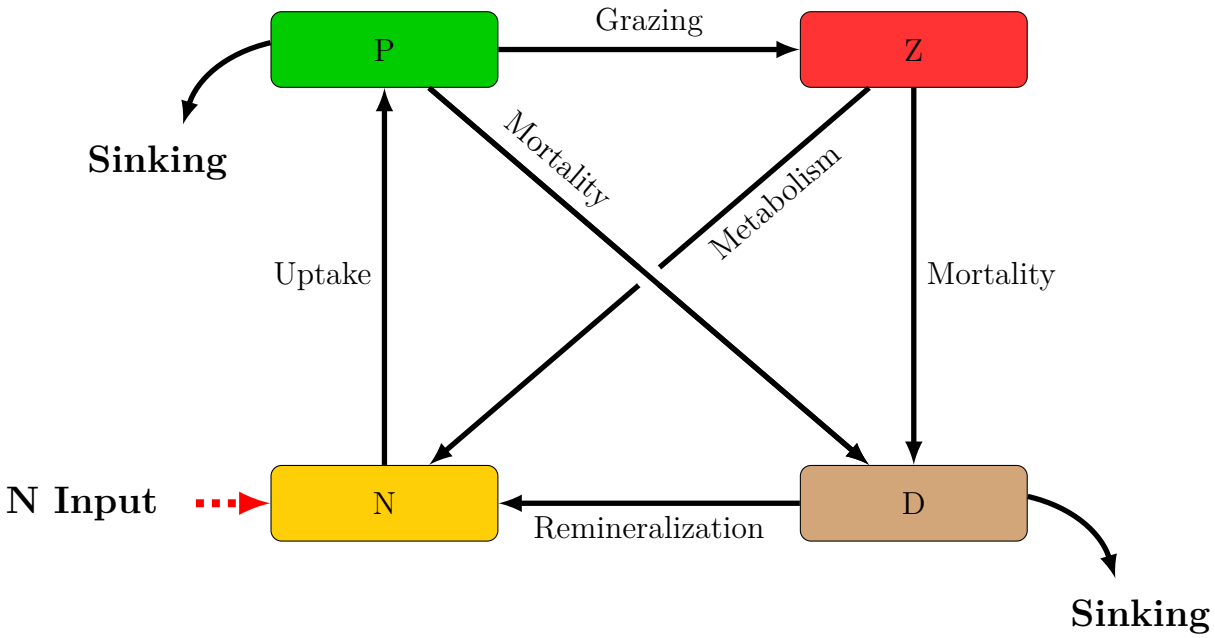

Figure 3.9: Schematic NPZD model.

Once the basic ecosystem model is operational, we will proceed to add a simulated input of Nitrogen in the Cohana bay which will simulate the input by the Katari river. This will allow us to observe the spacial distribution of these newly added nutrients as well as the evolution of the other state variables in the system.

In this section, we review the governing equations that make up the relevant processes of the NPZD model, then we will take a closer look at the implementation of this model into the hydrodynamic model. Finally we will validate this method by comparing the generated results with reality.

3.2.1 Governing equations

These equations make up the NPZD model. For most parameters, the Tian et al. (2015) values where used unless site-specific measures were available. The four major components of the model are resolved for each time step by solving their corresponding differential equations. The evolution of each components is computed as the following equation:

$$\frac{\partial N}{\partial t} + Advec(N) = -U_P + \lambda G_Z + \varepsilon f(T) D + Diff(N) \tag{3.13}$$

$$\frac{\partial P}{\partial t} + Advec(P) = U_P - G_Z - m_p f(T) P^2 + s_P \frac{\partial P}{\partial z} + Diff(P) \tag{3.14}$$

$$\frac{\partial Z}{\partial t} + Advec(Z) = \gamma G_Z - m_z f(T) Z^2 + Diff(Z) \tag{3.15}$$

$$\frac{\partial D}{\partial t} + Advec(D) = (1 - \gamma - \lambda) G_Z + m_p P^2 + m_z Z^2 - \varepsilon f(T) D + s_D \frac{\partial D}{\partial z} + Diff(D) \tag{3.16}$$

With the advection ($Advec$) and diffusion ($Diff$) terms for each component X as follow:

$$Advec(X) = \nabla_{\mathrm{h}} \cdot (uX) + \frac{\partial (wX)}{\partial z}\,, \tag{3.17}$$

$$Diff(X) = \nabla_{\mathrm{h}} \cdot (\kappa_{\mathrm{h}} \nabla_{\mathrm{h}} X) + \frac{\partial}{\partial z}\left(\kappa \frac{\partial X}{\partial z}\right)\,. \tag{3.18}$$

Starting with Eq. (3.13), we see that the stock of nitrogen is replenished on one side by mineralization of detritus and on another side by the zooplankton metabolism represented by the product of respiration with grazing. Nitrogen is then absorbed by phytoplankton through the uptake term.

Eq. (3.14) describes the evolution of phytoplankton (P) which is governed by four processes: growth directly linked to uptake U_P, grazing G_Z, mortality m_P, and sinking s_P. The mortality is influenced by temperature and population count. Temperatures that are far from the optimal induce a higher mortality and so does a crowded environment, this is represented by a mortality rate that greatly increases with P.

Eq. (3.15) describes the evolution of zooplankton (Z) which feeds on phytoplankton through grazing and joins the detritus stock through mortality. As for the phytoplankton, the mortality rate greatly increases with the zooplankton population, and is influenced by temperature.

Lastly in Eq. (3.16) we can see that the stock of detritus is replenished by the contribution of phytoplankton and zooplankton egestion and mortality. However, detritus are subject to sinking forces and remineralization thus contributing to the nitrogen compartment.

The uptake (U_P) and grazing (G_Z) terms can be further detailed since they depend largely on external factors:

$$U_P = \mu_{\max} f(N) f(I) f(T) P\,, \tag{3.19}$$

$$G_Z = \frac{g_{\max} f(T) Z P^2}{P^2 + K_P^2} \,. \tag{3.20}$$

Uptake is topped by a maximum growth rate for phytoplankton $\mu_{\max}$ and is influenced by the availability of nitrogen $f(N)$, phytoplankton response to light $f(I)$ and the effect of temperature $f(T)$ as shown in Eq. (3.19). These three terms are futher detailed in Eqs. (3.21), (3.22) and (3.24).
Grazing on the other hand (Eq. (3.20)) is limited by the zooplankton maximum grazing rate g_{max} and by the half-saturation constant for zooplankton grazing K_P, and is influenced by temperature.

Nitrogen availability is governed by a Michaelis Menten function characterised by the half-saturation constant for nitrogen uptake $K_N = 0.5$ [mmol N m^{-3}].

$$f(N) = \frac{N}{N + K_N} \tag{3.21}$$

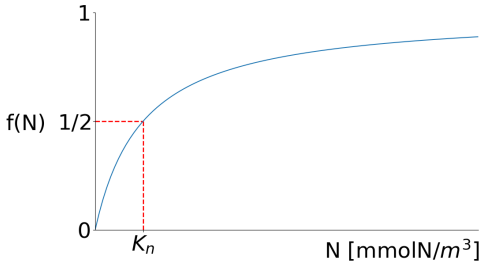

The effect of temperature on multiple biological rates is parameterized as an exponential function that evolves around an optimal temperature $T_{opt} = 20°$C.

$$f(T) = \mathrm{e}^{-a|T - T_{\mathrm{opt}}|} \tag{3.22}$$

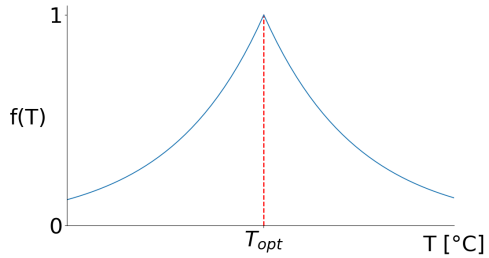

Solar radiation also plays an important role in our model since it is the driver of photosynthesis. Solar radiation reach the lake surface with a surface photosynthetically active radiation (PAR) of 275 W/m^2. The radiation make their way through the water column where they are progressively absorbed by pure water, phytoplankton, and detritus with their respective light attenuation constants k_W, k_p and k_D. This light attenuation is calculated as a function of water depth z, phytoplankton, and detritus concentrations as expressed in Eq. (3.23).

$$I(z) = I_0 \exp\left(-k_W z - k_P \int_z^0 P \mathrm{d}z - k_D \int_z^0 D \mathrm{d}z\right) \tag{3.23}$$

In the water column, phytoplankton can utilize this energy for photosynthesis. Nevertheless the amount of PAR that is effectively absorbed by phytoplankton $f(I)$ depends on the intensity of the radiation since effects such as light inhibition take place. Eq. (3.24)

was parameterized using the Platt et al. (1980) formulations where α and β are the light-photosynthesis slope and the inhibition coefficient, both in $[m^2 s^{-1} w^{-1}]$. We can see that the maximum efficiency is attained at 79 $[Wm^2]$ when the intensity is high enough to provide significant energy to phytoplankton but small enough to avoid damaging vegetation tissues.

$$f(I) = \left(1 - e^{-\alpha I/\mu_{\max}}\right) e^{-\beta I/\mu_{\max}} \tag{3.24}$$

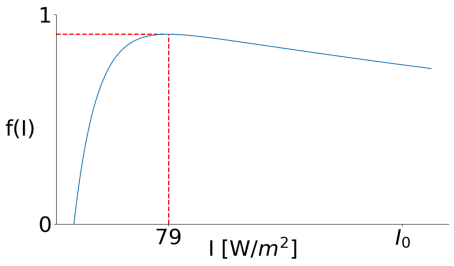

3.2.2 Initial conditions

As a starting point the NPZD model needs initial concentration values for the four state variables. These values were hard to come by due to the lack of available qualitative data, hence we had to derive suitable initial conditions based on the information at our disposal.

To find the initial values of the N component of our model, we mainly used the Cruz et al. (2014) data gathered during the July 2014 scientific cuise CR. 1407 (see Fig. 3.10).

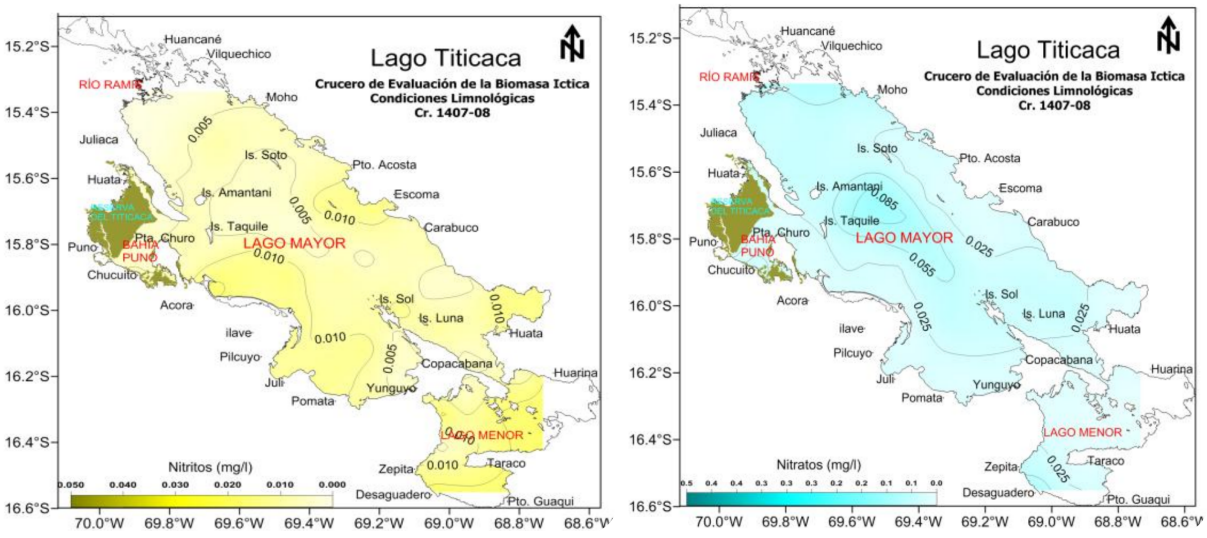

(a) NO_2 (mg/L) (b) NO_3 (mg/L)

Figure 3.10: Nitrite (a) and nitrate (b) concentrations (mg/l) in Lake Titicaca gathered by the CR.1407 scientific cruise. Source: Cruz et al. (2014)

The cruises objective was to gather multiple information regarding physical and chemical characteristics of the lake. 31 hydrographic stations and 80 surface stations where distributed throughout the lake. Sampling was carried out at different bathymetric levels

at the following depths (0, 25, 50, 75, 100, 150, 200 and 250 m). Both NO_2 and NO_3 values were available for the entire lake by combining superficial and profiles sampling stations.

We decided to use a homogeneous value throughout the lake as the initial condition of the N component. Indeed we realized that the model converged rapidly (within a few days) towards an equilibrium state. No need for a refined spatial distribution of nitrogen. To recall, the N component is defined as (NO_2 + NO_3 + NH_4), given the lack of available data and in the scope of this thesis, we chose to neglect ammonium concentrations. To compute this initial value of the N component, we thus started by averaging nitrite and nitrate values of the lake. We then computed the initial nitrogen based nutrients value by summing these average nitrite and average nitrate values. The total initial nitrogen value (NO_2 + NO_3) was then imputed as a homogeneous value for the whole lake. Again, given the lack of available data and in the scope of this thesis, we chose to neglect Ammonium concentrations.

For the initial phytoplankton, zooplankton and detritus values, we decided to maintain the same proportions between the four NPZD state variables as Tian et al. (2015). We computed the P,Z and D values in relation to the nutrient concentrations as shown in Table 3.3.

	N	P	Z	Z
Tian et al. (2015) (mmolN/m^3)	0.4	0.1	0.05	0.98
Our initial values (mmolN/m^3)	1.79	0.45	0.22	4.39
ratio	4.475	4.475	4.475	4.475

Table 3.3: Initial conditions for the N,P,Z and D values.

As previously mentioned, in the aim of identifying the impact of the error due to false initial conditions, we performed multiple runs of the model for different initial values. Since the equilibrium state seemed to be rapidly attained (within a few days), we concluded that the initial values did not strongly impact model predictions on the long run.

3.2.3 Model forcings

The main external forcings applied on this ecosystemic model are the physical forcings generated by the underlying model and the additional input of Nitrogen.

Physical forcings

The physical forcings terms that affect the NPZD model are generated by the underlying SLIM3D model for each element of the mesh. They are temperature and water currents.

Water currents affect the ecosystemic model driving the NPZD components through advection and diffusion. The horizontal diffusivity of the NPZD components is achieved

using the Okubo (1971) formulation. Water temperatures affect most of the processes mentioned for our ecologic model as they do in all natural ecosystems.

Nitrogen input

As a way to simulate the nitrogen input in the Cohana bay due to the Katari river discharge, an artificial nitrogen source was created on this location.

We generated an estimated amount of nutrients entering the Cohana bay during 2014 to 2015 by analyzing the flow rate and the concentrations of contaminants provided by different studies (see Table 3.4). As the only data available to make an estimation, these paperer provide nitrate concentrations for different dates and near the river output.

Paper	**Date of measure**	**$N0_3$ (mg/L)**
Lima et al. (2019)	March 2015	7
Ap et al. (2017)	June 2012	4.3
MMAyA (2014)	October 2014	1.26
K2/AP05/J13 (2013)	November 2013	45.65

Table 3.4: NO_3 concentrations provided by various studies.

Since the nitrate concentrations were not measured on the same year, we chose to make the hypothesis that the evolution of the discharge is similar each year during the period 2011 to 2015. Flow rates, gathered from the Geovisor VIBH of the Bolivian ministery of environment and water (Ministerio del Medio Ambiente y Agua (MMAyA)) seem to confirm this hypothesis (see Fig. 3.11).

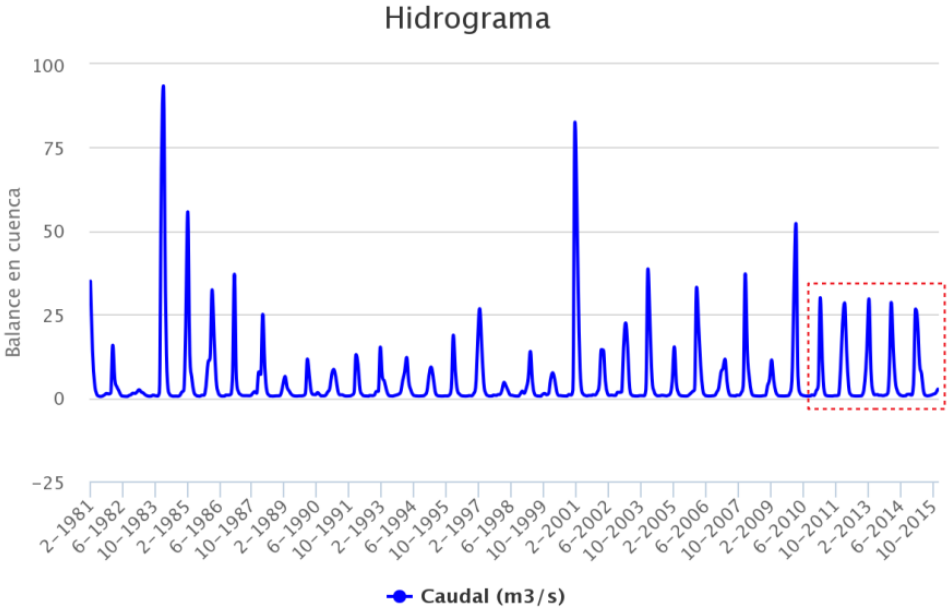

Figure 3.11: History of outflow (m/s) of the the Katari watershed. We can see that flow rate had the same aspect during the period of 2011 to 2015, with a peak flow at around 30 m/s. Source: Geovisor VIBH of the MMAyA.

Using the available data and following the shape of the discharge, we were able to build an approximation of the NO_3 discharge by the Katari river into the Cohana bay during 2014 and the beginning of 2015. (Fig. 3.12).

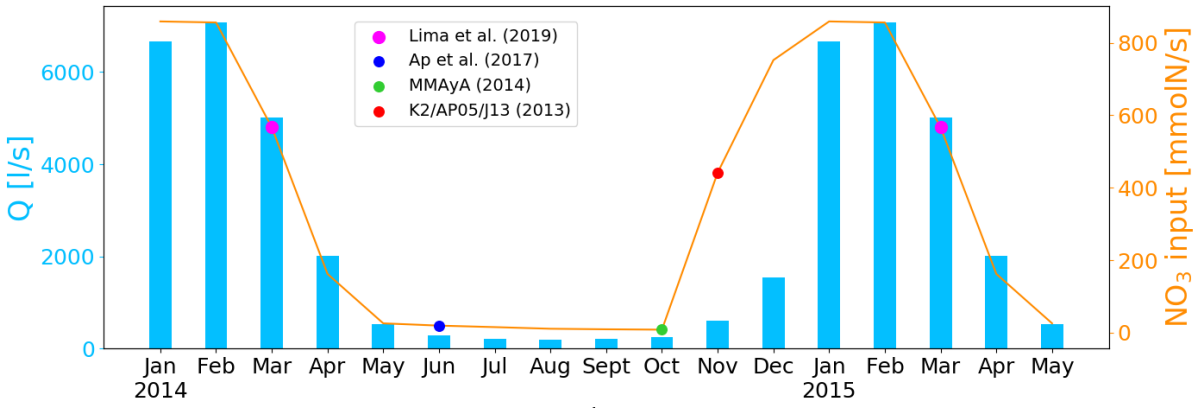

Figure 3.12: Discharge and estimated nitrite input from the Katari river

Lastly, since our model takes into account total nitrogen we had to add the NO_2 concentrations in order to build the N input (NH_4 was neglected). For this purpose we simply decided to keep the NO_3 to NO_2 ratio found In Lago Menor: for each mmolN/L of NO_2 we observed 12 mmolN/L of NO_3 as a global mean (Cruz et al., 2014). Our total nitrogen input was thus computed as follow:

$$\begin{aligned} N_{input} &= [NO3] + [NO2] \\ &= [NO3] + \frac{1}{12} * [NO3] \end{aligned} \tag{3.25}$$

It is clear that this method of estimation of the nitrogen based nutriments introduces a significant error and needs to be perfected but it will serves our purpose for the time being.

As for the location of the input, it was difficult to determine exactly the junction between the Katari river and Lago Menor since this area is a wetland and, thus, the lake perimeter is not clearly defined. We chose a unique point as the source of Nitrogen discharge (located at lon 535500.0, lat 8189700.0 UTM). With retrospective, we could of had used a segment or even multiple sources to better represent the span of the discharge.

3.2.4 Limitations concerning the NPZD model

Quality is dependent of the hydrodynamic model.

The quality of the NPZD model directly depends on the underlying hydrodynamical model. This dependency is inevitable but one should remain aware and make sure that the physical model is as optimal as possible. One way to evaluate the pertinence of the hydrodynamic model is by performing validations as we will do in Section 5.2.

Non-specific calibration due to lack of data.

As for the Hydrodynamic model, the difficulties encountered in the search of qualitative data have forced us to use parameters that are not specific to the lake therefore limiting the quality of the model outputs. As we will see in Section 5.2 this has an impact on the results.

Poorly approximated nitrogen input.

We used different sources to impute the nitrogen input concerning the junction of Katari with the Cohana bay but our method remains a rough estimate and can lead to significant error as seen in Section 4.4.

Limited ecological pathways.

Our ecosystemic model covers certain interactions between the four major components but it omits many others. For instance planktivorous fish or phosphorus availability where not taken into account. The model deals with simplified biological processes and is not species-specifics. It is not possible to implement the complexity of nature in one mathematical model, this is inevitable. Nevertheless it is important to identify the main ecological pathways of the environment that one wishes to study. On the other hand, the simplicity of the NPZD type model makes it a easier to calibrate since it requires less parameters than more complex models.

Static Solar radiation

Not so much as a limitation, it is interesting to mention that an additional forcing could be applied concerning solar radiance, for now, the PAR at the surface is introduced in the model as a constant I_0, but annual variations apply (Delclaux et al., 2007). Similarly to the solar radiation, several parameters are considered constant in time, this might affect the overall quality of our outputs.

4 | Results

In this section we will first analyze the outputs generated by our model. As previously mentioned, our model is able to provide a series of different outputs, we chose to mainly focus on a couple of them:

- **Horizontal components of water velocity** will be shown for the 15^{th} of March 2015, during the algal bloom event.
- **Water temperatures** will be shown as temperature profiles for all months of 2014. The spatial distribution will also be shown for the dates of the 15^{th} of February 2014, during the rainy season and the 15^{th} of August 2014, during the dry season when vertical mixing occurs.
- **Tracer** used to visualize the spread of contaminants will be shown for the year 2014.
- **NPZD components** will be shown for the 15^{th} of March 2015, during the algal bloom event.

All the results where extracted at midday.

4.1 Water velocity

The horizontal components of water velocities correspond to the u and v components of the velocity vector in [m/s]. As mentioned in Section 3.1.6, the wind and the surface temperature forcings are the main elements that drive the water circulation in the lake. Since these forcings change over time, the water currents on the surface of the lake can differ from one day to another. Fig. 4.1 shows Lake Titicaca on the 15^{th} of March 2015 at midday. We can see that horizontal velocities seem larger in the central part of the lake (maximum velocities around 2.5 cm/s), this corresponds to the deeper regions of the lake (see Fig. 3.2). We can see a circular motion in the center-east part of the lake. Taking a closer look at Lago Menor (Fig. 4.2), we can see that water velocities are less pronounced, with a maximum around 1 cm/s. In the Cohana bay, where the N input occurs, currents are quite slow (3mm/s) since it is very shallow area (maximum depth of 2m). Water comes from the south-west and makes its way towards the north of the bay.

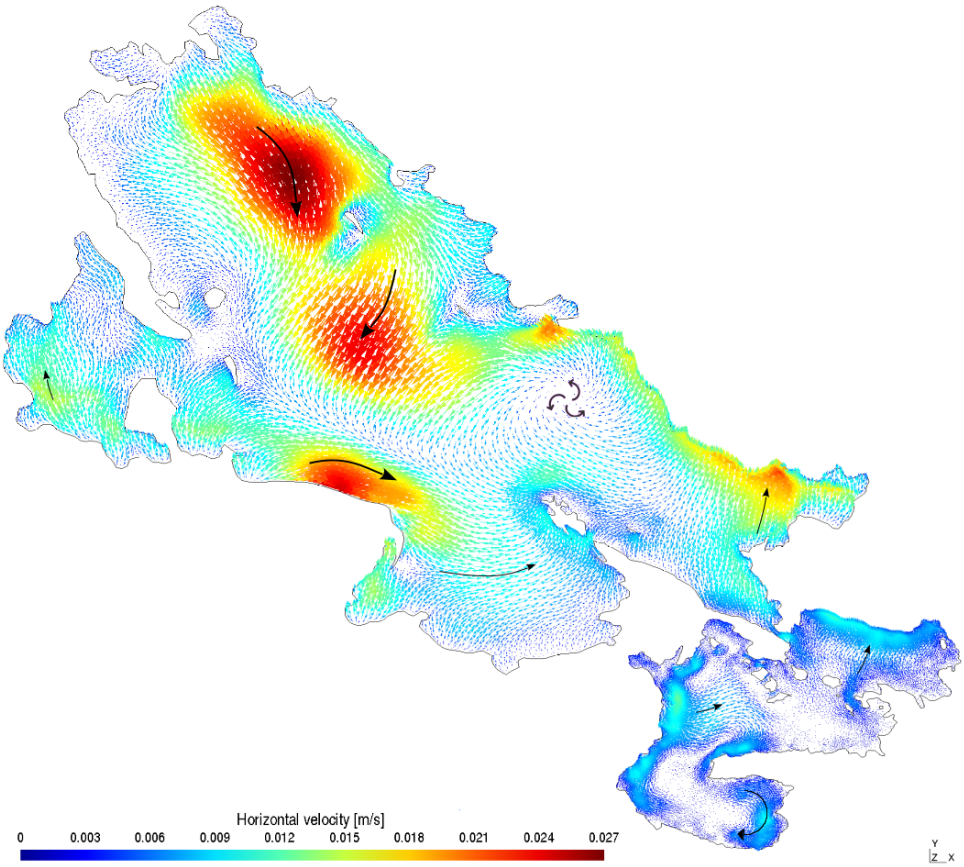

Figure 4.1: Water horizontal velocity (m/s) for the 15^{th} of March 2015 at midday.

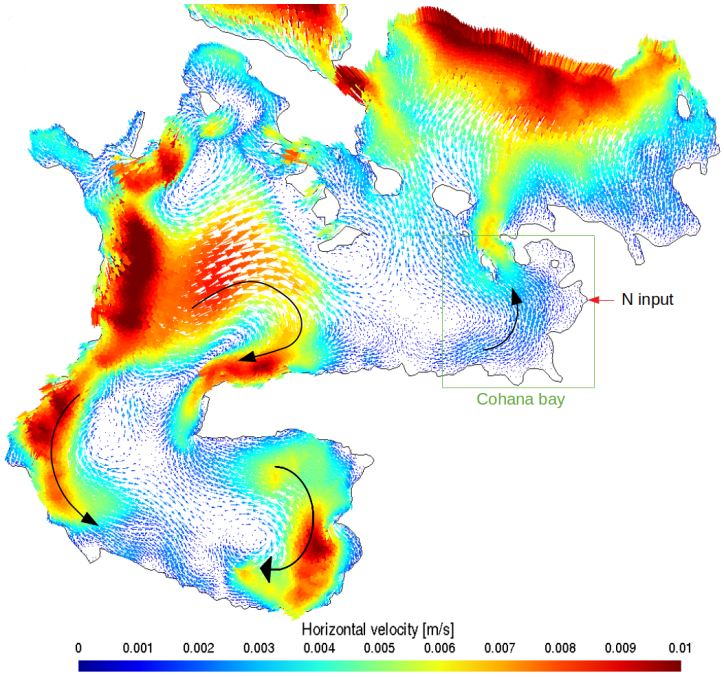

Figure 4.2: Water horizontal velocity (m/s) in Lago Menor for the 15^{th} of March 2015 at midday.

4.2 Water temperatures

The evolution of water temperatures within the lake is strongly dependent on the surface temperature forcing. We should keep in mind that this forcing was applied homogeneously on the entire lake which can lead to similar surface temperature values. As we saw in Section 3.1.6, surface temperatures present a seasonal variability. Therefore, we should be able to reproduce this variability in our results. Fig. 4.3 shows the annual evolution of the temperature profile taken at the coordinates 451826.10975, 8269107.8460 UTM (near the intersection of the A-A' and B-B' cross sections seen in Fig. 4.4).

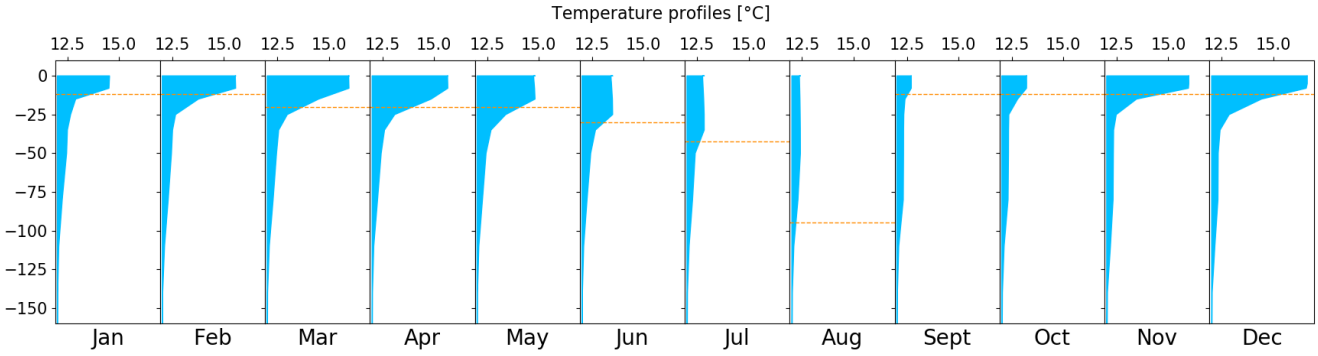

Figure 4.3: Annual evolution of the temperature profile. The temperature is shown in relation to depth for each months. The orange horizontal line represents the depth where the biggest temperature gap occurs, therefore symbolizing the approximate depth of the thermocline.

We can see that for the months of November to May 2014, when surface temperatures are hotter, there is a clear stratification of the lake temperatures. Indeed, the top 10m near the surface present temperatures around 15°C whereas cooler temperatures, around 12.5 °C, can be found bellow 25m. The temperature difference between these two depths is not done in a linear fashion, but rather as an abrupt change. At a certain depth, the water temperatures drop quickly. This rapid change of temperatures is called the thermocline, it is a thin layer that divides the upper mixed layer from the calm deep water below. We can see that for the period between June to October when the surface temperatures are cooler, the thermocline is much less defined or absent. This means that there is no longer the horizontal physical barrier that prevented the deep waters from mixing with the surface layers: we have vertical mixing over the entire water column. We can, thus, conclude that there is a clear difference in the temperature profiles between the months of February during the rainy season and of August at the peak of the dry season.

The spatial distribution of water temperatures for the the 15^{th} of February during the hotter rainy season is shown in Fig. 4.4. In this figure we can clearly see that surface temperatures seem very similar for the whole lake which is consistent with the forcing. However slightly cooler temperatures are present in the north eastern side of the lake.

In both cross sections, we can see that there is a clear stratification within the lake with warm waters near the surface. A closer look at the A-A' cross section shows that the warm water layer is deeper on the south western edge (A) than for the north-east counterpart (A'). This can be explained by the contribution of hot surface waters flowing towards the south-west during this period (see Appendix B). The waters on the north-eastern side seem to be subject to up-welling since we can see that the deeper and cooler waters are rising towards the surface (cross section A-A'). This phenomenon is likely caused by the wind that blows the surface waters towards the south-west therefore creating a local depression in the north-east. The deeper waters rise to the surface to fill in the gap.

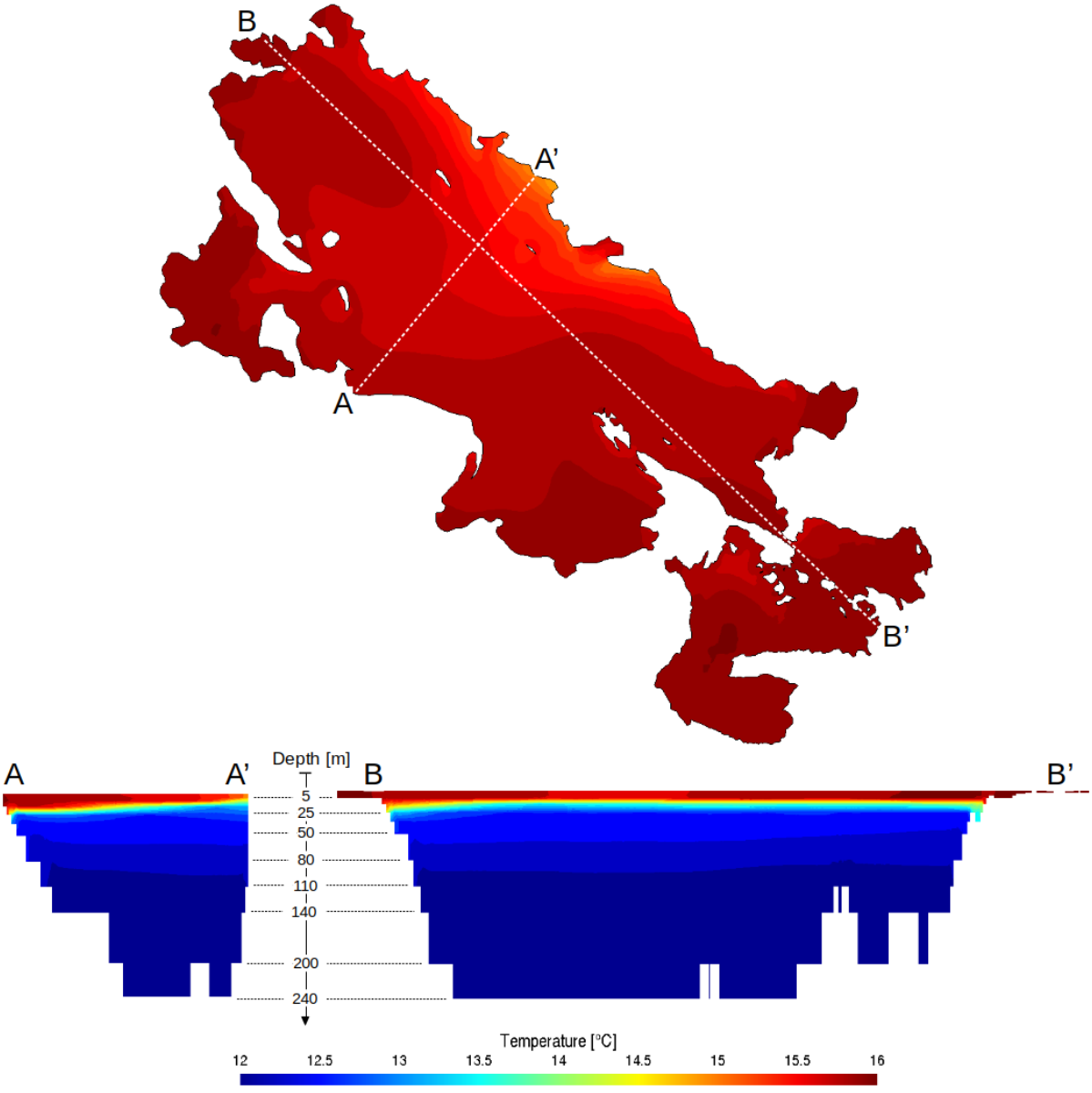

Figure 4.4: Water temperatures for the 15^{th} of February 2015 as seen from above as well as a cross section from points A to A' and a longitudinal cut from B to B'. Temperatures vary from 12 °C to 16 °C and the iso-temperature lines are plotted for every 0.1 °C.

The spatial distribution of water temperatures for the 15^{th} of August at the peak of

the cooler dry season is shown in Fig. 4.5. In comparison with the previous results, water temperatures in mid August are quite differently distributed. In general the lake surface temperatures are much lower, they fell from about 16°C in February to about 12.5°C in August.

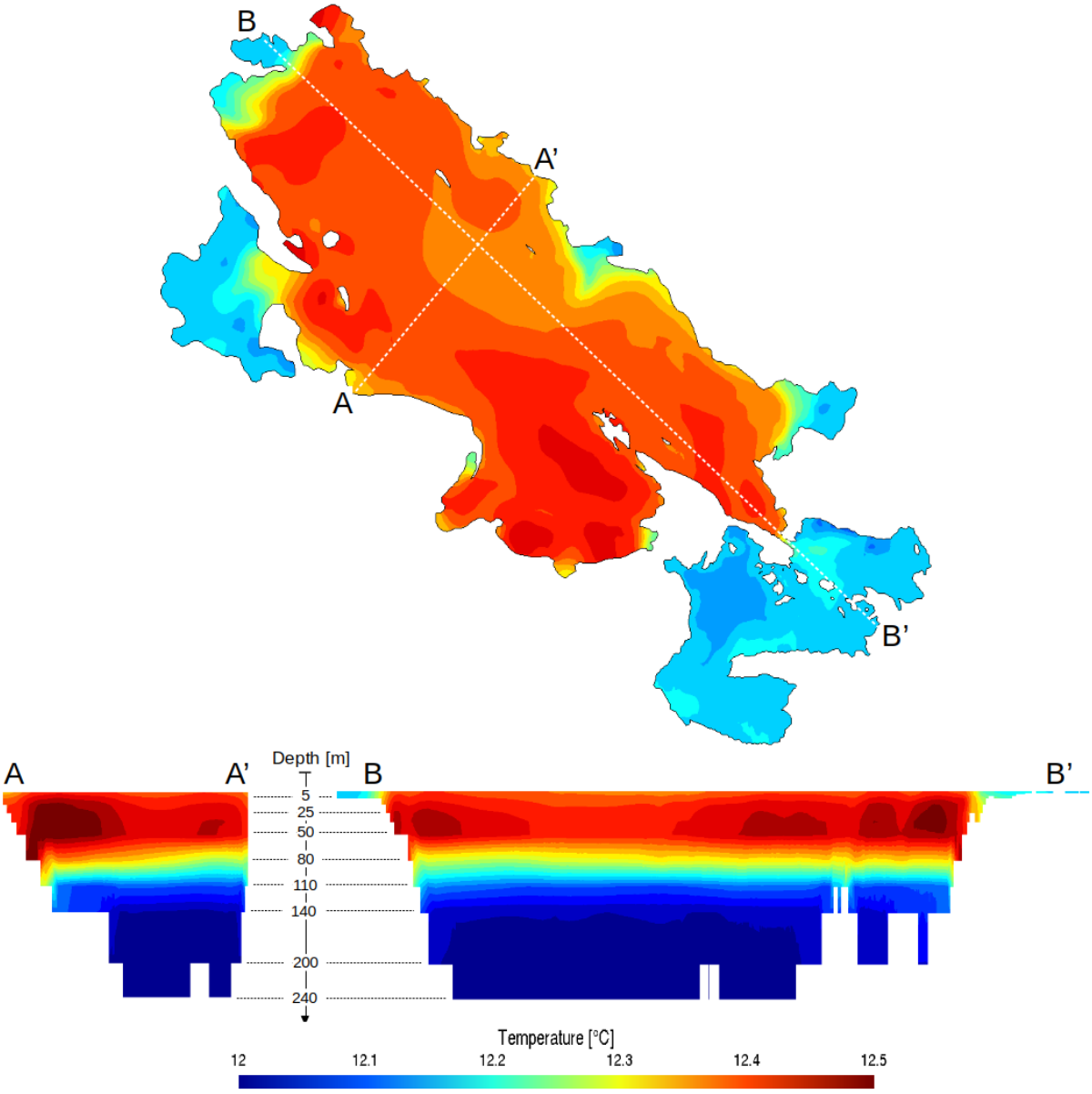

Figure 4.5: Water temperatures for the 15^{th} of August 2014 as seen from above as well as on a cross section from points A to A' and a longitudinal cut from B to B'. Temperatures vary from 12 °C to 12.5 °C and the iso-temperature lines are plotted for every 0.025 °C.

This is due to the lower atmospheric temperatures in this season which tend to cool the surface of the lake. In this figure we can also see that the shallower areas of the lake are cooler than the central core, this can be explained in part by the lakes thermal inertia. This thermal inertia tends to slow down the cooling. Indeed, the lake was previously warmer so the layers beneath the surface have stored heat, we can see this in both cross-sections, where hotter waters can be seen between the depths of 25m and 50m. Shallow

areas have a minor capacity to store heat since they have less volume. The mixing of the upper layers provide hot waters to the surface, this explains why shallow waters are cooler. By looking at both cross-sections, we can also see a difference in the vertical distribution of temperatures. Indeed, we have lost the clearly defined thermocline that was visible in February. The progressive cooling of the lake surface has brought surface temperatures to similar values as the deeper layers, this results in the loss of the physical barrier which separated these two compartments. Vertical mixing over the entire water column occurs. This enables sediments as well as biological or chemical particles to be transported from the depth to the surface layers.

4.3 Tracer

A particle tracer was implemented in our model in order to visualize the spread of chemical compounds such as nitrogen in the Cohana bay. The tracer was set to discharge a constant flux of 5 mmolN/s on the location of the Katari river output during the year 2014, this means that the seasonal variations of the discharge is not taken into account. This tracer serves as an indicator that allows us to better understand the spreading dynamic that is at play in this part of the lake.

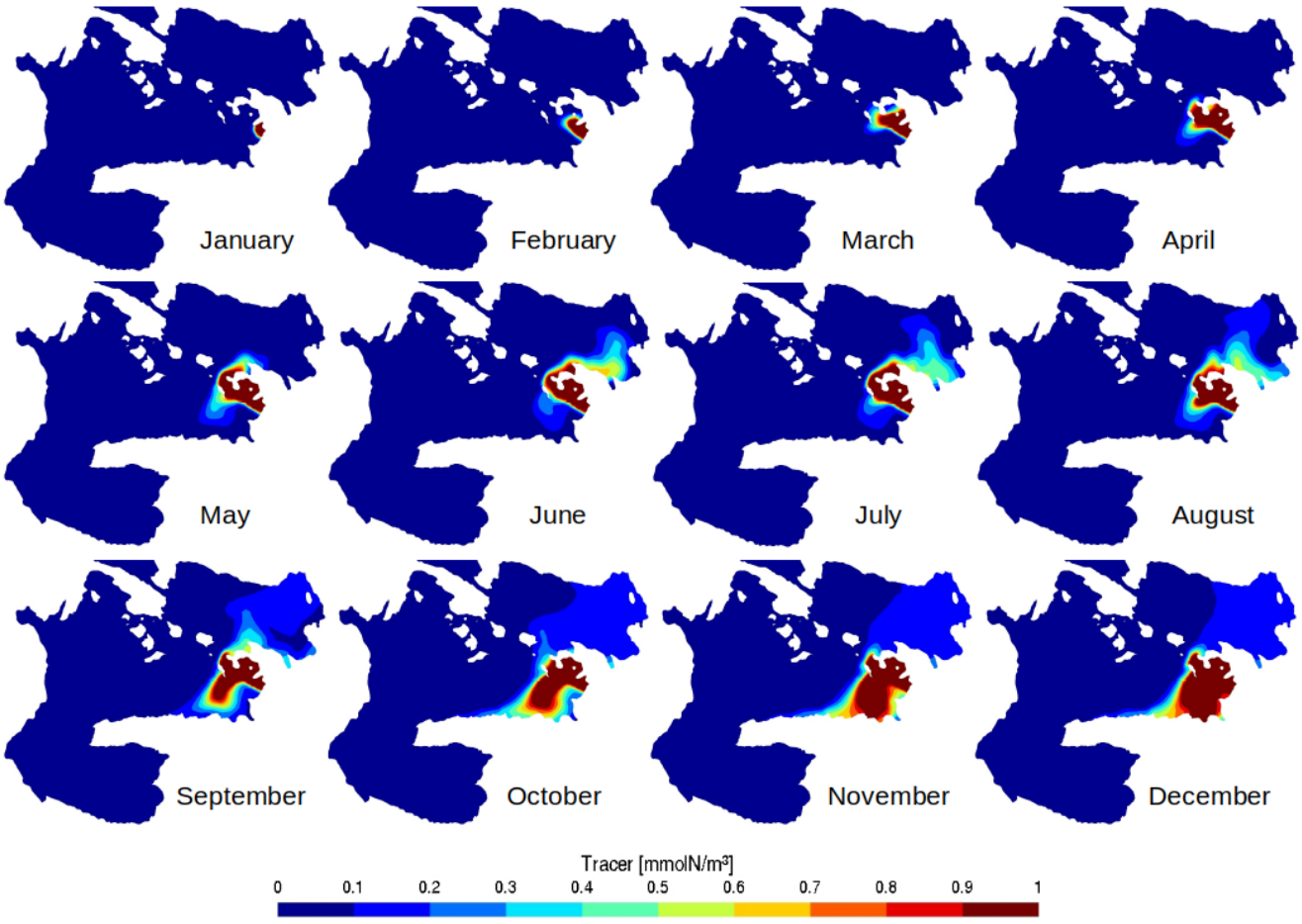

Figure 4.6: Tracer dispersion during the year 2014.

Fig. 4.6 shows the spread of this tracer within the Cohana bay. We can see that 15 days after the start of the simulation, the tracer is still confined in the vicinity of the river output. As time passes, we see that water currents tend to push the tracer towards the north-west. This displacement is slow given the weak currents in this area. When the particles reach the edge of the Puerto Perez peninsula, they are submitted to stronger currents. These currents drive the tracer towards the north-east and the south-west. During the months of May to August, the particles that make it passed the peninsula are spread by the currents towards the north-eastern part of Lago Menor following the coastlines. We observed that the tracer tends to accumulate near the input reaching maximum values around 34.2 mmolN/m^3 at the end of the year. Results where extracted on the 15^{th} at midday for each months.

4.4 NPZD components

Here we will take a look at the four main components of our ecosystemic model, similarly as the temperature results, we will focus on two dates: mid February and mid August.

4.4.1 Nitrogen

On Fig. 4.7 we can see that the nitrogen based nutrients (N) are found mainly in the depths of the lake (see cross sections A-A' and B-B'). This can be explained by the fact that detritus, which are also found in these areas (see Section 4.4.4) are the most important source of N through the remineralization process. We can also see in the cross-sections that there is a horizontal limit around 100m of depth, over which nitrogen is scarce. As we will see further on, just above this limit is where phytoplankton and zooplankton thrive. Phytoplankton consumes N, a valuable resource for their growth.

In Lago Menor and more particularly in the the Cohana bay, we can see that N plumes formed by the local currents are present. Yet we can see that there seem to be a concentration gap between the plume near the input point and the maxima located just underneath the Puerto Perez peninsula. This gap can be explained by the seasonality of the input of N. Looking back at Fig. 3.12, one can recall that between the months of January to April 2014, large amounts of N are poured in the Cohana bay. This is followed by six months of lower input intensity. As time passes the high concentrations of N are slowly transported towards the north-west. From November 2014 to March 2015 a new wave of N is generated. Between these two waves we can thus see a concentration gap. On the western shores of Lago menor, large amounts of N are present. This is due in part because of the transport of N originating from the Cohana bay but also because of the remineralization process of detritus that are present in the region.

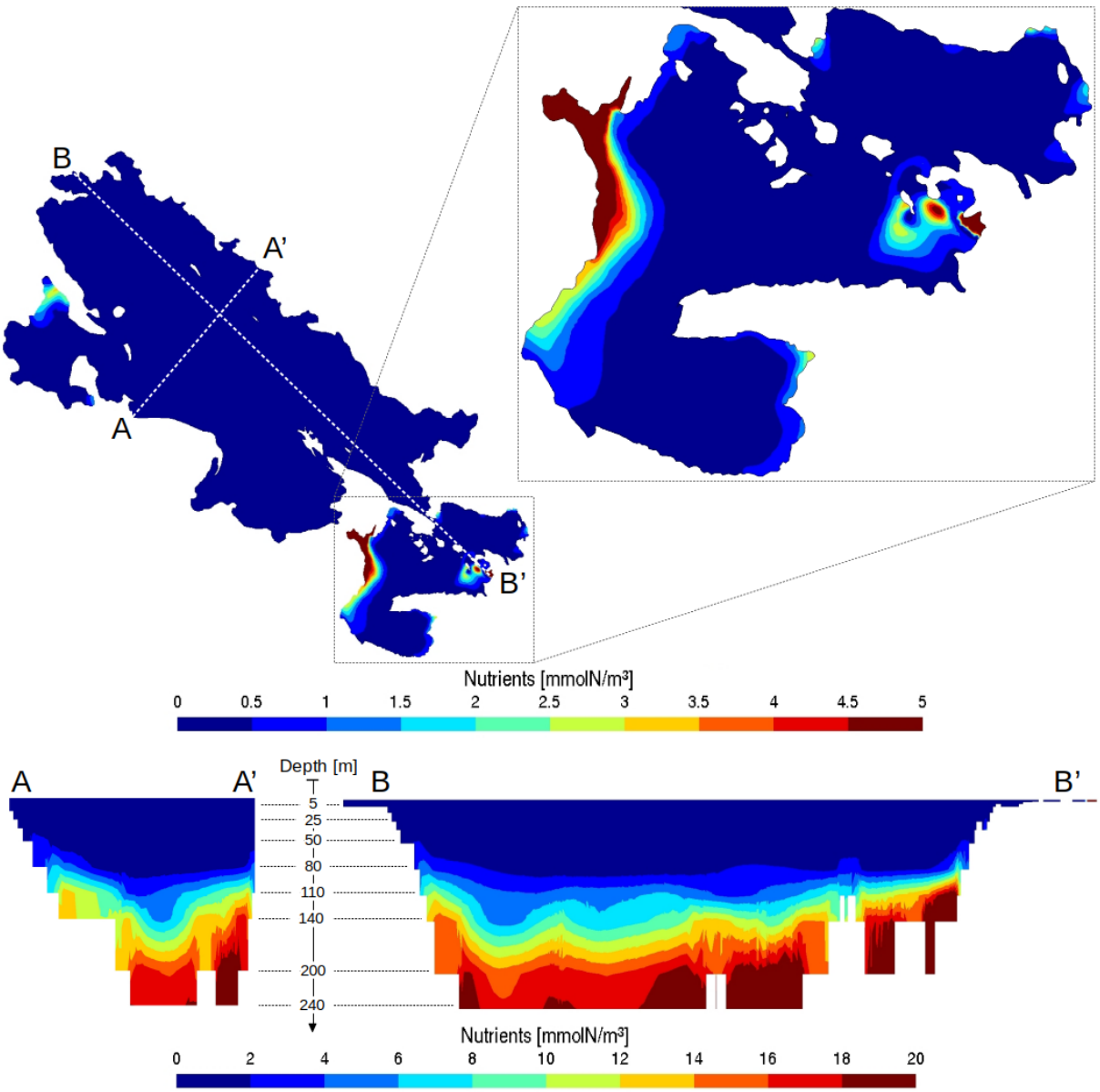

Figure 4.7: Nitrogen based nutrients concentrations in Lake Titicaca

4.4.2 Phytoplankton

On Fig. 4.8 we can see the previously mentioned horizontal layer in which phytoplankton thrives. This distribution can be explained by two main factors. Firstly, phytoplankton depends on the energy input from solar radiation. Therefore, since radiation is diminished with depth, P must stay close to the surface in order to benefit from it. The second factor is the availability of N, as we saw earlier, this element is mostly present in deeper waters and is indispensable for phytoplankton. The combination of these two constraints limit phytoplankton to this horizontal strip between 35m to 130m under the surface. In our model, phytoplankton is subject to sinking forces. This explains why we find some P concentrations under the optimal horizontal zone and near the bottom of the lake. In both cross sections, high phytoplankton concentrations are present near the edges of the

lake, this phenomenon can be explained looking at the nitrogen and detritus distributions. In these areas close to the edge, detritus tends to be lodged on the horizontal steps of the mesh. The remineralization process that takes place here is particularly efficient due to higher temperatures related to the proximity with the surface. The nitrogen provided greatly benefits phytoplankton which can proliferate. This phenomenon can be observed on cross-section B-B' near the Isla del Sol (center right). The low bathymetry in this area allows the detritus to be located in hotter waters, therefore, stimulating remineralization and thus, allowing the proliferation of phytoplankton.

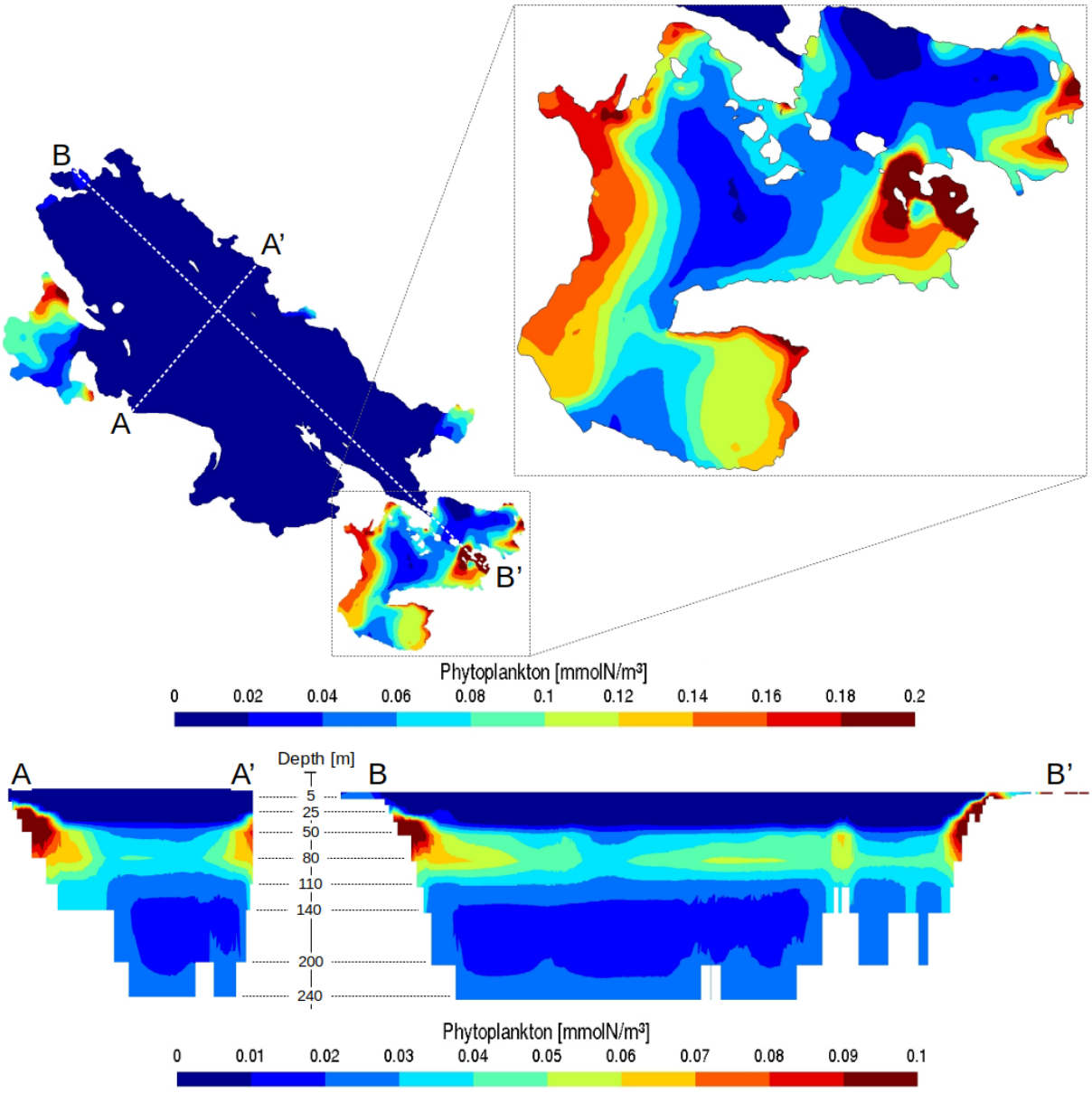

Figure 4.8: Phytoplankton concentrations in Lake Titicaca

In Lago Menor, we can see that phytoplankton is present in high concentrations in the Cohana bay which seems logical due to the high concentrations of N. Nevertheless, the distribution of P in this area is not homogeneous. This is the result of the combined

effects of current mixing and the different N input concentrations discharged. Some phytoplankton have passed the Puerto Perez peninsula and have relocated in the north-eastern part of Lago Menor, but we can also see that the western shores are also densely populated.

4.4.3 Zooplankton

In our models zooplankton feeds mainly on phytoplankton, therefore, it is normal to find it distributed alongside phytoplankton. Indeed, in Fig. 4.9, we can see the same horizontal layer for Z spanning between the depths of 30m to 110m. However, the top limit of this zone is not as clear as that of P since unlike phytoplankton, zooplankton does not require nitrogen based nutrients present in greater depths.

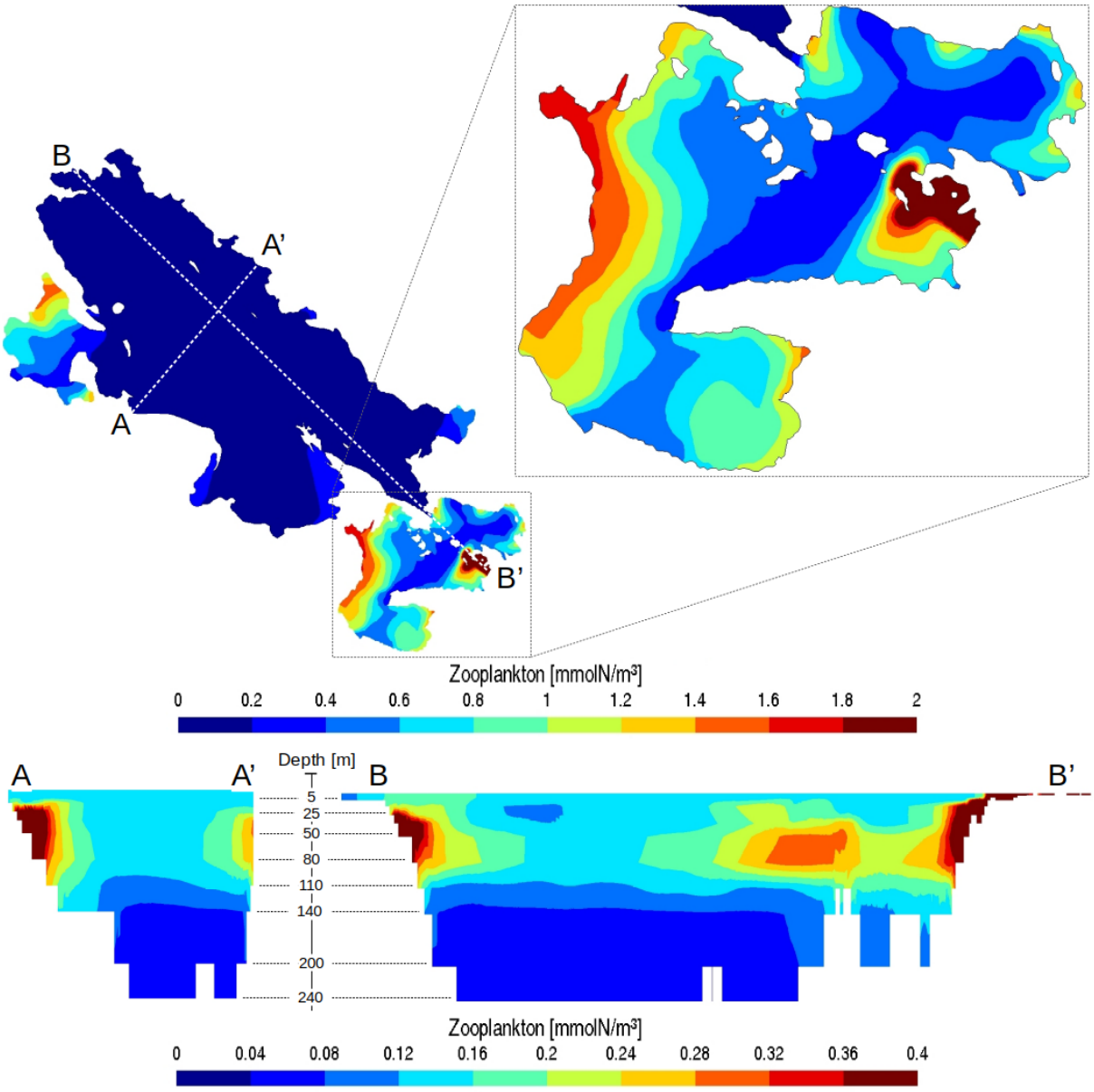

Figure 4.9: Zooplankton concentrations in Lake Titicaca

Grazing is favored by optimal temperatures (20°C) which can be found closer to the water surface, hence zooplankton concentrations are generally higher in shallow waters such as in Lago Menor or the Puno bay. Similarly as for P, we can clearly distinguish the high concentrations of Z located on the edges of the lake (see cross-sections). This is due to the lodged detritus phenomenon previously discussed, which provide sufficient phytoplankton to allow the proliferation of zooplankton in these areas.

In Lago Menor, consistently with what has been explained, zooplankton is distributed similarly to the phytoplankton.

4.4.4 Detritus

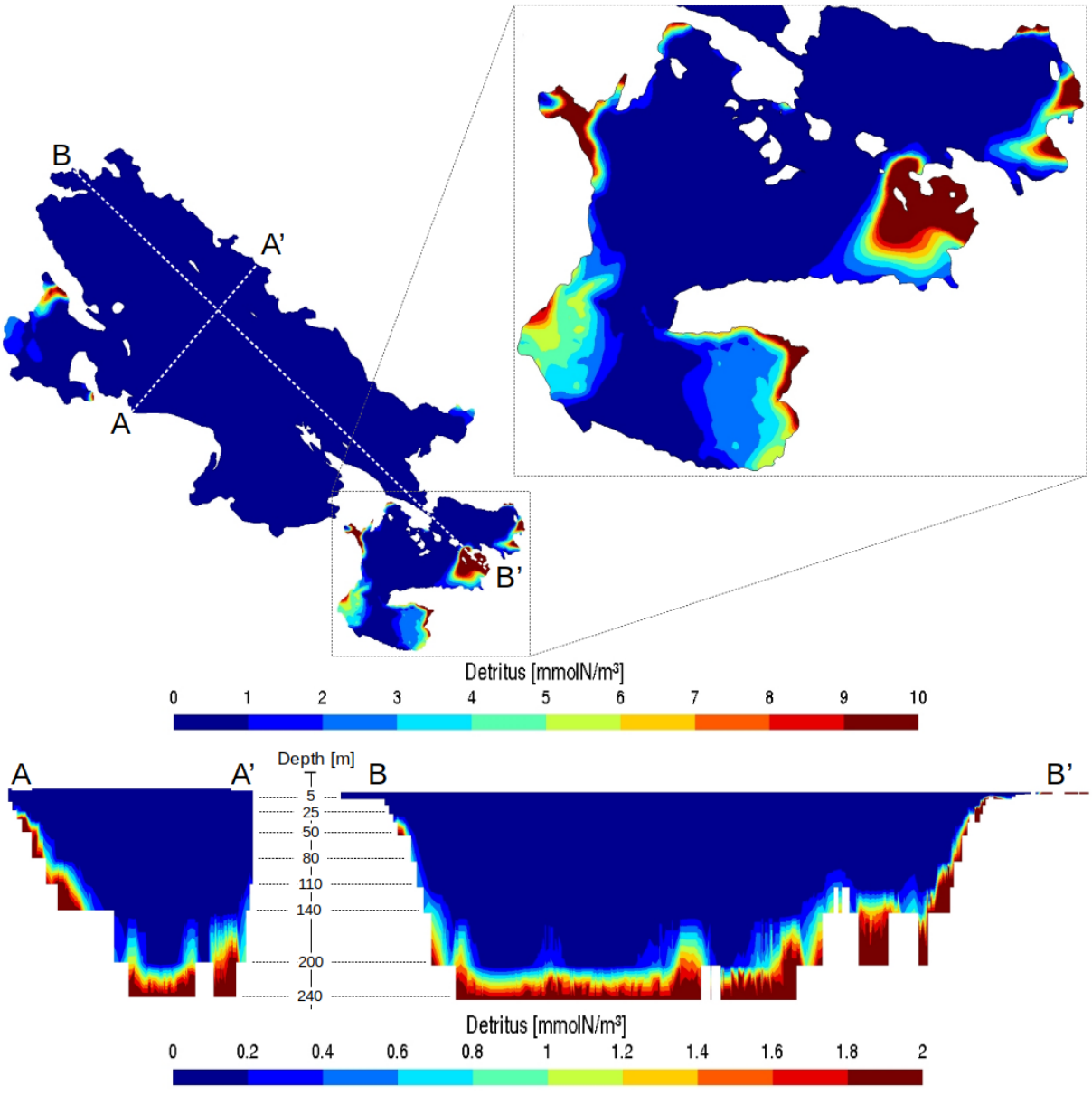

Figure 4.10: Detritus concentrations in Lake Titicaca

Detritus can be found mainly near the lake bottom where they tend to accumulate since they are subject to sinking forces (Fig. 4.10). We can see the lodged detritus previously mentioned, on the borders of the lake. The distribution of this component in Lago Menor reflects the distribution of P and Z since they are the main detritus providers through mortality. We have found that our model tends to accumulate large amounts of detritus in some punctual cavities on the bottom of the mesh. The trapped D in these cavities produce large amounts of N some times leading to large amounts of P and Z. As we will see in 5.2, this can lead to unrealistic simulations.

5 | Discussion

To determine the quality of the results obtained by our model, it is indispensable to carry out a validation process. In this section, we will mainly focus on the validations of both the hydrodynamic and the ecosystemic parts of our model by comparing our model outputs with field observations. In spite of the limited data at our disposal we were still able to shed some light on the quality of our model. This validation will provide means of knowing if our model is able to effectively simulate the hydrodynamics of the lake and if we are able to correctly represent the evolution of the main ecosystemic variables. In addition to this, we will recapitulate on the global limitations of our model and discuss how to enhance its performance. Elements of response to our main scientific question will then be brought forward. Finally, some potential applications of the model will be mentioned.

5.1 The Physical model validation

For the physical processes, we based our analysis on water temperatures. The aim of the validation is to see if our model is able to effectively reproduce the temperature profiles observed in July-August 2014 as well as the annual evolution of the thermocline during the year 2014.

Simulated temperatures coincide with in-situ observations

The main source for observation data was the technical report of the July 2014 scientific cruise CR. 1407 (Cruz et al., 2014).

In this study temperature profiles were taken on 31 locations (red triangles in Fig. 5.1). For these locations, temperatures were measured at different vertical depths. We can see that there are five main transects that cut through the lake (27 points without counting the Puno bay transect). For the blue dots, only surface temperatures are available. One of the transects passes trough Lago Menor: from the cities of Huarina to Desaguadero. The exact times of measurements were not provided for these data points, only the starting and ending date of the cruise (16^{th} of July to 3^{rd} of August) were mentioned.

For the validation of our model, we compared these observed temperature profiles with their respective simulated profiles in Fig. 5.2. Since the exact dates of measurements where not defined, we simply chose to show the simulated values extracted on the 15^{th} of

July 2014. This was considered an acceptable approximation even though it can lead to a biased analysis.

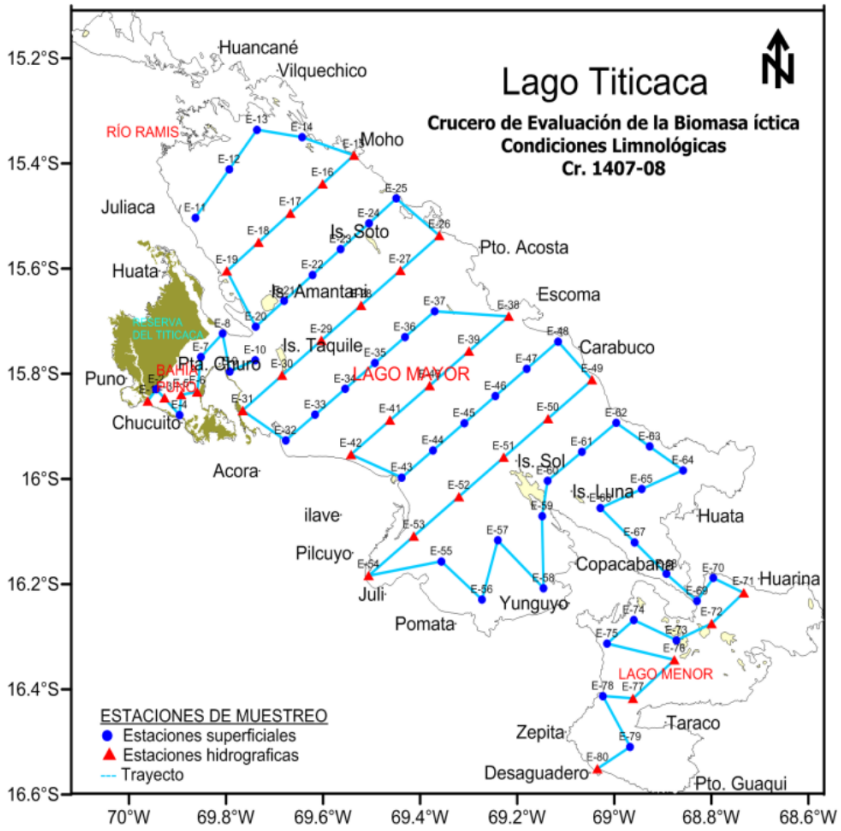

Figure 5.1: Sampling stations of the CR.1407 cruise. Hydrographic stations are shown with red triangles and superficial stations in blue. Source: Cruz et al. (2014)

We can see on Fig. 5.2, that the model is able to reproduce the observed data in most cases. The root mean squared error was computed (in red) for each location as follows:

$$RMSE = \sqrt{\frac{1}{n}\sum_{i=1}^{n}\left(modeled_i - observed_i\right)^2}$$

Where $modeled_i$ and $observed_i$ are the values at the depth i and n is the minimum nuber of available depths between the model outputs and the observations. This way, our model was compared only where both simulated and observed values exist. Indeed, for some locations, the model doesn't reach as deep as the observations, this is due to the shape of the mesh and the choice of vertical layers. The average RMSE value considering all locations is of 0.43°C. However we can clearly see that for the last transect, in Lago Menor, the model presents significant error, locations E-77 and E-80, for instance, have RMSE values close to 2°C. This error is in part linked to the skin temperature forcing applied on the top surface of the lake. This forcing, which was computed as a homogeneous value for the entire lake, does not take into account the spatial variability of the surface temperatures. We were also able to see that generally the model performs better in the deeper areas than in the shallow waters.

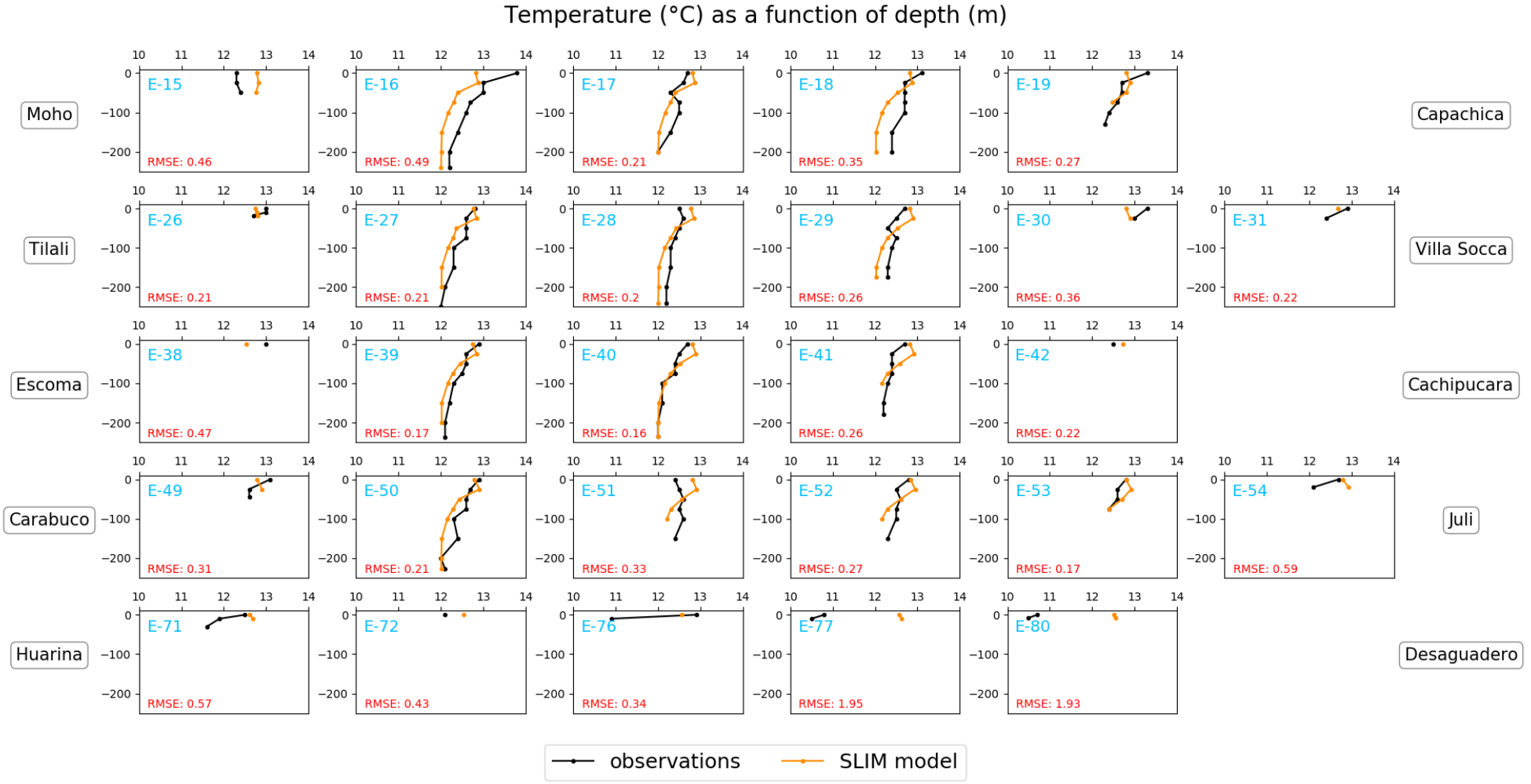

Figure 5.2: Temperature profiles over the 27 sampling points.

Each sampling station is represented by a graph showing temperature as a function of depth. The different transects shown in Fig. 5.1 are arranged horizontally spanning from north east cities (left) to the south west cities (right) according to the numbering.

Annual evolution of the thermocline is effectively reproduced

The second way to validate our model is to see if it can effectively reproduce the vertical mixing that should occur during the dry season. As we saw in Section 4.2 this is indeed the case. As the temperatures of the surface layers dropped, the thermocline disappeared, therefore allowing for the mixing with the lower layers. Looking back at Fig. 4.3, and comparing it with the observed monthly temperature profiles provided by Richerson (1992)(Fig. 5.3), we can see that our model was able to simulate the cooling of the top layers during the dry season similarly to the observations. However, a difference in the depths of the thermocline has to be noted. In our model this horizontal physical barrier is situated around 20 m whereas in Fig. 5.3 it is around 40 m. This suggests that our model has not been parameterized optimally. The surface temperature relaxation depth, which is the width of the water layer affected by the surface heating, was set to 12 m but could be changed to a deeper depth in order to better reproduce the observations.

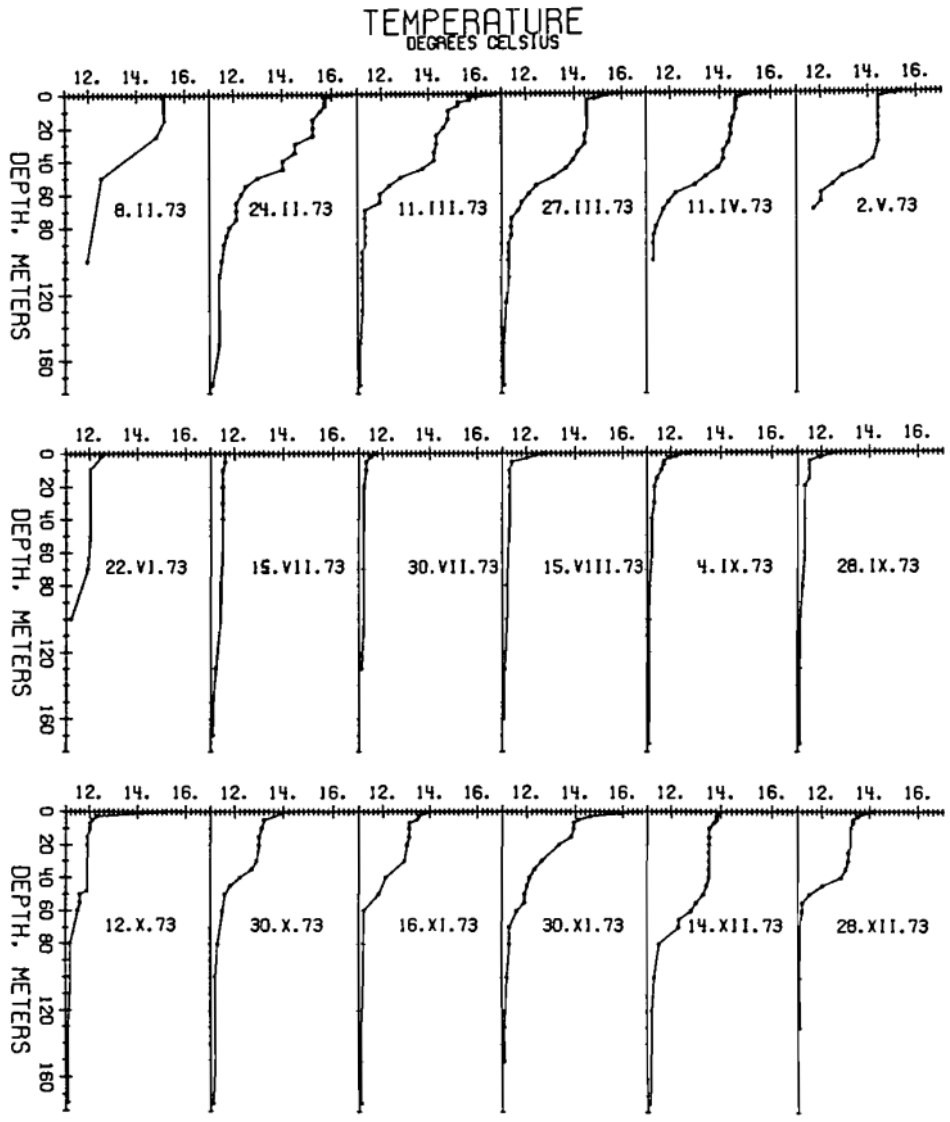

Figure 5.3: Annual evolution of the temperature profile in Lake Titicaca. Vertical mixing occurs during the dry season from June to October. Source: Richerson (1992)

Incomplete vertical mixing happens, as planned

Since the previously mentioned vertical mixing has an impact on the components of our NPZD model, we were able to visualize the mixing through the distribution of Phytoplankton and Zooplankton. Fig. 5.4 shows P and Z on the 15^{th} of August, we can see that phytoplankton and zooplankton have been dislodged from their horizontal thriving zone. Our model also allows us to identify the regions of the lake where the rise of phytopankton is the most pronounced (see Appendix D). Vertical currents have transported these components towards the surface, but not so much towards the depth. Indeed we can see that there still is a lower limit around 150 m under which neither P nor Z wanders. This is because a slight temperature gradient still remains between the surface (12.5°C) and the bottom of the lake (12°C), therefore the mixing does not happen on the entire water column. This concurrs with Richerson (1992), who says that mixing is often incomplete in Lago Mayor (see Appendix C). It is possible that colder years could lower the surface temperatures an additional half degree during July-August. In that case, temperatures in the deep would be hotter than the surface therefore allowing for complete vertical mixing. The less dense waters of the deep could move towards the surface, and the cooler surface waters would sink. Consequently, the deep waters would bring biological and chemical components from the depths towards the surface thus providing nutrients for P and Z.

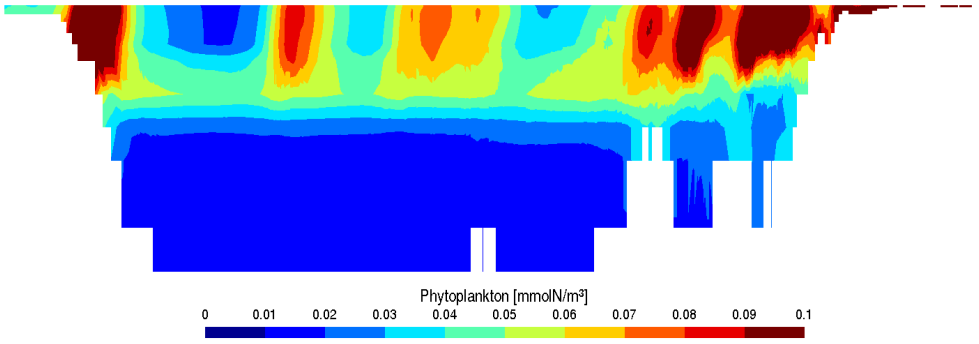

(a) Phytoplankton

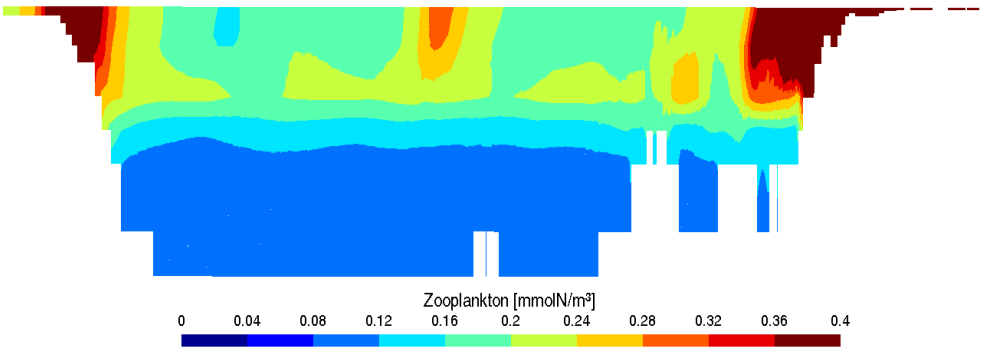

(b) Zooplankton

Figure 5.4: Phytoplankton and zooplankton during vertical mixing.

5.2 The NPZD model validation

As a mean of validation of the NPZD model we will first talk about the vertical distribution of phytoplankton in the lake. Then we will compare the simulated distribution of phytoplankton with satellite imagery of Lago Menor during the algal bloom event.

5.2.1 Vertical distribution of P in Lago Mayor

As we saw in Chapter 4, the phytoplankton in our model thrives in a horizontal zone between the depths of 35m to 130m. However, the scientific literature on the physico-chemical characteristics of Lake Titicaca suggest that pythoplankton thrives higher in the water column.

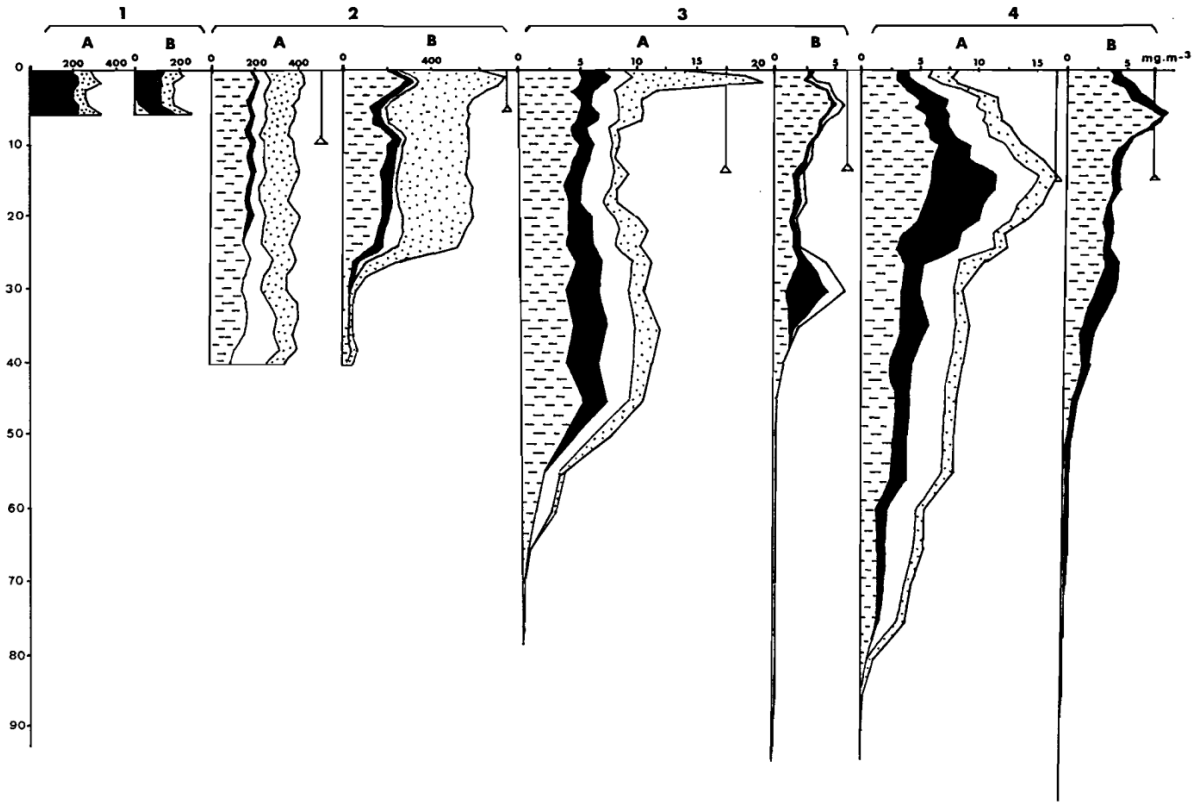

Figure 5.5: "Vertical algal biomass distribution in Lago Menor (left) and in Lago Mayor (right). 1: shallow zone of Lago Menor, 2: Chua Depression, 3:Lago Mayor close to Island of Moon, 4: close to Island of Sun; A: during mixing (13-15 July 1988), B: during stratification (14-16 December 1988). To the right of each profile is the Secchi depth reading (except the first station, where it was not possible). Dashes-cyanophytes; black-pyrrhophytes ". Source: Iltis (1992).

Firstly, Fig. 5.5 shows the vertical algal biomass distribution in Lago Menor and in Lago Mayor provided by Iltis (1992). We can see that the biomass maximum can be found at depths of 12m to 18m close to Island of Sun during mixing (4A) and between 5m to 8m during stratification (4B). Thus, phytoplankton is much closer to the surface than what our model simulated.

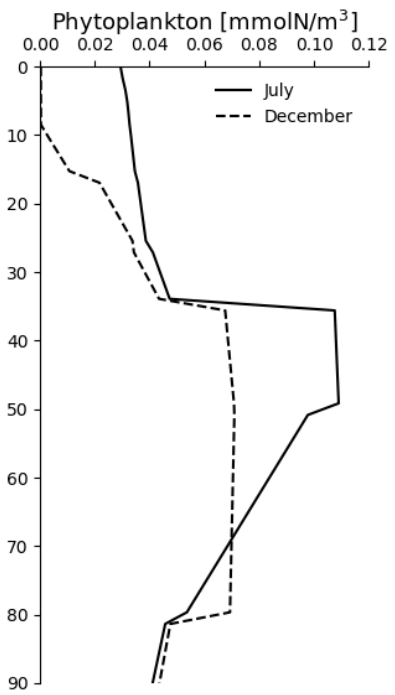

Figure 5.6: Vertical phytoplankton distribution between Isla del sol and Isla de la Luna.

Indeed, Fig. 5.6 shows the vertical profile of phytoplankton generated by our model on a point between Isla del Sol and Isla de la Luna and for the 15^{th} of July (during mixing) and the 15^{th} of December (stratification). These two islands are separated by 6.8 Km. We chose this intermediary point since no precise location of measurement was provided by Iltis (1992). We can clearly see that in our model, the maximum P mass during mixing is located between 35m and 50m which is much lower than the observations. Similarly, during the stratification period, our model simulates the maximum P concentrations between 35m to 80m whereas observations show a pronounced development of algae between 20m to 50m. This distribution of P is likely the result of an insufficient calibration of our model. Indeed, an increase in the light attenuation or the optimal temperature values could shift the thriving zone of P closer to the surface of the lake. Regarding the temporal evolution of P, we can see that during stratification, in December, the simulated P concentrations are generally smaller than during mixing. This is similar to the observed values of algal biomass on the locations of Isla del Sol and Isla de la Luna (3 and 4). This indicates that our model is able to reproduce the temporal evolution of P but in a less precise manner. Since the distribution of Z is closely related to the distribution of P, we conclude that zooplankton might also be misrepresented my our model.

5.2.2 Comparison with Landsat 8 image

Figure Fig. 5.7 shows the simulated phytoplankton for the 24^{th} of March at midday and a LANDSAT 8 image taken on the same date (Scene id: LC80010712015083LGN02). Unfortunately the satellite image doesn't cover the westernmost part of the lake on this date. The shape of the dispersion of phytoplankton just outside of Cohana bay seems satisfying. This indicates that the simulated currents managed to disperse the phytoplankton similarly as what happened during the bloom (see water curents in 4.2). However, we can see on the satellite image that some areas near the shores (yellow lines) are exempt of P. This is likely because these areas, including the Cohana bay, are in fact wetlands (see Appendix E), this might affect the transport of floating algae. Given that we didn't consider the specificities of these very shallow waters in our model, the presence in those areas is higher than in reality.

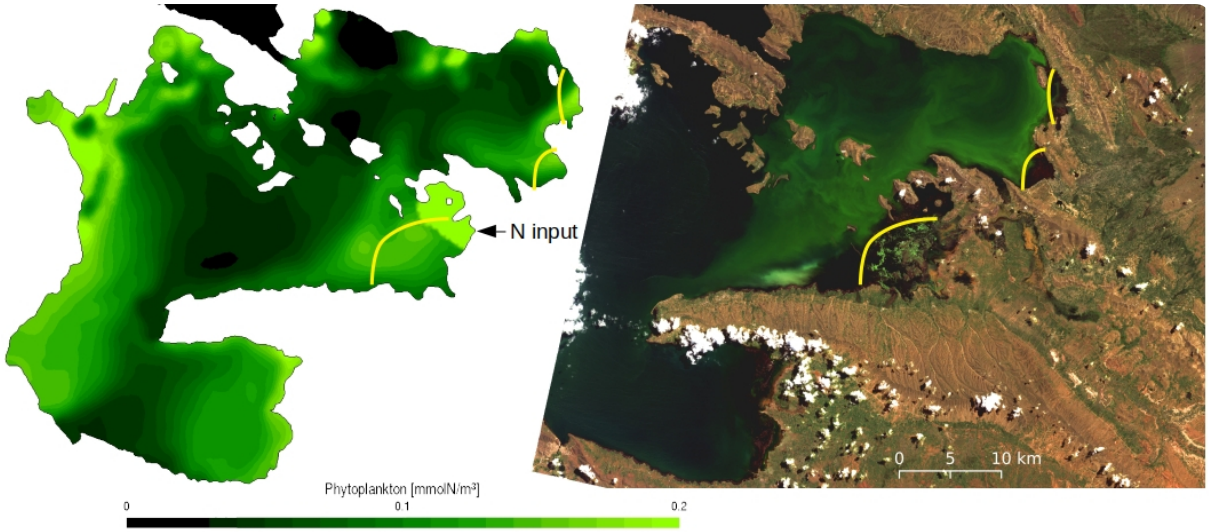

Figure 5.7: Comparison between simulated phytoplankton (left) and Landsat 8 image (right). The simulated phytoplankton concentration are shown in [mmolN/m^3].

Finally, the Lansat 8 image shows that the west side of Lago Menor is rather free of phytoplankton. Our model on the other hand, simulates large amounts of P near the western shore and down in the southern side of Lago Menor. This presence of P can be explained by the presence of detritus and nitrogen generated by the model in these regions but seems to be a misrepresentation of the reality. Some hypothesis that can explain the differences between the simulation and the satellite image can be advanced:

- The large amount of P could be related to the large amounts of D lodged in some cavities on the bottom of the mesh in the western side of Lago Menor.
- The satellite image shows only the visible surface algae whereas our model presents the Phytoplancton concentrations in water. This phytoplankton is not strictly in the form of floating algae and could thus be less visible on the western side of the lake in the Landsat 8 image.
- The erroneous values of the N input in the Cohana bay may lead to erroneous values of P in Lago Menor. As we mentioned earlier, one of the main difficulties encountered during this thesis has been to provide exact values of total nitrogen released by the Katari river over the period of interest. As one of the principal components of the NPZD model, nutrients have a significant effect on the distribution of P. We can, thus, understand that erroneous values of N lead to an incorrect dispersion of P in our model.
- Our model does not treat the effect of wind on the surface phytoplankton as it would be applied on the floating surface algae. These floating algae emerge partially out of the water thus creating more drag. Therefore, they are more subject to wind forces which can affect their dispersion throughout Lago Menor. Nevertheless, this could

be achieved using a Lagrangian particle tracker which would have a specific density and would be subject to wind drift velocities.

- Finally, another reason for this could simply be the insufficient calibration of the NPZD model.

A visual comparison with satellite imagery is clearly not an optimal validation process. Additional measurements should be taken in order to provide quantitative data that could be used to validate our model. Furthermore, a conversion from mmolN/m^3 of P to mg/m^3 of the Carteria sp. algae should be done in order to allow for the comparison of qualitative data.

In an atempt to better assess the distribution of phytoplankton in Lago Menor on the 24^{th} of March, we chose to cary out a more extensive analysis of the Landsat 8 image. For this purpose, we chose to observe Lago Menor using two different remote sensing methods: the normalized difference vegetation index (NDVI) and the chlorophyll *a* estimation algorithm for clear waters elaborated by Tenjo et al. (2014) (Chla). These two indices where obtained by performing the following raster calculations:

$$\text{NDVI} = \frac{(\text{NIR} - \text{Red})}{(\text{NIR} + \text{Red})} \tag{5.1}$$

$$\text{Chla} = 4.46 \left(\frac{\text{Geen}}{\text{Band1}} \right) - 0.55 \tag{5.2}$$

The bands used for this purpose are detailed in Table 5.1.

Bands	**Wavelengths**	**Name**
Band 1	0.43 - 0.45 µm	Costal/Aerosol
Band 3	0.53 - 0.59 µm	Green
Band 4	0.64 - 0.67 µm	Red
Band 5	0.85 - 0.88 µm	Near-Infrared

Table 5.1: Landsat 8 bands used in our analysis.

The results of these raster calculations are shown in Fig. 5.8. Firstly, in the top section of this figure we can see the NDVI index. Even though negative values of the NDVI usually do not have significant ecological meaning we realized that the shape of the bloom is well reproduced in this image. We can also see a strange pattern on the west side of the lake which is hard to interpret. It could simply be due to clouds formation, yet, we can see that it occurs only on top of the lake. It is thus hard to determine if there is any phytoplankton in this portion of the lake. The bottom section of the image shows estimates of chlorophyll *a* in [mg/m^3]. With this method we are able to detect the biggest patch of floating algae near the Cohana bay (also visible in Fig. 5.7) but it was harder to detect the smaller concentrations of chlorophyll *a*.

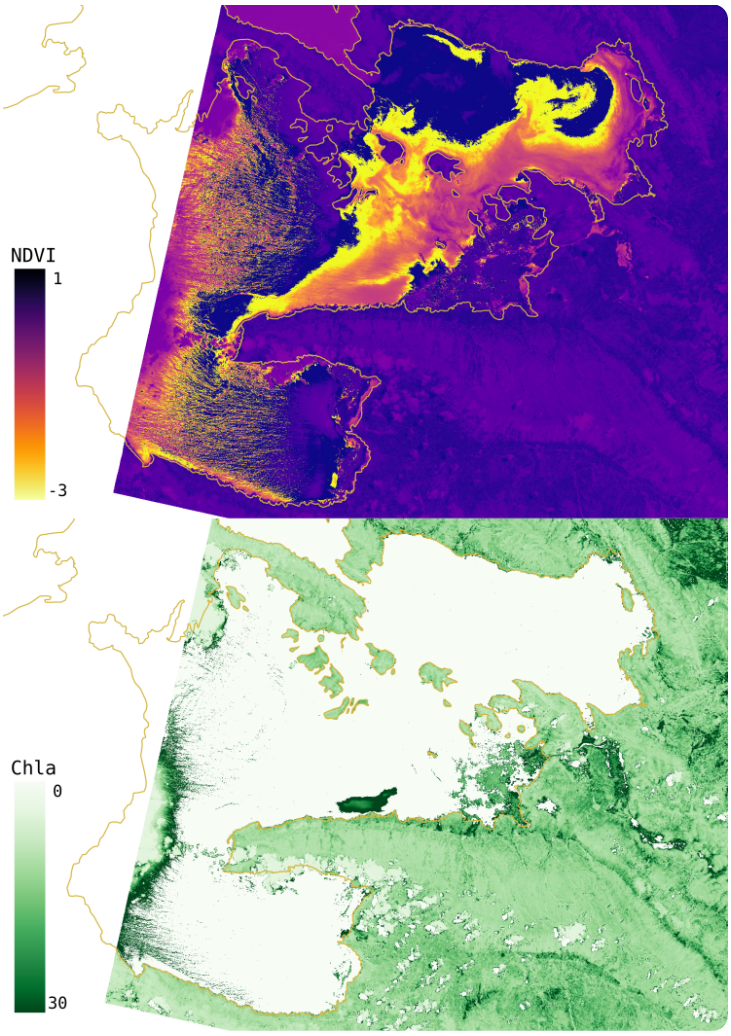

Figure 5.8: NDVI and the Tenjo et al. (2014) chlorophyll *a* index in Lago Menor.

This image also shows the presence of chlorophyll *a* on the western side of the lake. This could also be due to the effect of clouds. The doubt persists in relation to the presence or absence of phytoplankton on the western part of the lake.

Overall, this validation process for the NPZD model has yet to be conclusive. We saw that the model is able to partially simulate the shape of the algal bloom in the eastern part of the lake but that it overestimates phytoplankton concentrations on the west. However, it is important to keep in mind that a significant part of this error could be attributed to a poorly estimated N input in the Cohana bay. It would, thus, be premature to judge the performance of the NPZD model solely on this simulation. We can also say that in-situ observations can be greatly beneficial in order to make a more elaborate validation.

5.3 Limitations of our model

Given that this thesis is a first attempt of the application of our combined hydrodynamic and ecosystemic model, results are somewhat indicative. Our model is subject to multiple limitations mainly related to the quality of the inputs and to the calibration. We chose to elaborate on some of our models major drawbacks. These aspects, having been identified, can be treated in order to improve the performance of the model.

Lack of specificity of the ecosystemic model

One of the major limitations encountered during this thesis was the lack of availability of qualitative data and in-situ observations concerning the simulated dates which could help us calibrate our model. Within the framework of this thesis, multiple efforts have been

made to gather the best data available in the literature. In addition, many researchers have been contacted by mail but we received very few positive responses. This has lead us to use parameters with values that are non-specific to Lake Titicaca nor to the aquatic fauna, thus, that do not allow a realistic simulation of the water quality. A better calibration could be achieved by working in closer collaboration with local researchers and specialized scientists. This would enable better performance of the ecosystemic model.

Approximations regarding the N input in Cohana bay

With retrospective, we have considered our N input to be an incorrect estimate of the nitrogen discharge from the river Katari. Regarding the concentrations of N, it is difficult to generate such an estimate with little available data for the dates of our study. On top of this, NH_4 concentrations where not taken into account. As previously mentioned, this could cause errors in the simulation of the algal bloom. To counteract this issue, the N input must be recalculated. More importantly, for further applications, a more specific knowledge of the contaminant discharge must be known beforehand in order to effectively simulate its dispersion. Regarding the location of the N input, we chose to use a punctual source as the source of discharge. However, the Katari river meets with Lago Menor through a river delta, thus making it difficult to determine a single punctual source. To counter this, multiple punctual sources could be implemented.

Phosphorus not taken into account in our ecosystemic model

Our ecosystemic model was composed of, and limited to the N,P,Z and D components. We did not consider phosphorus as a limiting element since concentrations of soluble reactive phosphorus (SRP) available for phytoplankton growth are often high in Lake Titicaca relative to the amounts of dissolved inorganic nitrogen (DIN = NO_3^- + NO_2^- + NH_4^+). The DIN to SRP ratio, an indication of algal nutrient deficiency, being usually well below 10:1, suggests nitrogen limitation in Lake Titicaca (Iltis et al., 1992). Nevertheless, when N becomes more available, next to tributary rivers outputs for instance, phosphorus may become the limiting factor Carney et al. (1993). Thus, we consider that adding a phosphorus state variable to the model could be relevant and would allow for better estimations of algal bloom events.

Need for computational resources

In addition to the previously mentioned limitations, computational resources can, in some cases, be a limiting factor for the practical use of such a model. For this thesis, we decided to perform our simulation for the time period of 1^{st} January 2014 to the 1^{st} May 2015. The time-step was of 35 seconds (equations where resolved for every 35 sec), and results were extracted for a resolution of 6h. This gave us four outputs for each simulated day at the times of 00, 06, 12 and 18 UTC. Additionally, the 3D mesh was composed of approximately $209,680$ elements. To achieve this task, we were required to use the CECI (Consortium

des Équipements de Calcul Intensif) computer cluster. A total of 256 processors were used during approximately 9 days of calculations.

Nevertheless, the need for high performance computing should not be a major restriction since most applications of the model can be constrained to shorter simulation periods, smaller areas and/or less refined meshes.

5.4 Potential applications

The most interesting aspect of our model is the fact that it can be used for a variety of applications.

First of all, it can be greatly beneficial for any research regarding the hydrodynamics of the lake since it is able to reproduce realistic physical elements such as water currents, water temperatures but also density variations and surface elevation.

The spread of dissolved contaminants within the lake can also be simulated by our model. This allows for the study of different types of contamination by anthropogenic or natural sources. Similarly, the plastic pollution, a pertinent and current hot topic, could be addressed. The dispersion of floating particles can be simulated by SLIM3D, this could help to identify the main polluters and affected zones. Similarly, a study of the spread of heavy metals such as mercury could reveal the most affected zones of the lake.

The N, P, Z and D populations could serve as indicators to monitor the water quality in response to different stresses. However, additional elements such as dissolved oxygen concentrations could be computed by our model for a better water quality assessment.

Forecasting is one of the major assets of our model. Indeed, its basic inputs consist of the winds and surface temperature forcings, both are derived of global climate models which can provide predicted values for the future. Hence, our coupled SLIM3D-NPZD model could be used as a predictive tool. With this application in mind, it could be possible to run the model for different case scenarios, simulating the evolution of the lake for different forcings or different imposed stresses. This type of use of the model could be envisaged for the impact assessment of new environmental policies. Our model could also help in the sizing of water treatment facilities, for instance, in the Katari watershed. Indeed, by changing the amount of the nitrogen based nutrients input in the Cohana bay, we can predict the reaction of the NPZD ecosystem.

Lastly, if water inflows and outflows are explicitly taken into consideration, our model could be used to evaluate evolution of lake surface altitudes, therefore predicting potential floods.

Overall this model seems to have a large potential in environmental protection efforts as well as for scientific research.

6 | Conclusion

6.1 Summary

In this thesis, we have provided a new tool that can be used to study Lake Titicaca's hydrodynamics and water quality. This was achieved by coupling NPZD ecosystem-type model to an underlying hydrodynamic model. Our study focused on the entire Lake Titicaca, and we developed a case study on the smaller section of this lake: Lago Menor.

The simulation of the lake's hydrodynamics was covered by the 3D version of the Second-generation Louvain-la-Neuve Ice-Ocean Model. An unstructured mesh of Lake Titicaca was built and SLIM3D mobilized the finite elements method solving the three-dimensional hydrodynamic equations under the Boussi-nesq approximation on each element of this mesh. On top of this, we coupled a NPZD ecosystem-type model, which allowed us to simulate the evolution of the nitrogen based nutrients, phytoplankton, zooplankton and detritus within the lake for the period of January 2014 to May 2015. The model inputs were the bathymetry, surface temperatures as well as wind direction and speeds. Winds and surface temperatures represent the major forcings that affect the hydrodynamics of the lake, they were obtained from the NOAA's CFS and the ERA5 climate reanalysis models respectively.

With the goal of providing an example of the potential uses of this coupled SLIM3D-NPZD model for lake environments, we elaborated a case study. This study was centered on the Cohana bay, eastern part of Lago Menor, in which significant nitrogen discharge is caused by anthropogenic activities upstream in the Katari watershed. We simulated this contamination by introducing an artificial input of nitrogen to the lake. By these means we were able to simulate the contamination in phytoplankton similarly to the bloom event occurred in March-April 2015.

We chose to exploit the following results provided by the coupled SLIM3D-NPZD model:

- **Lake temperatures:** allowed us to study the evolution of the thermocline over the period of interest.
- **U and v components of water velocity:** allowed us to identify the principal water flow tendencies.
- **NPZD components:** showed us the spatial and temporal evolution of the nitrogen,

phytoplankton, zooplankton and detritus.

In order to evaluate the validity of our coupled SLIM3D-NPZD model, we compared our results with observed data.

The major bottleneck of this thesis has been the difficulty to find qualitative data regarding the physico-chemical characteristics of Lake Titicaca for the period of interest, therefore, making it hard to perform valid assessments of our models performance. In his thesis, Aguirre Céspedes (2009), who used the ELCOM model on Lake Titicaca, had already mentioned the lack of available observation data that could be used to validate such models. In spite of the limited data at our disposal we were still able to shed some light on the quality of our model.

For the hydrodynamic component, we were able to generate similar temperature profiles as those observed by the Cruz et al. (2014) scientific cruise. Additionnaly, we managed to replicate the annual evolution of the thermocline as described by Richerson (1992). This proves that our model is able to effectively simulate the hydrodynamics of Lake Titicaca.

As for the NPZD component, we compared the vertical phytoplankton distributions generated by our model with the distribution observed by Iltis (1992). This allowed us to see that our model tends to simulate phytoplankton lower in the water column than observed but was able to grasp the temporal evolution of this variable. Additionally, we compared the simulated bloom with satellite imagery for the 24^{th} of March 2015. We saw that our model was able to simulate a similar shape of phytoplankton spread as the one observed with the Landsat 8 image near the Cohana bay but that our model simulated unusual amounts of P on the western side of Lago Menor. Thus, we can say that our model globally covers the behavior and evolution of the different plankton communities but lacks in precision. This can be achieved with a better calibration that would take into account the specificity of Lake Titicaca.

Overall, the validation suggests that our coupled SLIM3D-NPZD model achieved the tasks of simulating Lake Titicaca's hydrodynamics but lacks a good calibration in order to correctly simulate water quality. Nevertheless, we were already able to foresee a few applications for this model. These range from the use of the model for research purposes to the forecasting and scenario analysis in more practical circumstances.

6.2 Elements of response to our main scientific question

To recall, our scientific question was the following: *How to grasp the complexity of Lake Titicaca in an easy to use model that enables water quality analyses and facilitates informed decision making?* Now that we have seen our results and have performed some validations of the model, our main question can be answered in three parts.

- *Were we able to grasp the complexity of Lake Titicaca including its hydrodynamics*

and its basic ecosystemic behavior?
As we saw in Chapter 4, the hydrodynamics of the lake have been fairly well simulated. We were able to reproduce the temperature evolutions throughout the period of interest in a realistic manner. However, a fine-tuning of the model is still required as some issues, that were earlier identified, need to be addressed. For instance, a deeper surface temperature relaxation depth needs to be implemented. This would lead to a better simulation of the thermocline. Furthermore, a σ-level type mesh should be used to bypass the lodged detritus phenomenon which generates unrealistic results. In spite of these errors related to the hydrodynamic model, the ecosystem of Lake Titicaca seems to have been globally well covered. Indeed, conserning the NPZD components, we saw that these behaved in a realistic manner. However, this ecosystemic model could be improved with a calibration more aligned with the specificity of the lake. This would allow to effectively simulate water quality.

- *Is our model easy to use?*
We consider that it is, indeed, easy to use. As described in Table 3.2, the NPZD model is composed of only 4 state variables and 6 governing processes. It requires the calibration of 19 parameters, some more important than others, and needs initial values of N,P,Z and D. This means it is easier to calibrate than models of greater complexity which some times have more than 20 state variables and many more governing processes. However, we have to mention the need for site-specific data for this calibration. For the hydrodynamic component, the following inputs have to be provided: winds, surface temperatures and the bathymetry. Yet, nowadays, these are all accessible data.

- *Does it facilitate informed decision making?*
At this stage, we cannot conclude that this is indeed the case. A better validation needs to be conducted primarily on the NPZD component in order to better assess the quality of our model. In any case, a better calibration of the latter seems indispensable. Moreover, an improved estimation of the N input in the Cohana bay is needed in order to simulate a more realistic forcing. Once these corrections are applied, our model could be used for a variety of applications ranging from testing solutions for treating the algal bloom, to studying the impact of preventive actions such as building water treatment facilities.

6.3 Future research suggestions

During this thesis, we have laid down the groundwork for a useful/powerful model that could serve as a predictive tool in the efforts of preserving the natural environment of Lake Titicaca. As we have mentioned, the next step that needs to be done with this model is to perform a calibration that would better take into account the specificity of the Lake. For this purpose, research could be done in order to find the best match for the parameters of the NPZD model.

Once this calibration is performed, several additions to this model could be implemented. For instance, in order to better estimate the amount of the nutrients provided by the Katari river, more work should be done taking into account the different sources of contamination of the watershed and the evolution of the water discharge in time. Pluviometry and water runoff measures could also be leveraged to build predictions regarding the N discharge into the Cohana bay.

With regard to the implementation of the ecosystemic component to SLIM3D, it would be interesting to replicate our model on other water bodies. This way, the performance of the NPZD model linked with SLIM3D could be tested for distinct environments.

The NPZD ecosystem-type is not the only ecosystemic model available in the literature, It would be interesting to couple SLIM3D to other types of ecosystemic models that would take into account other state variables such as phosphorus or bacteria. By comparing their performance we would be able to identify which model works best for water quality analysis of Lake Titicaca.

Finally, more work could be done in order to find a way to better simulate the dynamics of the spread of contaminants in the wetlands.

References

Achá, D., Guédron, S., Amouroux, D., Point, D., Lazzaro, X., Fernandez, P. E., and Sarret, G. (2018). Algal Bloom Exacerbates Hydrogen Sulfide and Methylmercury Contamination in the Emblematic High-Altitude Lake Titicaca. *Geosciences*, 8(12):438.

Aguirre Céspedes, C. A. (2009). Simulación numérica de la hidrodinámica del Lago Titicaca, frente a las costas de la ciudad de Puno en el Perú. *Universidad Nacional Mayor de San Marcos*.

Anderson, T. R. (2005). Plankton functional type modelling: running before we can walk? *Journal of Plankton Research*, 27(11):1073–1081.

Ap, D., Duwig, C., Spadini, L., Uzu, G., Guedron, S., C. Morel, M., Cortez, R., Ramos Ramos, O., Chincheros, J., and Martins, J. (2017). How Uncontrolled Urban Expansion Increases the Contamination of the Titicaca Lake Basin (El Alto, La Paz, Bolivia). *Water, Air, & Soil Pollution*, 228.

Carney, H. J., Binford, M. W., Marin, R. R., and Goldman, C. R. (1993). Nitrogen and phosphorus dynamics and retention in ecotones of Lake Titicaca, Bolivia/Peru. *Hydrobiologia*, 251(1):39–47.

Chudnoff, S. (2009). A Water Quality Assessment of the Rio Katari River and its Principle Tributaries, Bolivia. *Water Resources Professional Project Reports*.

Cruz, R. C., Cruz, L. L., Calderon, J., Puntaca, L., Casa, C., Yujra, E., Amaru, G., and Mamani, H. S. (2014). CRUCERO DE EVALUACIÓN DE RECURSOS PESQUEROS Y CONDICIONES LIMNOLÓGICAS DEL LAGO TITICACA – CR. 1407.

Cruz, R. C., Mamani, H. S., Quispe, C. V., Canales, G. R. V., and Herrera, L. E. (2013). CRUCERO DE EVALUACIÓN DE RECURSOS PESQUEROS Y CONDICIONES LIMNOLOGICAS DEL LAGO TITICACA – CR. 1310- 2013.

Dejoux, C., ed., Iltis, A., and ed. (2013). Lake Titicaca : a synthesis of limnological knowledge. page 611.

Delandmeter, P., Lambrechts, J., Legat, V., Vallaeys, V., Naithani, J., Thiery, W., Remacle, J.-F., and Deleersnijder, E. (2018). A fully consistent and conservative vertically adaptive coordinate system for SLIM 3d v0.4 with an application to the thermocline oscillations of Lake Tanganyika. *Geoscientific Model Development*, 11(3):1161–1179.

Delclaux, F., Coudrain, A., and Condom, T. (2007). Evaporation estimation on Lake

Titicaca: a synthesis review and modelling. *Hydrological Processes*, 21(13):1664–1677.

Duwig, C., Archundia, D., Lehembre, F., Spadini, L., Morel, M. C., Uzu, G., Chincheros, J., Cortez, R., and Martins, J. M. F. (2014). Impacts of Anthropogenic Activities on the Contamination of a Sub Watershed of Lake Titicaca. Are Antibiotics a Concern in the Bolivian Altiplano? *Procedia Earth and Planetary Science*, 10:370–375.

Friedrichs, M. and E. Hofmann, E. (2001). Physical control of biological processes in the central equatorial Pacific Ocean. *Deep-sea Research Part I-oceanographic Research Papers - DEEP-SEA RES PT I-OCEANOG RES*, 48:1023–1069.

Fulton, E. A., Smith, A. D. M., and Johnson, C. R. (2003). Effect of complexity on marine ecosystem models. *Marine Ecology Progress Series*, 253:1–16.

Gammons, C. H., Slotton, D. G., Gerbrandt, B., Weight, W., Young, C. A., McNearny, R. L., Cámac, E., Calderón, R., and Tapia, H. (2006). Mercury concentrations of fish, river water, and sediment in the Río Ramis-Lake Titicaca watershed, Peru. *The Science of the Total Environment*, 368(2-3):637–648.

Guedron, S., Point, D., Acha C., D., Bouchet, S., Baya, P., Tessier, E., Monperrus, M., Molina, C., Groleau, A., Chauvaud, L., Thebault, J., Amice, E., Alanoca, L., Duwig, C., Uzu, G., Lazarro, X., Bertrand, A., Bertrand, S., Barbraud, C., and Amouroux, D. (2017). Mercury contamination level and speciation inventory in Lakes Titicaca & Uru-Uru (Bolivia): Current status and future trends. *Environmental Pollution*, 231:262–270.

Heinle, A. and Slawig, T. (2013). Internal dynamics of NPZD type ecosystem models. *Ecological Modelling*, 254(C):33–42.

Ibáñez Luna, C., Hugueny, B., Esquer Garrigos, Y., Zepita, C., and Gutierrez, R. (2014). Biodiversidad íctica en el lago titicaca. In *Línea base de conocimientos sobre los recursos hidrológicos e hidrobiológicos en el sistema TDPS con enfoque en la cuenca del Lago Titicaca*, pages 134–153.

Iltis, A. (1992). Phytoplankton : quantitative aspects and population. In Dejoux, C. and Iltis, A., editors, *Lake Titicaca : a synthesis of limnological knowledge*, volume 68 of *Monographiae Biologicae*, pages 182–195. Kluwer Academic, Dordrecht.

Iltis, A., Carmouze, J.-P., Lemoalle, J., Arze, C., Quintanilla, J., Guyot, J. L., Wasson, J.-G., Calle, H., Richerson, P. J., Wurtsbaugh, W. A., Vincent, W. F., Vincent, C. L., Carney, H. J., and Tapia, R. A. (1992). Physico-Chemistry. In Dejoux, C. and Iltis, A., editors, *Lake Titicaca: A Synthesis of Limnological Knowledge*, Monographiae Biologicae, pages 89–160. Springer Netherlands, Dordrecht.

IPCC, editor (2014). *Climate Change 2013 - The Physical Science Basis: Working Group I Contribution to the Fifth Assessment Report of the Intergovernmental Panel on Climate Change*. Cambridge University Press, Cambridge.

Jackett, D. R., McDougall, T. J., Feistel, R., Wright, D. G., and Griffies, S. M. (2006). Algorithms for density, potential temperature, conservative temperature, and the freezing temperature of seawater. *Journal of Atmospheric and Oceanic Technology*,

23(12):1709–1728.

K2/AP05/J13 (2013). Informe de auditoría sobre el desempeño ambiental respecto a la contaminación hídrica en la cuenca del río Katari y la Bahía de Cohana. Informe no publicado. Ministerio de Medio Ambiente y Agua, Ministerio de Minería y Metalurgia, Ministerio de Relaciones Exteriores, Gobierno Autónomo Departamental de La Paz, Gobiernos Autónomos Municipales de El Alto, Viacha, Laja, Pucarani y Puerto Pérez, Empresa Pública y Social de Agua y Saneamiento (EPSAS), Empresa Municipal de Aseo de El Alto (EMALT) y el Fondo Nacional de Inversión Productiva y Social (FPS), La Paz. 268 p.

Kawamiya, M., Kishi, M. J., and Suginohara, N. (2000). An ecosystem model for the North Pacific embedded in a general circulation model: Part I: Model description and characteristics of spatial distributions of biological variables. *Journal of Marine Systems*, 25(2):129–157.

Kroll, O., Hershler, R., Albrecht, C., Terrazas, E. M., Apaza, R., Fuentealba, C., Wolff, C., and Wilke, T. (2012). The endemic gastropod fauna of Lake Titicaca: correlation between molecular evolution and hydrographic history. *Ecology and Evolution*, 2(7):1517–1530.

Lavenu, A. (1991). Formación geológica y evolución. *El Lago Titicaca: Síntesis Del Conocimiento Limnológico Actual*.

Lazzaro, X., Rybarczyk, H., Meziane, T., Hubas, C., Lamy, D., Point, D., Martinez, J., Guedron, S., Duwig, C., Groleau, A., Rocha Lupa, S., P. Alcoreza Ortiz, M., Lanza, W., J. Flores, A., Loayza Torrico, E. Z., Ibañez Luna, C., Nuñez-Villalba, J., Gamarra Peralta, C., Villanueva Quispe, C., and Acha C., D. (2016). Accelerated eutrophication in Lake Titicaca : historical evolution, mechanisms, monitoring, and observatory approach.

Lima, I. Q., Muñoz, M. O., Ramos, O. E. R., Bhattacharya, P., Choque, R. Q., Aguirre, J. Q., and Sracek, O. (2019). Hydrochemical assessment with respect to arsenic and other trace elements in the Lower Katari Basin, Bolivian Altiplano. *Groundwater for Sustainable Development*, 8:281–293.

Martinez Gonzales, I., Zuleta Roncal, R., Pancheco Miranda, A., and Sanjines Gotilla, J. (2007). Co-operation on the Lake Titicaca. *UNESCO-IHP*, page 118.

meteoblue (2019). Weather archive Isla del Sol, https://www.meteoblue.com/en/weather/forecast/archive/isla-del-sol_bolivia_3904119.

MMAyA (2014). ANEXO 2: TABLAS DE DATOS. In *Informe de Monitoreo de Calidad Hídrica Cuenca Katari*. Ministerio de Medio Ambiente y Agua.

Molina, C., Lazzaro, X., Guedron, S., and Acha C., D. (2017). Contaminación de la Bahía de Cohana, Lago Titicaca (Bolivia) : desafíos y oportunidades para promover su recuperación.

Monroy, M., Maceda-Veiga, A., and de Sostoa, A. (2014). Metal concentration in water, sediment and four fish species from Lake Titicaca reveals a large-scale environmental

concern. *Science of The Total Environment*, 487:233–244.

Naithani, J., Darchambeau, F., Deleersnijder, E., Descy, J.-P., and Wolanski, E. (2007). Study of the nutrient and plankton dynamics in Lake Tanganyika using a reduced-gravity model. *Ecological Modelling*, 200(1):225.

Okubo, A. (1971). Oceanic diffusion diagrams. *Deep Sea Research and Oceanographic Abstracts*, 18(8):789–802.

Olascoaga, M. J., Idrisi, N., and Romanou, A. (2005). Biophysical isopycnic-coordinate modelling of plankton dynamics in the Arabian Sea. *Ocean Modelling*, 8(1):55–80.

Platt, T., Gallegos, C., and Harrison, W. (1980). Photoinhibition of photosynthesis in natural assemblages of marine phytoplankton. *Journal of Marine Research*, 38:687–701.

Pérez, W. (2015). Dos toneladas de ranas, peces y aves mueren en el Titicaca - La Razón.

R. Hood, R., E. Kohler, K., P. McCreary, J., and Smith, S. (2003). A four-dimensional validation of a coupled physical–biological model of the Arabian Sea. *Deep Sea Research Part II: Topical Studies in Oceanography*, 50:2917–2945.

Richerson, P. (1992). The thermal stratification regime in Lake Titicaca. *Lake Titicaca. A Synthesis of Limnological Knowledge (C. Dejoux \& A. Iltis, Editors)*, pages 120–130.

Ronchail, J., Espinoza, J. C., Callède, J., and Lavado, W. (2014). Evolucion del nivel del Lago Titicaca durante el siglo XX. page 16.

Salvarredy-Aranguren, M. M., Probst, A., Roulet, M., and Isaure, M.-P. (2008). Contamination of surface waters by mining wastes in the Milluni Valley (Cordillera Real, Bolivia): Mineralogical and hydrological influences. *Applied Geochemistry*, 23(5):1299–1324.

Scannone, F. (2016). What is eutrophication? Causes, effects and control.

Tenjo, C., Ruiz-Verdú, A., Delegido, J., Peña, R., and Moreno, J. (2014). Determinación de componentes ópticamente activos en aguas continentales a partir de imágenes Landsat-8. *UD y la geomática*, (9):37–46.

Tian, R., Chen, C., Qi, J., Ji, R., Beardsley, R. C., and Davis, C. (2015). Model study of nutrient and phytoplankton dynamics in the Gulf of Maine: patterns and drivers for seasonal and interannual variability. *ICES Journal of Marine Science*, 72(2):388–402.

Vallaeys, V., Kärnä, T., Delandmeter, P., Lambrechts, J., Baptista, A., Deleersnijder, E., and Hanert, E. (2018). Discontinuous Galerkin modeling of the Columbia River's coupled estuary-plume dynamics. *Ocean Modelling*, 124.

WWDR, U. (2003). *Water for people, water for life: the United Nations world water development report; a joint report by the twenty-three UN agencies concerned with freshwater*. UNESCO Publishing Paris.

Appendices

A | Land use (2010)

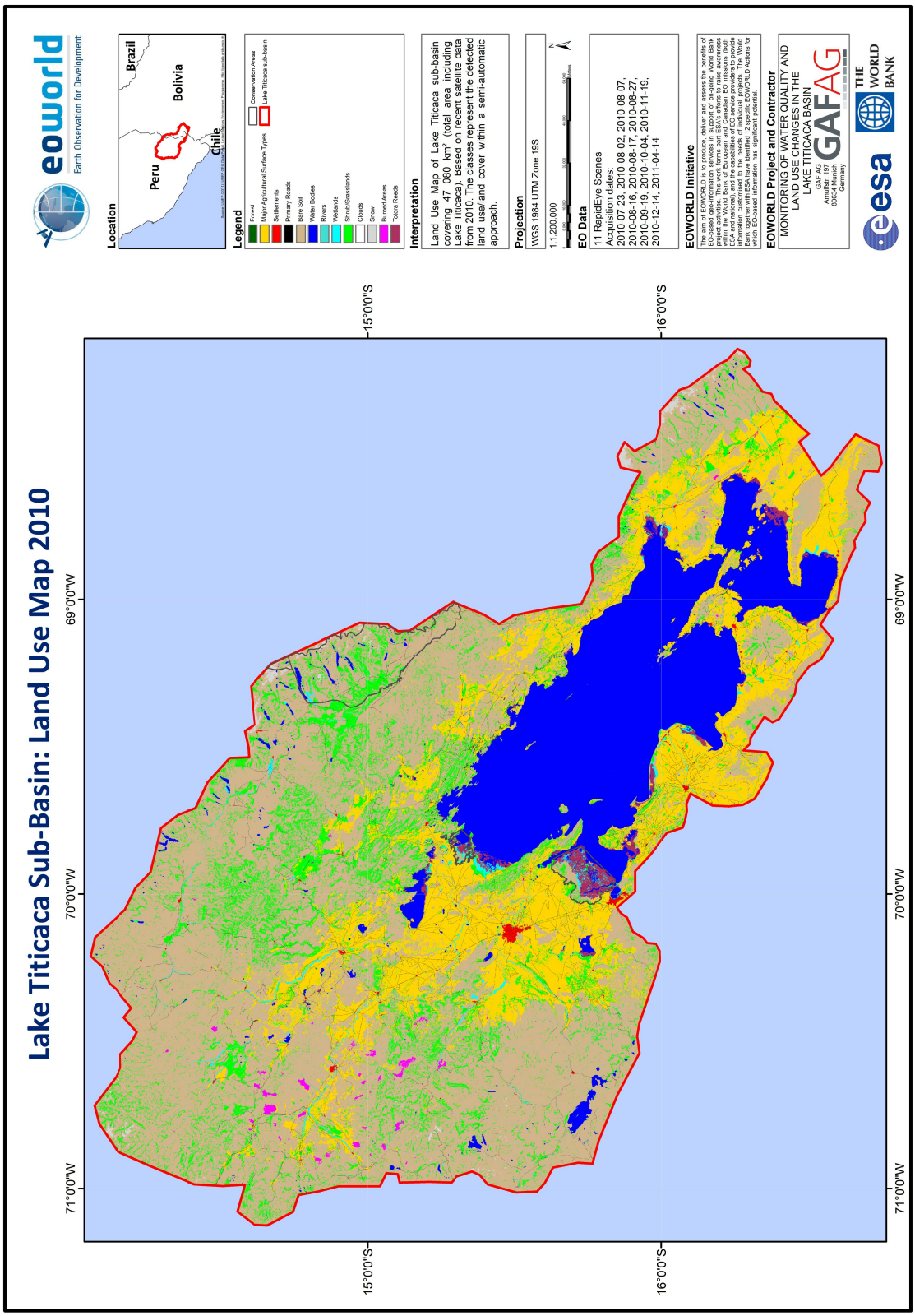

Figure A.1: Land use (2010), we can see that the most present type of landuse around Lake Titicaca consist of "Major Agricultural Surface Types"(orange) and "Shrubs/Grasslands" (green). "Bare soil" is represented in brown.

B | Horizontal water velocity (February 2014)

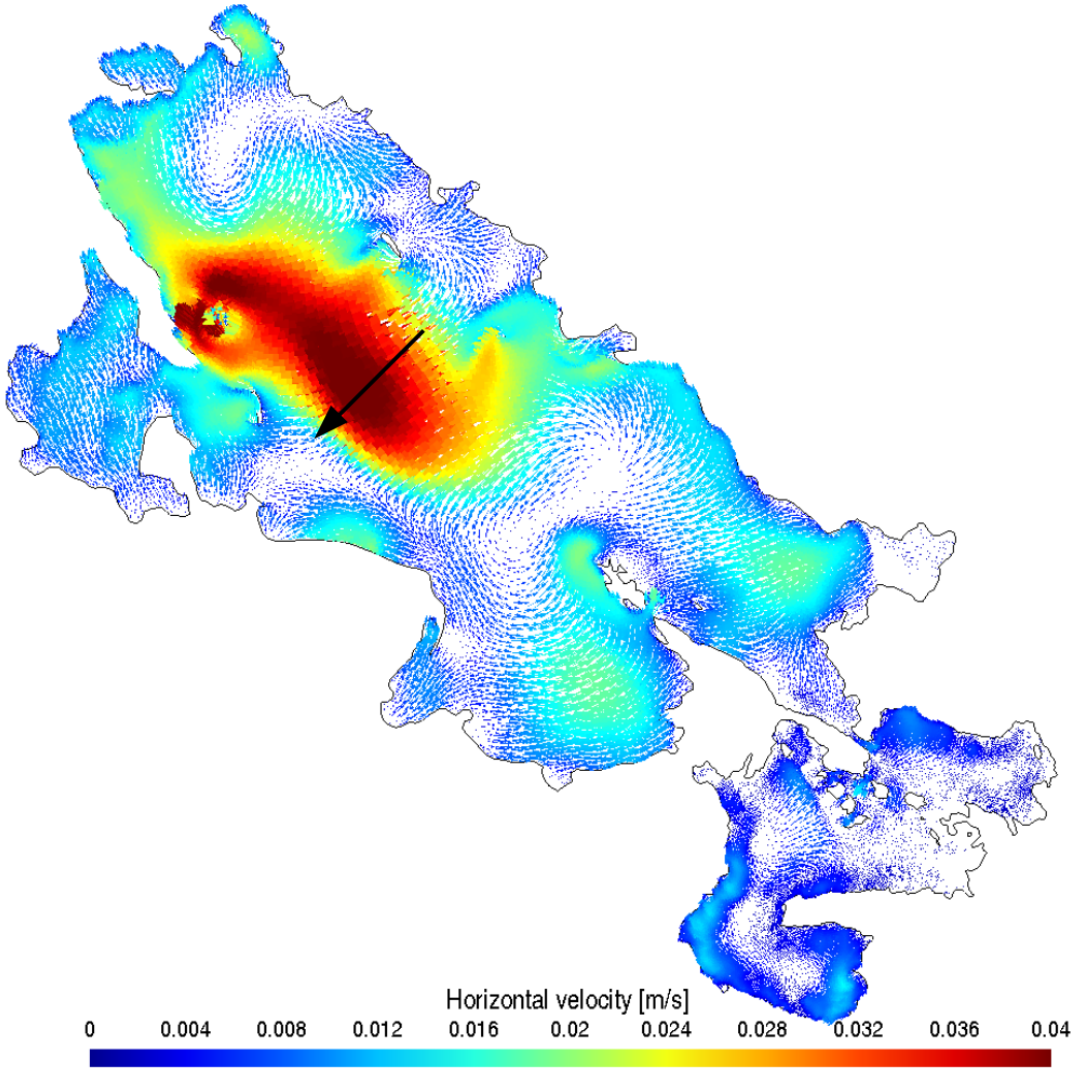

Figure B.1: Water horizontal velocity (m/s) for the 15^{th} of February 2014 at midday. We can see that currents in the northen center part of the lake flow mainly towards the south-west.

C | Monomictic property of the lake

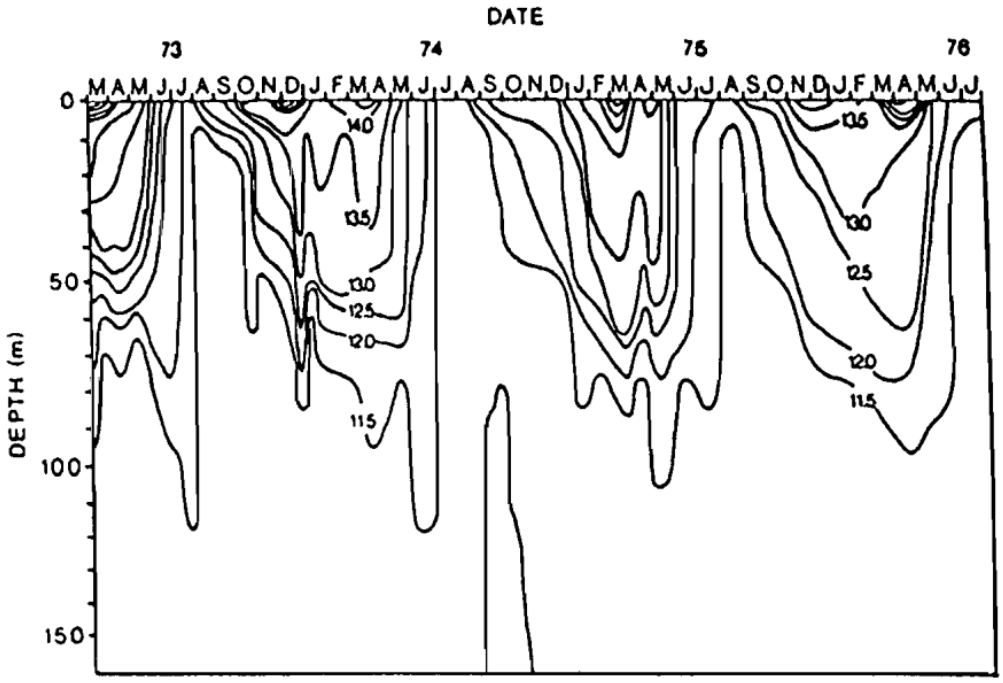

Figure 2. Isotherms in°C versus depth and time for the 1973–1976 period (Taylor and Aquize Jaen, 1984).

Figure C.1: We can see that temperatures homogenize during July-August when vertical mixing occurs. Source: Richerson (1992)

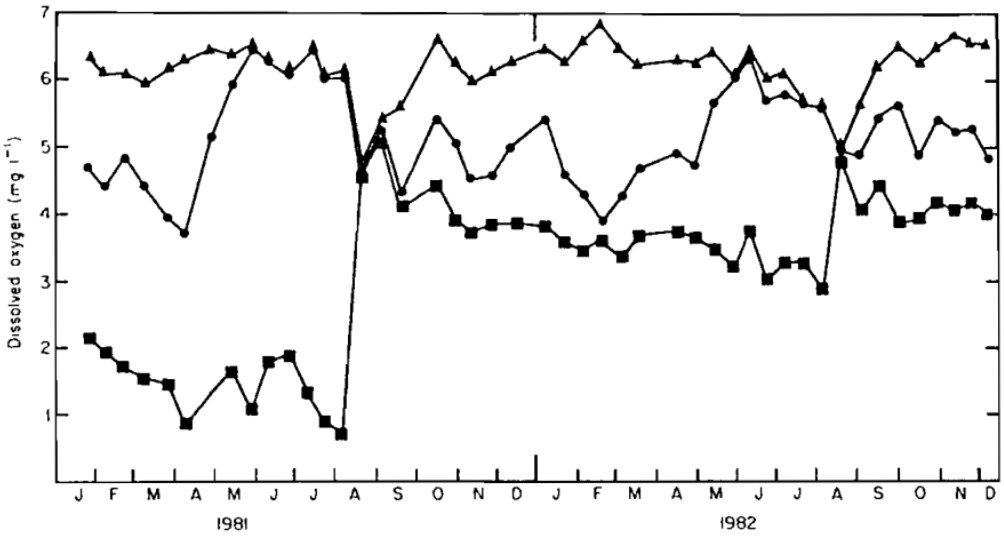

Figure 3. Dissolved oxygen concentrations at three depths in Lago Grande. 20 m, ▲; 50 m, ●; 150 m, ■ (Vincent *et al.*, 1985).

Figure C.2: Mixing occurs in August. We can see that on that month, dissolved oxygen concentrations are homogeneous throughout the water column between the surface to 150m of depth. Source: Richerson (1992).

D | Phytoplankton on the 15^{th} of August

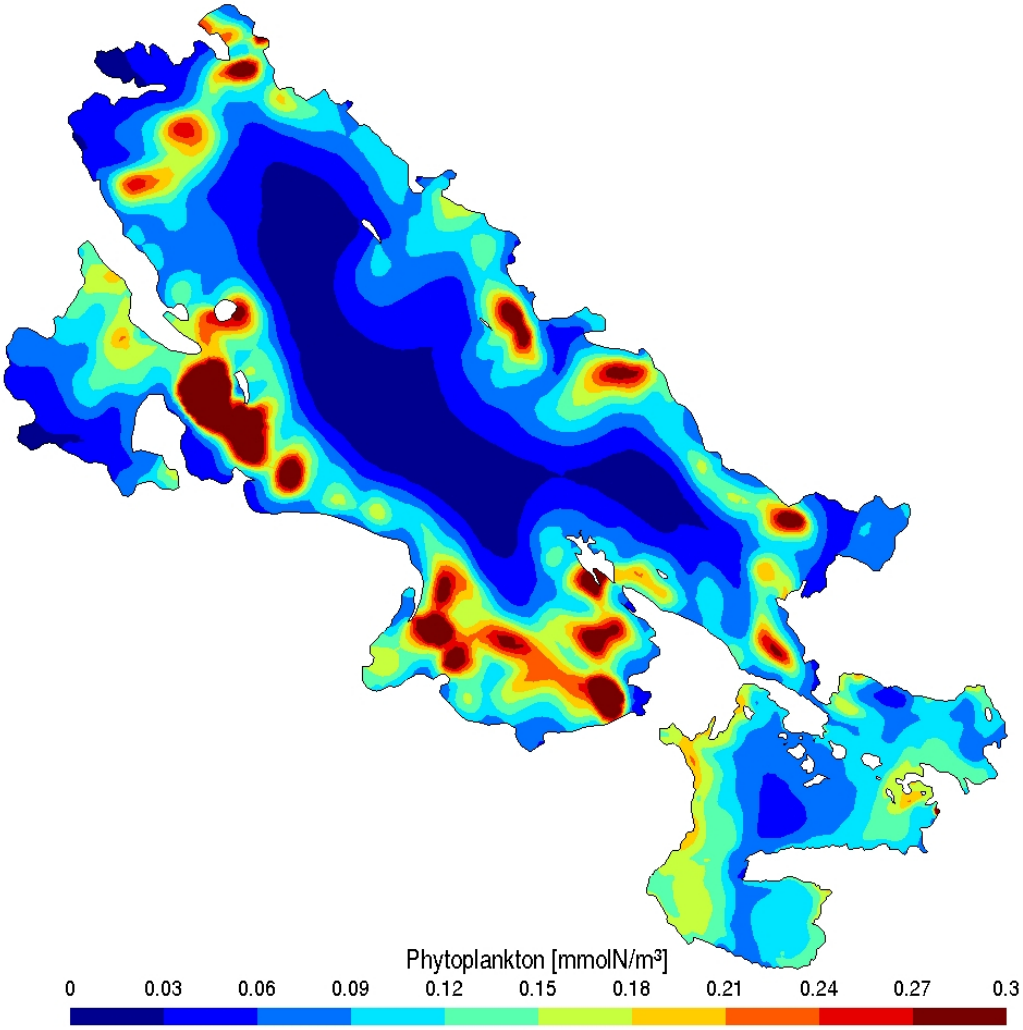

Figure D.1: Phytoplankton in LakeTiticaca on the 15^{th} of August as seen from above. We can see that P concentrations are high near the borders of the lake.

E | Flood prone areas

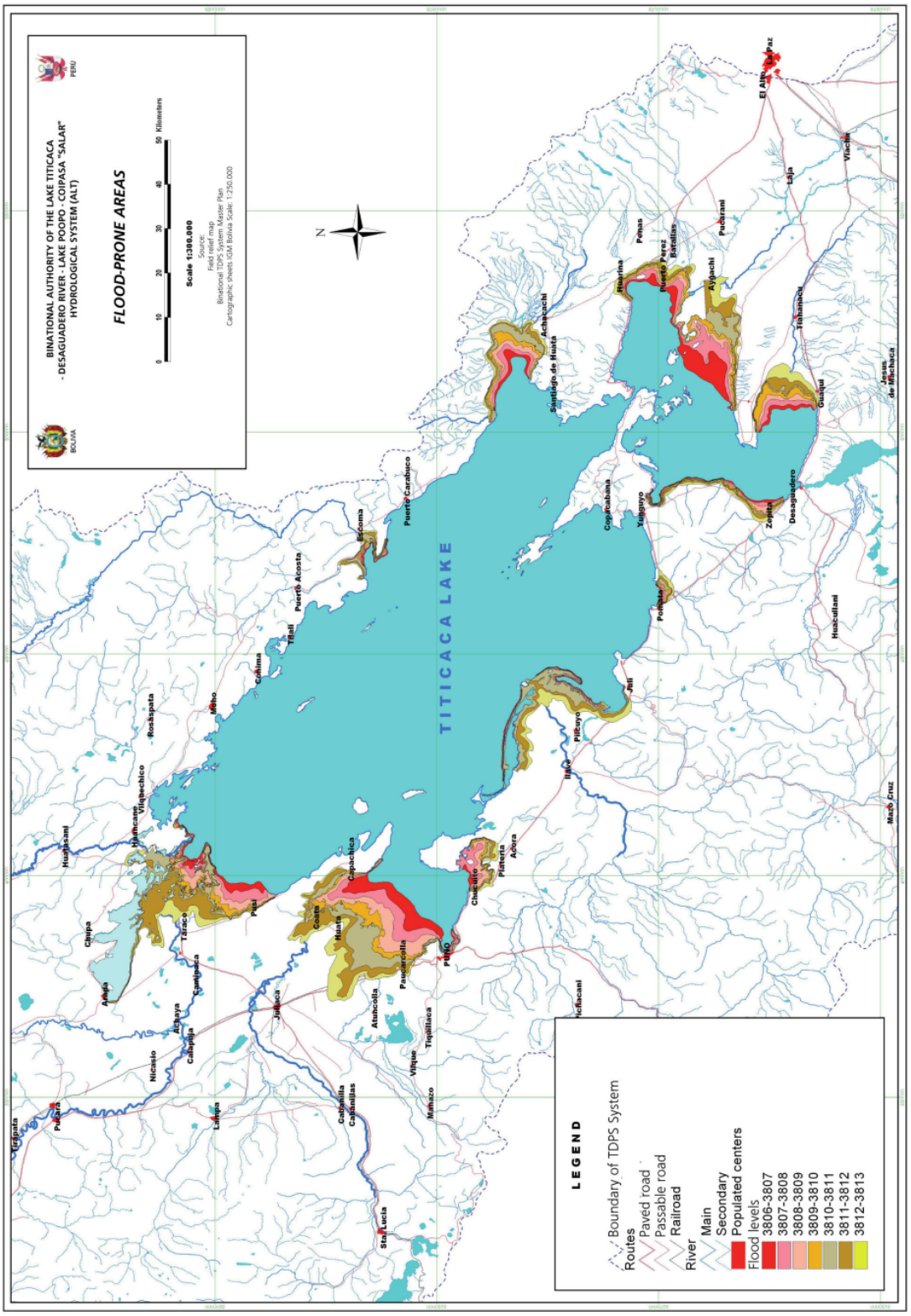

Figure E.1: Flood prone areas.

F | Chlorophyll a (August 2011)

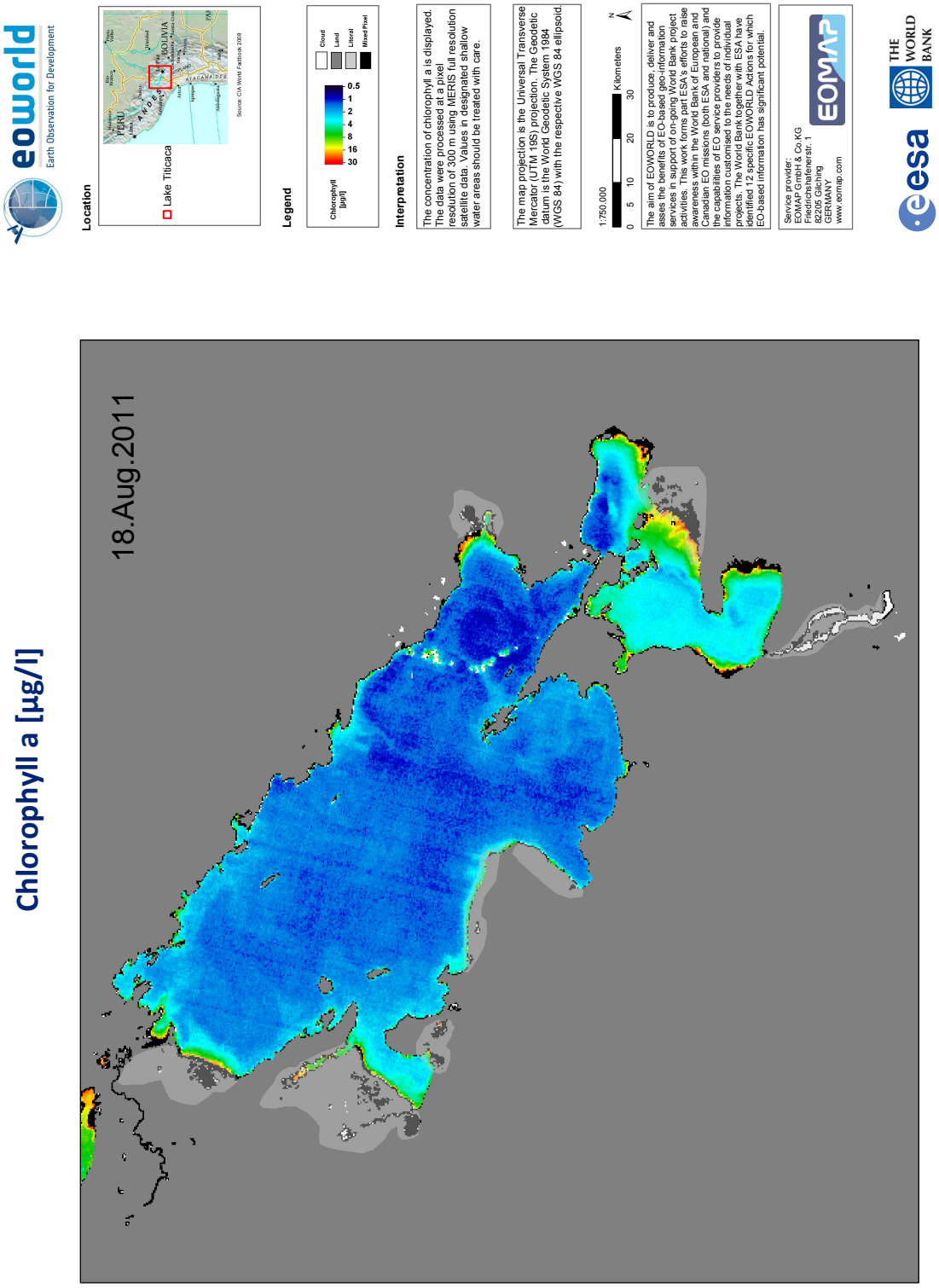

Figure F.1: Chlorophyll a (August 2011). We can see that Chlorophyll a is mostly present in Lago Menor and in shallow waters.

A coupled 3D hydrodynamic and ecosystemic model of Lake Titicaca.

How to grasp the complexity of Lake Titicaca in an easy to use model that enables water quality analyses and facilitates informed decision making?

François Duquesne

Mathematical models are essential in the quest to better understand the human impact on the world's ecosystems. In this thesis, we have provided a new tool that can be used to study Lake Titicaca's hydrodynamics and water quality. This was achieved by coupling NPZD (for Nitrogen-based nutrients, Phytoplankton, Zooplankton and Detritus) ecosystem-type model to an underlying three dimensional hydrodynamic model: the 3D version of the Second-generation Louvain-la-Neuve Ice-Ocean Model. SLIM3D leverages the finite elements method to solve the three-dimensional hydrodynamic equations on each element of an unstructured 3D mesh. Our study focused on the entire Lake Titicaca, and we developed a case study on the smaller section of this lake: Lago Menor. Indeed, in the Cohana bay, eastern part of Lago Menor, a significant nitrogen discharge is caused by anthropogenic activities of the upstream Katari watershed. This discharge is most likely responsible for the algal bloom event occurred in March-April 2015. We thus applied a nitrogen forcing to our NPZD ecosystem-type model in order to replicate the proliferation of phytoplankton. Our model covered the period of January 2014 to May 2015 and required the following inputs: the bathymetry, surface temperatures, and the horizontal wind speeds. Winds and surface temperatures are the major forcings that affect the hydrodynamics of the lake. The results generated by the coupled SLIM3D-NPZD model we chose to exploit were: lake temperatures, the u and v components of water velocity, and the NPZD components. Overall, the validation of our our coupled SLIM3D-NPZD model suggests that the tasks of simulating Lake Titicaca's hydrodynamics was achieved but that our model lacks a more site-specific calibration in order to correctly simulate water quality. We managed to simulate the bloom of 2015 but observed some erroneous simulations in other parts of the lake. Nevertheless, we were able to foresee a few promising applications for this coupled model. These range from the use of the model for research purposes to the forecasting and analysis of different contamination scenarios. We have thus manged to implement a fairly simple ecosystemic model that could be used as a predictive tool in the planification for the environmental protection of Lake Titicaca. Offering new opportunities for research and expanding the potential uses of the SLIM hydrodynamic model.

Université catholique de Louvain

Faculté des bioingénieurs

Croix du Sud, 2bte L7.05.01, 1348 Louvain-La-Neuve, Belgique | www.uclouvain.be/agro